



Reinforced Concrete Frame Element with Axial-Shear-
Flexural Interaction Under Cyclic Loading

Worathep Sae-Long

A Thesis Submitted in Partial Fulfillment of the Requirements for the Degree of
Doctor of Philosophy in Civil Engineering

Prince of Songkla University

2019

Copyright of Prince of Songkla University



Reinforced Concrete Frame Element with Axial-Shear-
Flexural Interaction Under Cyclic Loading

Worathep Sae-Long

A Thesis Submitted in Partial Fulfillment of the Requirements for the Degree of
Doctor of Philosophy in Civil Engineering

Prince of Songkla University

2019

Copyright of Prince of Songkla University

Thesis Title Reinforced Concrete Frame Element with Axial-Shear-
Flexural Interaction Under Cyclic Loading

Author Mr.Worathep Sae-Long

Major Program Civil Engineering

Major Advisor

.....
(Prof. Dr.Suchart Limkatanyu)

Examining Committee :

.....Chairperson
(Assoc. Prof. Dr.Nattapong Damrongwiriyanupap)

.....Committee
(Assoc. Prof. Dr.Kittisak Kuntiyawichai)

.....Committee
(Assoc. Prof. Dr.Woraphot Prachasaree)

.....Committee
(Dr.Wichairat Kaewjuea)

.....Committee
(Prof. Dr.Suchart Limkatanyu)

The Graduate School, Prince of Songkla University, has approved this thesis as partial fulfillment of the requirements for the Doctor of Philosophy Degree in Civil Engineering

.....
(Prof. Dr.Damrongsak Faroongsarng)
Dean of Graduate School

This is to certify that the work here submitted is the result of the candidate's own investigations. Due acknowledgement has been made of any assistance received.

..... Signature
(Prof. Dr.Suchart Limkatanyu)
Major Advisor

..... Signature
(Mr.Worathep Sae-Long)
Candidate

I hereby certify that this work has not been accepted in substance for any degree,
and is not being currently submitted in candidature for any degree.

..... Signature

(Mr.Worathep Sae-Long)

Candidate

ชื่อวิทยานิพนธ์	แบบจำลองโครงข้อแข็งคอนกรีตเสริมเหล็กที่มีปฏิสัมพันธ์ระหว่างแรงในแนวแกน-แรงเฉือน-แรงดัดภายใต้แรงแผ่นดินไหว
ผู้เขียน	นายวรเทพ แซ่ล่อง
สาขาวิชา	วิศวกรรมโยธา
ปีการศึกษา	2561

บทคัดย่อ

ในงานวิจัยนี้นำเสนอแบบจำลองโครงข้อแข็งคอนกรีตเสริมเหล็กสำหรับการวิเคราะห์เสาคอนกรีตเสริมเหล็กซึ่งมีลักษณะการออกแบบเหล็กตามขวางหรือเหล็กปลอกซึ่งไม่เพียงพอต่อการต้านทานแรงแผ่นดินไหว โดยเสาลักษณะนี้ถูกนิยามว่า เสาแบบ Non-ductile และมักจะพบในโครงสร้างโครงข้อแข็งคอนกรีตเสริมเหล็กซึ่งถูกออกแบบและก่อสร้างก่อนที่จะมีมาตรฐานการออกแบบโครงสร้างคอนกรีตเสริมเหล็กต้านทานแรงแผ่นดินไหวดังเช่นในปัจจุบัน แบบจำลองโครงข้อแข็งในการศึกษานี้สร้างมาจากวิธีการกระจัดและใช้สมมติฐานทฤษฎีคานของ Timoshenko ในการอธิบายการเปลี่ยนแปลงความเครียดตลอดหน้าตัดของเสา จากสมมติฐานดังกล่าวแรงในแนวแกนและแรงดัดจะมีปฏิสัมพันธ์กันอัตโนมัติ ในขณะที่ผลของแรงเฉือนไม่ได้มีปฏิสัมพันธ์กับแรงทั้งสอง แต่ผลของปฏิสัมพันธ์ระหว่างแรงเฉือนและแรงดัดจะถูกใส่เข้าไปผ่านทางความสัมพันธ์ระหว่างแรงเฉือนและความเครียดเฉือน ความสัมพันธ์ระหว่างแรงเฉือนและความเครียดเฉือนในงานวิจัยนี้ได้ปรับปรุงมาจากงานวิจัยของ Mergos และ Kappos (ปี 2008 และ 2012) โดยการลดลงของกำลังรับแรงเฉือนเนื่องมาจากอิทธิพลของการเปลี่ยนแปลงรูปเนื่องจากการดัดในช่วงอินอีลาสติก ถูกพิจารณาในความสัมพันธ์ดังกล่าวร่วมกับแบบจำลองการทำนายกำลังรับแรงเฉือนของคอนกรีตเสริมเหล็กที่เรียกว่า แบบจำลองกำลังรับแรงเฉือน UCSD ภายใต้วิธีการกระจัดมักจะพบปรากฏการณ์ที่เรียกว่า Shear locking เพื่อหลีกเลี่ยงปรากฏการณ์ดังกล่าว ในงานวิจัยนี้ได้ใช้ฟังก์ชันการกระจัดที่เรียกว่า Linked displacement interpolation functions ในการประมาณฟังก์ชันการกระจัดสุดท้ายความสำคัญของการพิจารณาผลของแรงเฉือนและปฏิสัมพันธ์ระหว่างแรงเฉือนและแรงดัดในการประเมินผลตอบสนองของเสาคอนกรีตเสริมเหล็กถูกนำเสนอและอธิบายผ่านตัวอย่างทั้ง 3 นอกจากนี้ตัวอย่างนี้เหล่านี้ยังถูกใช้ในการพิสูจน์ความแม่นยำและความสามารถในการทำนายพฤติกรรมที่ซับซ้อนของเสาคอนกรีตเสริมเหล็กแบบ Non-ductile

Thesis Title	Reinforced Concrete Frame Element with Axial-Shear-Flexural Interaction Under Cyclic Loading
Author	Mr.Worathep Sae-Long
Major Program	Civil Engineering
Academic Year	2018

Abstract

This thesis presents the reinforced concrete (RC) frame element for the analysis of the RC columns characterized by light and insufficiently detailed transverse reinforcement. This type of column is defined as the “*non-ductile*” RC column and also found in the existing RC frame buildings designed and constructed before the introduction of modern seismic codes. The frame element in this study is derived based on the displacement-based formulation and the Timoshenko beam kinematics assumption is used to describe the variation of strains along the RC cross-section at the fiber section level. As a result, the axial-flexure interaction is automatically taken into the element stiffness matrix while shear action uncouples with those actions. The shear-flexure interaction is taken into account via the shear hysteretic curve. The presented shear force and shear strain relation in the shear hysteretic curve is adopted and modified from the research work of Mergos and Kappos (2008 and 2012). The degradation of shear strength due to the influence of inelastic flexural deformations is accounted in this modified shear hysteretic curve within the framework of the so-called “*UCSD Shear-Strength Model*” . Linked displacement interpolation functions are used to solve the problematic phenomenon known as “*shear locking*” in the Timoshenko frame element. Finally, the importance of including shear response and shear-flexure interaction in the evaluation of the non-ductile RC columns are presented and discussed through the three numerical examples. Furthermore, the numerical examples are employed to verify the model accuracy and its capability to predict rather complex responses of the non-ductile RC columns.

Acknowledgements

This work would not have succeeded without the support of my advisor, Prof. Dr. Suchart Limkatanyu, who always cares all my work, study, and family's life since I was a master student. I delight and be lucky that have an experience working with him. He is my idol in many lifestyles both work and family's life, such as seeking knowledge, friendship, and socializing. He always supports both finance and education. Sometimes, he comes with a little snack and gives to me. I feel have the power to move on and feel thankful to him.

I deeply thank Prince of Songkla University for support by Scholarship Awards for Thai Ph.D. Student under Thailand's Education Hub for Southern Region of ASEAN Countries though I receive only one over three of this education fund.

I would like to thank the faculty of Engineering, Prince of Songkla University for the Scholarship after I miss the Scholarship Awards for Thai Ph.D. Student under Thailand's Education Hub for Southern Region of ASEAN Countries.

Special thanks go to a senior lecturer Mr. Wiwat Sutiwipakorn for reviewing and correcting the English of my journal papers, and all his advice in English language.

Lots of thanks are also due to Assoc. Prof. Dr. Woraphot Prachasaree, Asst. Prof. Dr. Passagorn Chaiviriyawong, Asst. Prof. Dr. Paramet Luathep, Asst. Prof. Dr. Jareerat Sakulrat, Assoc. Prof. Dr. Tanit Chalermyanont, Asst. Prof. Dr. Chatchawin Srisuwan, Assoc. Prof. Dr. Thaniya Kaosol, Dr. Wichairat Kaewjuea, Asst. Prof. Dr. Sakchai Prechaverakul, Asst. Prof. Sitthichai Piriyaakontorn, Dr. Ornkamon Wang-a-pisit, and Asst. Prof. Dr. Tanan Chub-uppakarn for giving their knowledge and friendships.

I would like to thank Assoc. Prof. Dr. Pattamad Panedpojaman for the experience of working and other opportunities in the work which are given to me. Moreover, he always gives the snacks to me. I feel thankful to him.

Thanks are also due to Ms.Supit Nontasorn, Ms.Kamonwan Songnam, and Ms.Jiraporn Yuangyai for their help in the accuracy of all documents and their supports.

The author is very enjoying to my friends that have studied in the same department and thank for entertaining moments.

Finally, big thanks to my family for their moral and financial support.

Worathep Sae-Long

Contents

	Page
Abstract	v
Acknowledgements	vii
Contents	ix
List of Tables	xiii
List of Figures	xiv
List of Symbols	xvii
Chapter 1: Introduction	1
1.1 Background and Rationale	1
1.2 Objectives	4
1.3 Scope	4
1.4 Advantages	5
Chapter 2: Literature Review	6
2.1 Introduction	6
2.2 Shear Mechanism of Reinforced Concrete	6
2.2.1 Equilibrium in the shear span	7
2.2.2 The mechanism of shear resistance	9
2.3 Shear Strength Models	14
2.3.1 ACI 318-14	15
2.3.2 ASCE-ACI Committee 426 Proposal	15
2.3.3 Ang et al. and Wong et al.	16
2.3.4 Watanabe and Ichinose	17
2.3.5 Priestley et al.	19
2.3.6 FEMA-273 Seismic Rehabilitation Guidelines	22
2.3.7 Sezen and Moehle	23
2.4 Beam Theories	24

Contents (Continuous)

	Page
2.5 General Finite Element Formulation of Reinforced Concrete Frame Element Including Shear Responses and Shear-Flexure Interaction Effects	26
2.5.1 Models based on the concept of truss analogy with uniaxial material constitutive models	28
2.5.1.1 Guedes's Modelling Approach	28
2.5.1.2 Martinelli's Modelling Approach	30
2.5.1.3 Ranzo and Petrangeli's Modelling Approach	31
2.5.1.4 Marini and Spacone's Modelling Approach	32
2.5.1.5 Mergos and Kappos's Modelling Approach	34
2.5.2 Models based on the 2D or 3D suitable constitutive model	36
2.5.2.1 Petrangeli's Modelling Approach	37
2.5.2.2 Vecchio and Collins's Modelling Approach	38
2.5.2.3 Bentz's Modelling Approach	40
2.5.2.4 Remino's Modelling Approach	41
2.5.2.5 Bairan's Modelling Approach	42
2.5.2.6 Kagermanov and Ceresa's Modelling Approach	43
2.5.2.7 Kotronis's Modelling Approach	44
2.5.2.8 Saritas's Modelling Approach	45
Chapter 3: Element Formulation	48
3.1 Introduction	48
3.2 A Set of Governing Equations of Timoshenko Frame Element (Strong Form)	48
3.2.1 Equilibrium	48
3.2.2 Compatibility	50
3.2.3 Section Force-Deformation Relations	51
3.3 Displacement-Based Formulation of Timoshenko Frame Element (Weak Form)	55
3.3.1 Formulation	55
3.3.2 Linked displacement interpolation functions	58

Contents (Continuous)

	Page
Chapter 4: Element State Determination	62
4.1 Introduction	62
4.2 Structure State Determination	62
4.3 Element State Determination	64
4.4 Convergence Criterion	67
4.5 Numerical Integration	69
Chapter 5: Material Constitutive Laws	70
5.1 Introduction	70
5.2 Concrete Constitutive Model	70
5.2.1 Stress-strain relation for concrete in compressive zone	71
5.2.2 The hysteretic response of concrete model under cyclic loading	73
5.3 Reinforcing Steel Constitutive Model	74
5.3.1 Stress-strain relation for reinforcing steel	75
5.3.2 The hysteretic response of reinforcing steel model under cyclic loading	76
5.4 Shear Constitutive Model	78
5.4.1 The Undamaged Primary Curve	79
5.4.2 Modified Mergos-Kappos Shear-Flexure Interaction Procedure	83
5.4.3 The Hysteretic Shear Force-Shear Strain Responses	91
5.4.3.1 The Monotonic Shear Force–Shear Strain Relation	91
5.4.3.2 The Behavior During Unloading State	93
5.4.3.3 The Behavior During Reloading State	93
5.4.3.4 The Reduced Shear Force-Shear Strain Envelope Due to the Crack Opening	96
Chapter 6: Numerical Verification of Model	98
6.1 Introduction	98
6.2 Flexure-Shear critical R/C members	98
6.2.1 Example I: Column 2CLD12	99

Contents (Continuous)

	Page
6.2.2 Example II: Column 2CMH18	106
6.3 Shear critical RC member	113
6.3.1 Example III: Column Specimen No. 1-1	113
Chapter 7: Conclusions	118
7.1 Summary	118
7.2 The Development and Future Work	119
References	120
Appendix A	136
Appendix B	139
Author's Biography	145

List of Tables

Table		Page
4-1	Step in element state determination for RC frame element analysis based on displacement-based formulation	65

List of Figures

Figure		Page
1-1	Damaged columns from 1971 San Fernando earthquake	2
1-2	Damaged bridge piers from 1995 Kobe earthquake	2
2-1	Mechanism of concrete shear resistance	7
2-2	Equilibrium of beam in the shear span	9
2-3	Beam actions on the concrete cantilever in the shear span	11
2-4	Arch action in idealised beam due to slip effect	12
2-5	Concrete cantilevers acting as struts	12
2-6	Truss analogy	14
2-7	Shear force versus displacement ductility of Ang and Wong model	17
2-8	Watanabe and Ichinose approach model	19
2-9	Strength of concrete shear resistant versus curvature ductility demand	21
2-10	Definition of D' for transverse reinforcement contribution	21
2-11	Axial load component of shear strength	22
2-12	Kinematics description of the Timoshenko beam element before deformation and after deformation	25
2-13	Strain distributions of Timoshenko element	26
2-14	Truss analogy of Guedes and Pinto model	29
2-15	Compatibility and Equilibrium of structure system	30
2-16	Planer structural assemblage for truss mechanism	31
2-17	Hysteretic shear force-shear strain response of Ranzo and Petrangeli model	32
2-18	Section shear law of Marini and Spacone	33
2-19	Mergos and Kappos element model	34
2-20	The initial shear force-shear strain primary curve without shear-flexural interaction	35

List of Figures (Continuous)

Figure		Page
2-21	Definition of GA_{eff}	36
2-22	Fiber section mechanics	38
2-23	Dual-section approach of Vecchio and Collins	39
2-24	The Modified Compression Field Theory of smeared cracks	40
2-25	The fiber stress and strain conditions of Rose-Shing model	41
2-26	The equilibrium conditions of Bairen's model	43
2-27	State of art of Kagermanov and Ceresa model	44
2-28	La Bordiere damage model of concrete	45
3-1	A differential segment of frame element	50
3-2	Fiber discretization of RC frame cross-section	53
3-3	Uniaxial cyclic constitutive laws of concrete, steel, and shear	54
3-4	Tonti's diagram for Timoshenko frame element: differential equations (Strong form)	55
3-5	The modified Tonti's diagram for Timoshenko frame element: displacement-based formulation (Weak form)	56
3-6	A standard linear Timoshenko frame element	61
4-1	Structure state determination by Newton-Raphson solution at load step k	63
4-2	Element state determination at load step k	66
4-3	Section state determination at load step k	67
5-1	Constitutive model of concrete under cyclic loading in compression	73
5-2	Menegotto and Pinto steel hysteretic model	75
5-3	Definition of curvature parameter R in Menegotto-Pinto reinforcing steel model	77
5-4	The undamaged primary curve of shear constitutive model	82

List of Figures (Continuous)

Figure		Page
5-5	The damaged primary curve of shear constitutive model	85
5-6	Three cases of the incremental shear force-shear strain relation	87
5-7	The step-by-step algorithm for iterative procedure within the shear-flexure interaction procedure	90
5-8	The hysteretic of shear model	92
6-1	The specimen geometry of column 2CLD12	100
6-2	The lateral load-displacement response of the end column 2CLD12	101
6-3	The hysteretic shear responses of column 2CLD12 at various monitoring sections	103
6-4	Shear force vs curvature ductility at the end of column 2CLD12 (Section I)	106
6-5	The specimen geometry of column 2CMH18	107
6-6	The lateral load-displacement response of the end column 2CLD12M	108
6-7	The hysteretic shear responses of column 2CMH18 at various monitoring sections	110
6-8	Shear force vs curvature ductility at the end of column 2CMH18	113
6-9	The specimen geometry of column No. 1-1	114
6-10	The lateral load-displacement response of the end column No. 1-1	115
6-11	The hysteretic shear responses of column No. 1-1 at various monitoring sections	117

List of Symbols

Symbol	Definition
A_g	= The gross cross sectional area
A_m	= The cross-section area of the m^{th} fiber in the section
A_v	= The area of the transverse reinforcement
b	= The section width
$\mathbf{B}_{TB}(x)$	= The sectional deformation-displacement matrix
c	= The neutral axis depth
C	= The compression force
C_d	= The diagonal compression struts
d	= The section depth
$\mathbf{d}(x)$	= The element sectional deformation vector
$\Delta\mathbf{d}(x)$	= The sectional deformation increments
$\mathbf{D}(x)$	= The element sectional force vector
D'	= The distance measured parallel to the applied shear between centers of the longitudinal reinforcement
D_c	= The column diameter for circular section
D'_c	= The core diameter measured to the centerline of transverse hoop for circular section

List of Symbols (Continuous)

Symbol	Definition
$\mathbf{D}_R(x)$	= The sectional resisting forces
dx	= An infinitesimal segment
d_1	= The damage factor which accounts for the loss of section strength
d_2	= The damage factor which accounts for the loss the ability of section to dissipate energy
E_c	= The concrete elastic modulus
$E_{dissipated}$	= The energy absorption
$E_{elastic}$	= The energy absorption at yield
E_m	= The modulus of the m^{th} fiber in the section
E_s	= The steel elastic modulus
E_t	= The tangent stiffness
E_0	= The initial slope of Menegotto and Pinto steel model
f'_c	= The concrete compressive cylinder strength (in MPa)
f_{ca}	= The corresponding stress due to arch action in Watanabe and Ichinose model (1991)
F_{ci}	= The concrete strut forces for Guedes's model

List of Symbols (Continuous)

Symbol	Definition
f_{ct}	= The corresponding diagonal compression stress due to truss action in Watanabe and Ichinose model (1991)
f_t'	= The nominal tensile strength of concrete
f_v	= The stirrups or transverse reinforcement stress
F_{wy}	= The transversal steel tie forces for Guedes's model
f_y	= The yield strength of reinforcing steel
f_{yv}	= The yield strength of transverse reinforcement
G	= The shear modulus
G_A	= The lumped shear stresses transmits across the crack by aggregate interlocking into a single force
GA_{eff}	= The effective sectional shear stiffness
GA_{ref}	= The reference shear stiffness
GA_{rel}	= The reloading sectional shear stiffness for shear model
GA_s	= The sectional shear stiffness
GA_0	= The uncracked shear stiffness
GA_1	= The cracked shear stiffness
h	= The section height

List of Symbols (Continuous)

Symbol	Definition
h'	= The width of concrete core for concrete model
jd	= The distance between line of thrust and tensile force of the flexural reinforcement
jt	= The distance between upper and lower chords of the analogous truss
K	= A parameter which accounts the strength increase because of the confinement for concrete model
\mathbf{K}	= The element stiffness matrix
$\mathbf{k}(x)$	= The sectional stiffness matrix
k_d	= The factor depending on the displacement ductility demand
k_{FEMA}	= The ductile factor for FEMA-273 model
k_ϕ	= A factor depending on the influence of curvature ductility demand on the concrete shear strength V_c
L	= The element length
L_a	= The shear span
L_a / h	= The shear span ratio
\mathbf{L}_{TB}	= The Timoshenko frame differential operator
M	= Bending moment

List of Symbols (Continuous)

Symbol	Definition
$M(x)$	= The sectional bending moment
N	= The compressive axial force
$N(x)$	= The frame sectional axial force
$\mathbf{N}_{TB}(x)$	= The displacement interpolation function matrix
n_{fib}	= A number of fibers in the section
\mathbf{P}	= The element nodal forces
$\mathbf{p}(x)$	= The element distributed load vector
\mathbf{P}_p	= The equivalent load vector due to the distributed load $\mathbf{p}(x)$
$P_y(x)$	= The transverse distributed load
\mathbf{Q}	= The element resisting force vector
R	= The parameter for controlling shape of the transition curve for Menegotto and Pinto steel model
R_0	= The value of the parameter R during first loading for Menegotto and Pinto steel model
s	= The spacing of transverse reinforcement
s_c	= The depth of the critical cantilever section
s_h	= The center to center spacing of stirrups or hoop set for concrete model

List of Symbols (Continuous)

Symbol	Definition
T	= The tensile force
ΔT	= A bond force due to the increase of the tensile force in the flexural reinforcement between adjacent cracks
T_s	= The resultant of all stirrup force across the diagonal crack
\mathbf{U}	= The element nodal displacements
$\Delta \mathbf{U}$	= The incremental of element nodal displacements
$u(x)$	= The horizontal displacements field
$\mathbf{u}(x)$	= The sectional displacement vector
$\Delta \mathbf{u}(x)$	= The incremental of displacement vector
$\delta \mathbf{u}(x)$	= A vector collecting compatible virtual displacement fields
$\delta \mathbf{U}^T \mathbf{P}$	= The boundary terms that can be obtained during the integration by parts
$u_{ps}(x)$	= The plane section displacement field based on Euler Bernoulli beam theory for Bairan's model
$u_w(x)$	= The imposing distortion-warping displacement field
$u_0(x)$	= The sectional axial displacement at reference axis
V	= Shear force
ΔV	= The incremental sectional shear force

List of Symbols (Continuous)

Symbol	Definition
$v(x)$	= The transverse displacements field
$V(x)$	= The sectional shear force
v_A	= The shear stresses transferred across the crack by the average of the aggregate interlocking
V_a	= The axial-force shear strength
v_b	= The basic shear stress for ASCE-ACI Committee 426
V_c	= The concrete contribution of shear strength
ΔV_c^{deg}	= The reduction in sectional shear force associated with the concrete shear strength degradation
V_{cr}	= The cracking shear force
V_{cz}	= The shear force across the compressive zone
V_d	= A dowel force transferred across the crack by the flexural steel reinforcement
V_{Rd}	= The shear capacity suggested by Eurocode 2 (1991)
V_{Rdc}^*	= The force of the concrete member under zero axial load
V_{Rds}	= The force of steel stirrups for Marini and Spacone's model
V_s	= The transverse-reinforcement shear strength

List of Symbols (Continuous)

Symbol	Definition
V_t	= The total external shear force
V_u	= The shear strength
V_{u0}	= The initial shear strength without the degradation of shear strength due to the increasing of the sectional curvature ductility demand
V_y	= Shear force at the longitudinal reinforcement yielding for the first time
V_0	= The non-degraded sectional shear force
$v_0(x)$	= The sectional transverse displacement
w	= The weight factor
W_{str}	= The work (Energy) at the structural level
x_a	= The distance from the total external shear force to the combination of shear force across the compressive zone
y	= The distance from the horizontal axis to considerate point with normal in vertical direction
y_m	= The distance from the reference axis x of the m^{th} fiber in the section
Z	= The slope of the softening branch for concrete model
α_b	= A parameter to be determined from the limit Euler-Bernoulli condition of vanishing shear strain

List of Symbols (Continuous)

Symbol	Definition
α_c	= the modification factor for the concrete shear strength of Ang et al. (1989) and Wong et al. (1993) model
β	= The angle between the column axis and the line connecting the centers of the flexural compression zones at the top and the bottom of the column ends
β_t	= The web reinforcement angle to the horizontal
$\Delta\gamma$	= The incremental sectional shear strain
$\gamma(x)$	= The sectional shear strain
γ_{ch}	= The shear strain at a break point
γ_{cr}	= The cracking shear strain
γ_{nu}	= The last shear strain for complete negative unloading
γ_{pu}	= The last shear strain for complete positive unloading
γ_{st}	= The shear strain corresponding to the verge of transverse reinforcement yielding
γ_{truss}	= The shear strain corresponding to the yielding of transverse reinforcement based on the truss analogy approach
γ_u	= The ultimate shear strain
$\gamma_{xy}(x)$	= The sectional shear strain

List of Symbols (Continuous)

Symbol	Definition
γ_y	= The shear strain at the longitudinal reinforcement yielding for the first time
ε_c	= The concrete strain
ε_{c0}	= The concrete strain at maximum stress in compression
ε_{cu}	= The strain at concrete crushing
ε_s	= The steel strain
$\varepsilon_{xx}(x)$	= The sectional axial strain
ε_y	= The strain at yield point
$\varepsilon_0(x)$	= The sectional axial strain at reference axis
θ	= The angle between the column axis and the direction of the diagonal compression struts
$\theta(x)$	= The sectional rotation
κ	= The axial-force modification factor
λ	= The member-aspect-ratio modification factor
λ_{aci}	= The modified factor to reduce the concrete strength for ACI 318-14 code
λ_{FEMA}	= A coefficient of the concrete shear resisting mechanism for FEMA-273 model
λ_1	= The parameter accounting for the axial load

List of Symbols (Continuous)

Symbol	Definition
λ_2	= The parameter accounting for the member aspect ratio
λ_3	= The parameter accounting for the amount of transverse reinforcement
μ_d	= The displacement ductility demand
μ_φ	= The curvature ductility demand
ξ_x	= The pinching parameters in x direction
ξ_y	= The pinching parameters in y direction
ρ_v	= The volumetric of transverse reinforcement
σ_c	= The compressive stress of concrete
σ_m	= The normal stress of the m^{th} fiber in the section
σ_s	= The stress of reinforcing steel
σ_{st}	= A stress shift in the linear yield asymptote for Menegotto and Pinto steel model
σ_{xx}	= The stress in x-direction
σ_y	= The stress at yield point
σ_{yy}	= The stress in y-direction
σ_1	= The principal stress in 1-direction
σ_2	= The principal stress in 2-direction

List of Symbols (Continuous)

Symbol	Definition
τ_{xy}	= The shear stress
ϕ	= The angle characterized by the member axis and the direction of diagonal struts
$\phi(y)$	= The shear sectional interpolation function for Saritas's model
$\Phi(GA_{eff})$	= The residual function
φ	= The crack angle inclination of 45 degrees
$\varphi(x)$	= The sectional curvature

CHAPTER 1

Introduction

1.1 Background and Rationale

Nowadays, the reinforced concrete structures (RC-Structures) have been extensively used in the structural engineering works, such as building, highway, pavement and bridge structures etc. The older RC frame buildings with the poor performance, especially the RC buildings designed and constructed prior to the introduction of modern seismic codes, have still existed in the most countries. During the past and recent devastating earthquakes (e.g. the 1967-Caracas earthquake, the 1968-Tokachi-Oki earthquake, the 1971-San Fernando earthquake, the 1989-Loma Prieta earthquake, the 1994-Northridge earthquake, 1995-the great Hanshin earthquake or Kobe earthquake, the 1999-Kocaeli earthquake, the 1999-Taiwan earthquake, the 2008-Wenchuan earthquake, and the 2009-Honduras earthquake), it has been observed that those frame buildings are severely damaged or even completely collapsed as shown in Figure 1-1 and 1-2. To examine the cause of the resulting damages and collapses of those frame structures, several researchers (e.g. Wight and Sozen; 1975; Ghee et al., 1989; Li et al., 1995; Yalcin 1997; Lynn et al., 2001; Hamilton et al., 2002; and Sezen, 2002) conducted the experiments on RC columns to investigate the behavior of those columns under seismic load. From the study results of some research works [Lynn et al., 2001; and Sezen, 2002], it can indicate that those columns are characterized by the lightly and insufficiently detailed transverse reinforcement that corresponds to the study results in the several research works (e.g. Lynn et al., 1996; and Kim et al., 2013). Moreover, it is found that the most damaged mechanism of those columns is related to shear that is the main cause of column damages and collapses [Moehle et al., 2001; Sezen et al., 2003; and Dogangun, 2004]. However, although those columns have initially been designed to withstand shear force associated with the flexural yielding, it may fail in shear because of the increase of inelastic flexural deformations (Plastic-hinge

formation) which affect on the shear capacity [Ghee et al., 1989; Watanabe and Ichinose, 1991; Priestley et al., 1993; Biskinis et al., 2004; Sezen and Moehle, 2004]. It relies on the fact that when the width of the cracks associated with the inelastic flexural deformations increase, the capability of the concrete shear transfer between the aggregate interlock is also reduced and leads to the degradation of the shear capacity.

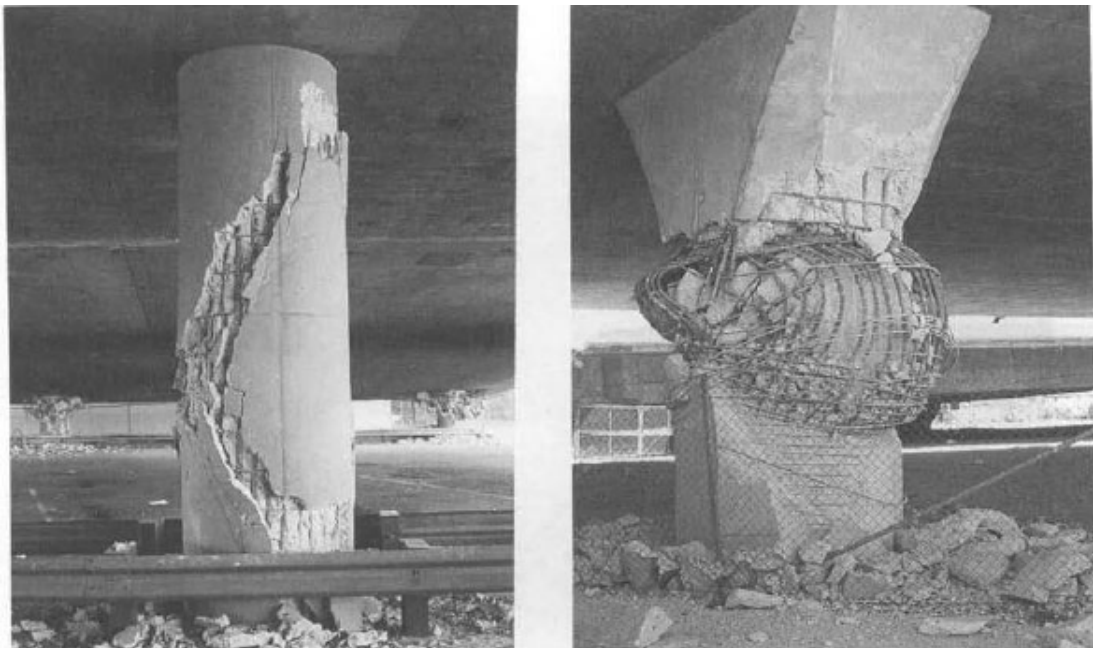


Figure 1-1 Damaged columns from 1971 San Fernando earthquake [Alim, 2014]



Figure 1-2 Damaged bridge piers from 1995 Kobe earthquake [Ghasemi et al., 1996]

According to the failure types of the RC columns under seismic load, the research work of Ceresa et al. (2008) divides the failure types into three categories detected by the shear span ratio $\frac{L_a}{h}$, that is the ratio between the shear span L_a and section depth h . The first failure type is the shear failure mode that is dominated when the value of shear span ratio is lesser than 2.5 ($\frac{L_a}{h} < 2.5$) while the second failure mode is the members with the value of shear span ratio between 2.5 and 5 ($2.5 \leq \frac{L_a}{h} \leq 5$). This type of member is classified as the flexural-shear critical member. The shear-flexural interaction is also observed in this type of members. Finally, the last failure type is the flexural failure mode which is found in the members with the value of shear span ratio over 5 ($\frac{L_a}{h} > 5$). In addition to the most damages and collapses of the columns as above discussed in the first paragraph, the most failures can be classified in the shear failure and flexural-shear failure, especially the flexural-shear failure. The behavior of shear-flexural interaction effects within the flexural-shear critical member (Leading to the degradation of shear strength capacity) corresponds to the results of experiments on RC columns as above discussed. Thus, the shear-flexural interaction effects may be the main cause of column damages and may lead to the failure in shear.

To evaluation of those existing building's performance as above discussed in the first and second paragraphs, the development of efficient and reliable RC frame models for the maintainable preparation, minimum levels of the economic investment, and reduction of the damaged risk on those columns to withstand the future earthquakes are still required in the earthquake engineering. Although there are many RC frame models which are accepted and used in the engineering practice, the development of RC frame model capable of the effects of flexure-shear interaction, including inelastic shear response, and the failure prediction in shear is still a challenging and open-ended problem.

1.2 Objectives

This research focuses on the development of frame element model which accounts the shear-flexural interaction effects for seismic analysis of the non-ductile RC columns. The developmental approach needs to be the simple but accurate model and the input properties parameters on the proposed model are closely based on the engineering properties in the practice.

The main objectives of this research are:

1.2.1 To propose the new method to predict the shear stiffness with shear-flexural interaction effects after plastic hinge forming for non-ductile RC column analysis.

1.2.2 To discuss the importance of considering the shear response and shear-flexure interaction effects in the non-ductile RC column analysis.

1.2.3 To prove the performances of the proposed RC frame element when compared to the previous models (e.g. Mergos and Koppas model (2008); and the frame element based on Euler-Bernoulli beam theory).

1.3 Scope

Limitations of this study can be expressed as:

1.3.1 The frame element is based on Timoshenko beam theory.

1.3.2 The frame element model is based on the small-deformation hypothesis.

1.3.3 Effective of Poisson's ratio is neglected in this study.

1.3.4 The range of the used parameters is based on the criteria of each equation.

1.4 Advantages

The benefits of this research can be explained as follow:

1.4.1 The analytical responses from this research model can use to investigate, evaluate, and design R/C frame buildings under cyclic loading.

1.4.2 The model in this research can be applied with the engineering application software.

1.4.3 The model in this research is the basic model of the RC frame element subjected to the cyclic loading which can develop into a real simulation in the future.

1.4.4 The proposed model is convenient and straightforward for use in practical engineering because of the input parameters within the proposed model based on the reinforced concrete properties that are commonly found in the practice.

CHAPTER 2

Literature Review

2.1 Introduction

In this chapter presents the brief summary of the shear mechanism of reinforced concrete, the shear strength models, the classical beam theories and the overview of the element formulation strategies with including shear responses and the reflection of shear-flexure interaction effects. It can be divided into the four major parts. The first part mentions the behavior of reinforced concrete for resisting of the shear mechanism. The second part refers to the prediction models of the shear capacity of reinforced concrete. The third part talks about the used classical beam theories in this study while the last part shows the summary of element formulation strategies with accounting the shear effect into the response analysis and discusses to the overview of state-of-the-art to include the shear-flexure interaction in the response analysis.

2.2 Shear Mechanism of Reinforced Concrete

The shear resisting mechanism of the reinforced concrete can describe through the principal stress analysis in Figure 2-1 (a). Shear force and bending moment always combine in the multi-axial stress state. During the applied load, the diagonal crack of concrete occurs at which the principal tensile stress reaches to the tensile capacity of concrete. The crack pattern is approximated inclination of 45 degrees ($\phi = 45^\circ$) and is always found in the diagonal line shown in Figure 2-1 (b). While the crack width increases, the ability of the concrete to transfer principle tensile stresses is also reduced.

Figure 2-1 (b) shows the relation between the internal forces and external forces from the free body diagram of RC beam, which is cleaved across the inclined crack. It can be observed that the external shear force V is resisted by the

shear stresses which transmitted in the uncracked compression zone, shear stresses which transmitted along the crack plan by aggregate interlock, dowel forces due to the flexural steel bar, and residual tensile stresses that transmitted across the crack plane [Ceresa et al., 2008].

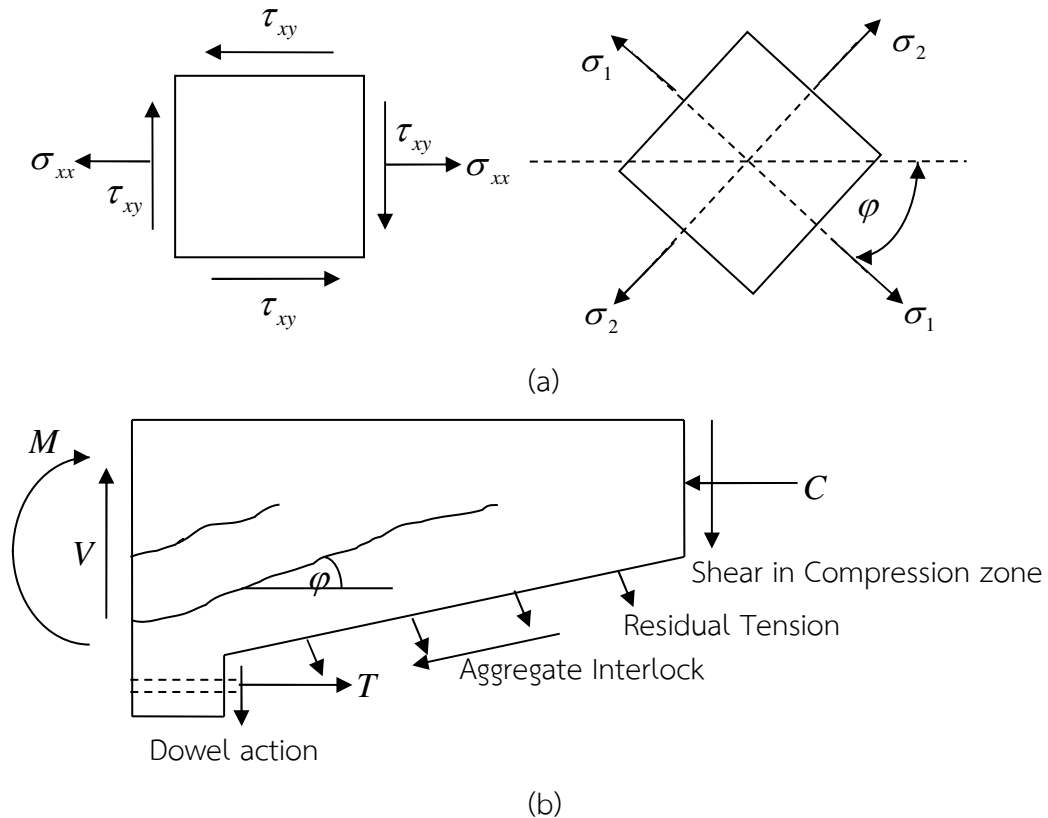


Figure 2-1 Mechanism of concrete shear resistance: (a) principal stress; and (b) external and internal actions in beam [Ceresa et al., 2008]

2.2.1 Equilibrium in the shear span

The equilibrium of the shear span can define by considering a part of the simply supported beam with the constant of shear force as shown in Figure 2-2 (a). The total external shear force V_t is resisted by the combination of shear force across the compressive zone V_{cz} , a dowel force transferred across the crack by the flexural steel reinforcement V_d , and shear stress transferred across the crack by the

average of the aggregate interlocking ν_A . Thus, the total external shear force V_t can be written as:

$$V_t = V_{cz} + V_A + V_d \quad (2-1)$$

To simplify for the consideration of the equilibrium equation of Eq. (2-1), the shear stresses transmitted across the crack by aggregate interlocking ν_A can be lumped into a single force G_A , which is defined by the line of action across two distinct points as shown in Figure 2-2 (b). After that, the equilibrium of the free body can be represented through the force polygon as shown in Figure 2-2 (c).

The resisting moment of beam M can be written as:

$$M = x_a V_t = jd(T + V_d \cot \theta) \quad (2-2)$$

where x_a is a distance from the left support; jd is the distance between line of thrust and tensile force of the flexural reinforcement; and T is the tensile force. For beam without the transverse reinforcement, the dowel force transferred across the crack by the flexural steel reinforcement V_d cannot be developed because this force reacts directly on the concrete cover at which the dowel force V_d is low. Thus, the resisting moment is simplified by neglecting the term of the dowel force ($V_d = 0$) and can be simply expressed by

$$M = Tjd \quad (2-3)$$

It needs to note that the bending moment and tension force, correspond to each other in Figure 2.2 (b) and Eq. (2-3), don't occur in the same section of the beam. The tensile force in the longitudinal reinforcement bar at a distance $x_a - jd \cot \theta$ from the left support depending on the bending moment at a distance x_a from the left support. Thus, it is clear that the increase in the steel stresses is governed by the slope of idealized diagonal crack. When the angle θ is less than 45° , the moment arm $jd \cot \theta$ can be approximated by the section depth d [Park and Paulay, 1975].

equilibrium of beam system, the internal shear force equation can be rewritten as shown in Eq. (2-4).

$$V = \frac{dM}{dx} = \frac{d}{dx}(Tjd) = jd \frac{dT}{dx} + T \frac{d(jd)}{dx} \quad (2-4)$$

From the Eq. (2-4), the internal shear force V is expressed in the two terms. The first term presents the behavior of the true prismatic flexural member by the variation of the internal tension force $\frac{dT}{dx}$ with the constant lever arm jd while the second term shows the variation of the lever arm $\frac{d(jd)}{dx}$ with the constant tension force T . In the elastic beam theory, the bond between concrete and steel reinforcement is assumed to be perfect (Non-slip). From this assumption, the lever arm of the second term in Eq. (2-4) is assumed as a constant term. In other words, the variation of the lever arm is equal to zero ($\frac{d(jd)}{dx} = 0$). Thus, the Eq. (2-4) can be reduced into Eq. (2-5).

$$V = jd \frac{dT}{dx} \quad (2-5)$$

According to Eq. (2-5), this equation is referred to as “*beam action*” in the shear span and is accepted in the analysis of prismatic flexural members [Park and Paulay, 1975]. The beam action can consider from the simply supported beam in Figure 2-2 (a). Each block may be considered into the cantilever action as shown in the Figure 2-3. Under perfect beam assumption as above described, the external forces (N , M , and V) are resisted by the internal forces, such as a bond force due to the increase of the tensile force in the flexural reinforcement between adjacent cracks $\Delta T = T_1 - T_2$, shear stresses at the two faces of the crack v_{a1} and v_{a2} , and the dowel forces across the flexural reinforcement V_{d1} and V_{d2} . It can be observed that the external moment is resisted by the bond force ΔT . Moreover, the flexural of concrete resistance depends on the tensile strength of concrete and the critical section depth s_c .

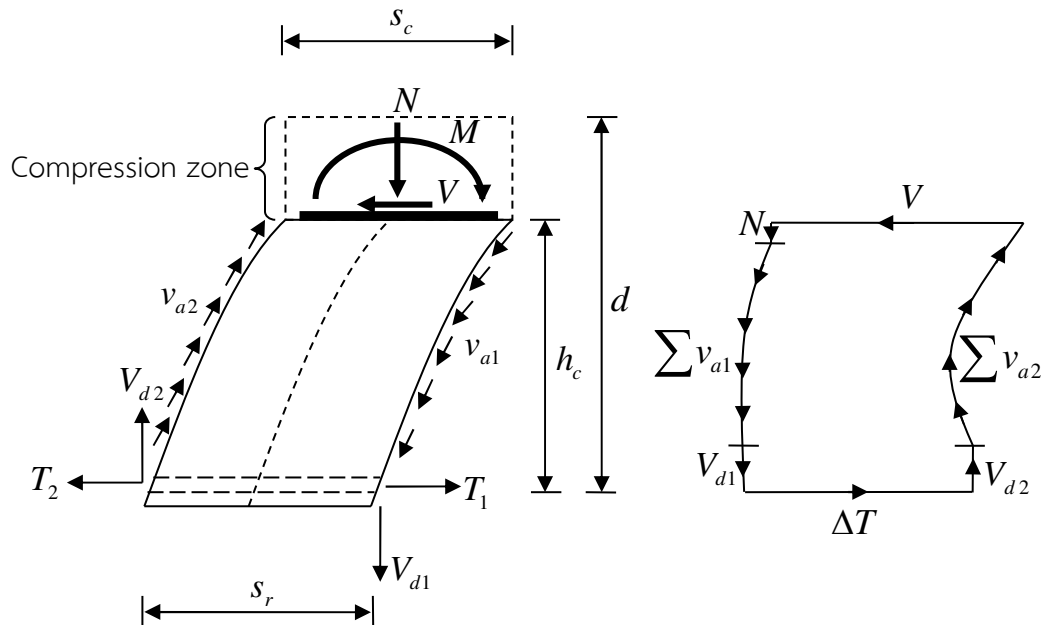


Figure 2-3 Beam actions on the concrete cantilever in the shear span

[Park and Paulay, 1975]

In case of only second term of Eq. (2-4), it refers to the case of the bond between concrete and steel reinforcement is destroyed along the entire of shear span (Complete loss of bond transfer). From this reason, the tensile force T cannot change ($\frac{dT}{dx}=0$) and the external force is resisted only by the inclined internal compression as shown in Eq. (2-6). This case is referred to as “*arch action*” in the shear span [Park and Paulay, 1975]. The strength of arch action depends on the inclination of the line of thrust in Figure 2-4.

$$V = T \frac{d(jd)}{dx} \quad (2-6)$$

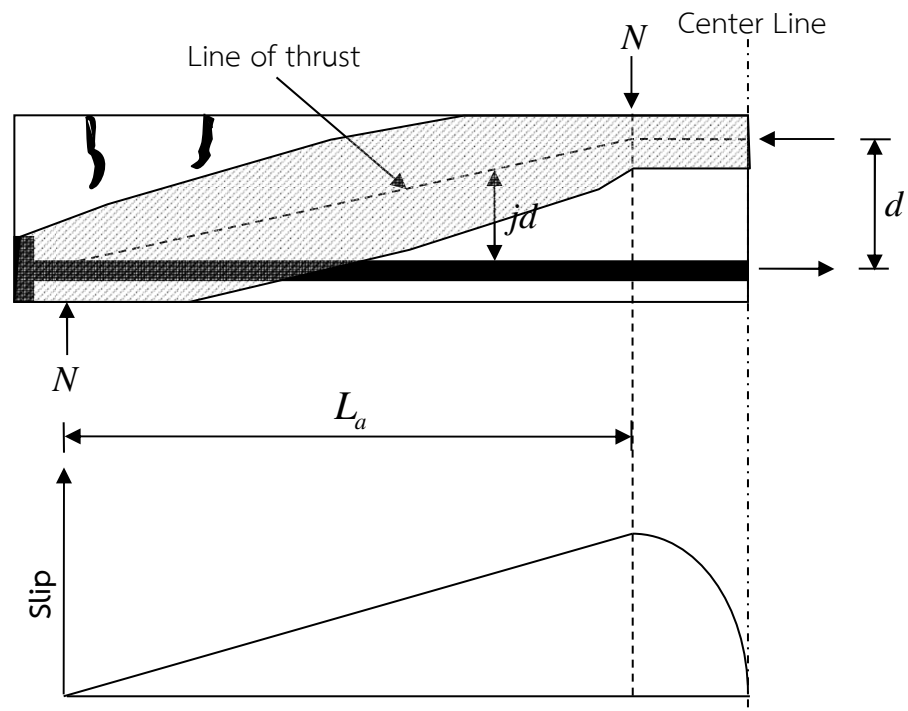


Figure 2-4 Arch action in idealised beam due to slip effect [Park and Paulay, 1975]

According to above explanation on the beam action, the cantilever system in Figure 2-3 does not consider the resisting force from web reinforcement, such as stirrups or transverse reinforcement. However, when the system includes the resisting force by the web reinforcement, the bond force ΔT is also resisted by the combination of aggregate interlock, flexural, and dowel action of cantilever system. Another bond force $\Delta T'$ can define in term of “truss action” as shown in Figure 2-5.

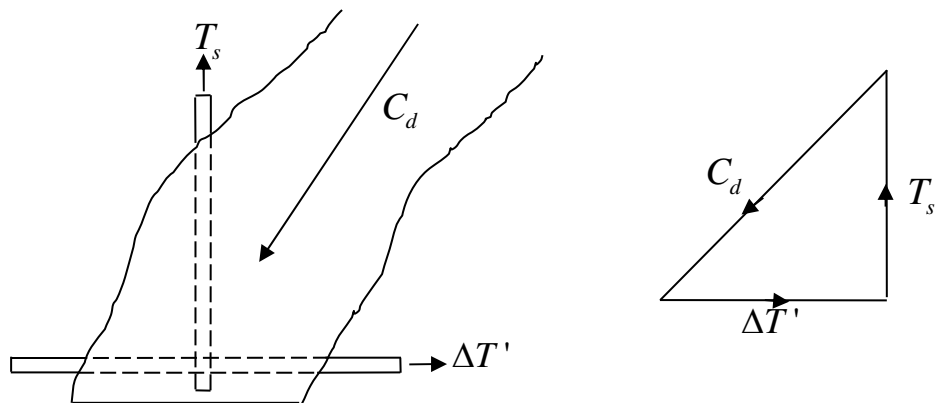


Figure 2-5 Concrete cantilevers acting as struts [Park and Paulay, 1975]

The behavior of the truss action is similar to the perfect beam action (The lever arm of the second term is the constant), but it includes another bond force $\Delta T'$ as shown in Figure 2-5. The force in truss can be determined from the considerations of equilibrium only. From the analogous truss in the Figure 2-6, the external shear force (truss mechanism) V_s is resisted by the diagonal compression struts C_d which incline at an angle of the concrete strut θ to the horizontal axis, and the resultant of all stirrup force across the diagonal crack T_s which incline at an angle β_t to the horizontal axis. The relation between the external shear force and internal shear force can be written as:

$$V_s = C_d \sin \theta = T_s \sin \beta_t \quad (2-7)$$

From the geometry of the analogous truss, the spacing of stirrups s can be defined as:

$$s = jd (\cot \theta + \cot \beta_t) \quad (2-8)$$

From the Eq. (2-7) and Eq. (2-8), the external shear force V_s can be written as:

$$V_s = \frac{A_v f_v (jd \sin \beta_t (\cot \theta + \cot \beta_t))}{s} = \frac{T_s}{s} \quad (2-9)$$

where A_v is the web reinforcement area with the spacing s ; and f_v is the stirrup stress. It is crucial to point out that the advantages of the stirrups or transverse reinforcement in beam action are the resisting shear force that attempts to extend the crack of concrete, suppressing flexural tensile stresses in the cantilever blocks by the average of the diagonal compression force C_d , limiting the crack opening, preventing the loss of bond, and providing the confinement [Park and Paulay, 1975]. Thus, the resisting shear force by the truss mechanism is an important component which plays an essential role on the shear capacity of the reinforced concrete members.

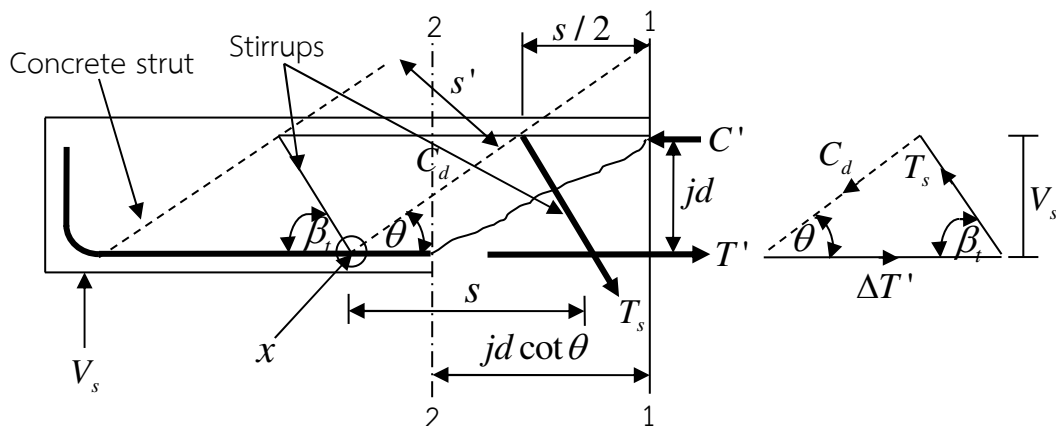


Figure 2-6 Truss analogy [Minelli, 2005]

2.3 Shear Strength Models

During the last several decades, the several researchers (e.g. Wight and Sozen, 1973; Nagasaka, 1982; Umehara and Jirsa, 1982; Bett et al., 1985; Ohue et al., 1985; Imai and Yamamoto, 1986; Zhou et al., 1987; Ang et al., 1989; Arakawa et al., 1989; Amitsu et al., 1991; Lynn et al., 1996; Priestley and Benzoni, 1996; Xiao and Martirosyan, 1998; Aboutaha et al., 1999; Sezen, 2002; Sezen and Moehle, 2004) conducted a set of experiments on columns for the study of the reinforced concrete column behaviors under the constant axial load and cyclic lateral load. The specimens of their experiments were varied with the different the column properties, such as the longitudinal and transverse reinforcement ratio, shear span ratio and axial load ratio etc. Among these experiments, the several shear strength models for reinforced concrete have been proposed in the research community [Ghee et al. 1989; Watanabe and Ichinose 1991; Priestley et al., 1993; Sezen, 2002] and applied in the several building codes [Cai and Degree, 2017]. The shear strength equations were developed and established by the different approaches from those experiments in terms of the property parameters of the reinforced concrete column.

From most of the shear strength models, the shear strength of reinforced concrete column V_u is considered to be the summation of the

contributions of concrete V_c and reinforcement V_s for resisting shear force as shown in Eq. (2-10).

$$V_u = V_c + V_s \quad (2-10)$$

Some shear strength models proposed in literatures can be summarized and expressed in the following:

2.3.1 ACI 318-14 (2014)

The shear strength model proposed by ACI 318-14 is the criteria for design of RC column under axial load. The shear strength equation V_u is the contributions of shear resisting force from the concrete V_c and transverse reinforcement V_s as shown in Eq. (2-10). The concrete contribution of shear strength equation is given by

$$V_c = 2 \left(1 + \frac{N}{2000A_g} \right) \lambda_{aci} \sqrt{f'_c} b d \quad (2-11)$$

The contribution of the transverse reinforcement can calculate by

$$V_s = \frac{A_v f_{yv} d}{s} \quad (2-12)$$

where N is the compressive axial force; A_g is the gross cross sectional area; f'_c is the concrete compressive cylinder strength; b is the section width; d is the section depth; λ_{aci} is the modified factor to reduce the concrete strength; A_v is the transverse reinforcement area with a spacing s ; and f_{yv} is the yield strength of transverse reinforcement.

2.3.2 ASCE-ACI Committee 426 Proposal (1973, 1977)

In 1973, a report on the shear strength of reinforced concrete members was published by the ASCE-ACI Joint Committee 46. The report discussed the cause of shear failure of RC members that observed from the damaged response

after the 1971-San Fernando earthquake. Later, a revised version of this report was published in 1977.

The shear strength model of ASCE-ACI Committee 426 is similar to the ACI 318-02 code that the shear strength equation is the contributions of concrete and transverse reinforcement as shown in Eq. (2-10). The transverse reinforcement contributions V_s can calculate from Eq. (2-12) while the concrete contributions V_c for the rectangular column can calculate by

$$V_c = v_b \left(1 + \frac{3N}{f'_c A_g} \right) 0.8 A_g \quad (2-13)$$

The basic shear stress v_b can calculate by

$$v_b = (0.067 + 10 p_v) \sqrt{f'_c} \leq 0.2 \sqrt{f'_c} \quad (2-14)$$

where p_v is the volumetric ratio of transverse reinforcement.

2.3.3 Ang et al. (1989) and Wong et al. (1993)

The shear strength model of Ang et al. (1989) and Wong et al. (1993) is established from a set of the circular cantilever column experimental tests under uniaxial [Ang et al., 1989] and multidirectional cyclic lateral displacement [Wong et al., 1993]. This model accounts the strength degradation suggested by ATC-6 relationship as shown in Figure 2-7. Moreover, the contribution of shear strength model is similar to ACI 318-02 that can calculate from Eq. (2-10).

The initial concrete mechanism of shear resisting is given by

$$V_c = 0.37 \alpha_c \left(1 + \frac{3N}{f'_c A_g} \right) \sqrt{f'_c} 0.8 A_g \quad (2-15)$$

The truss mechanism of shear resisting for circular column can calculate by

$$V_s = \frac{\pi A_v f_{yv} D'_c}{2s} \quad (2-16)$$

where D'_c is the core diameter measured to the centerline of transverse hoop for circular section; and α_c is the modification factor for the concrete shear strength and can determine from bending moment M , shear force V , and the column diameter for circular section D_c as shown in Eq. (2-17).

$$\alpha_c = \frac{2}{(M / VD_c)} \geq 1.0 \quad (2-17)$$

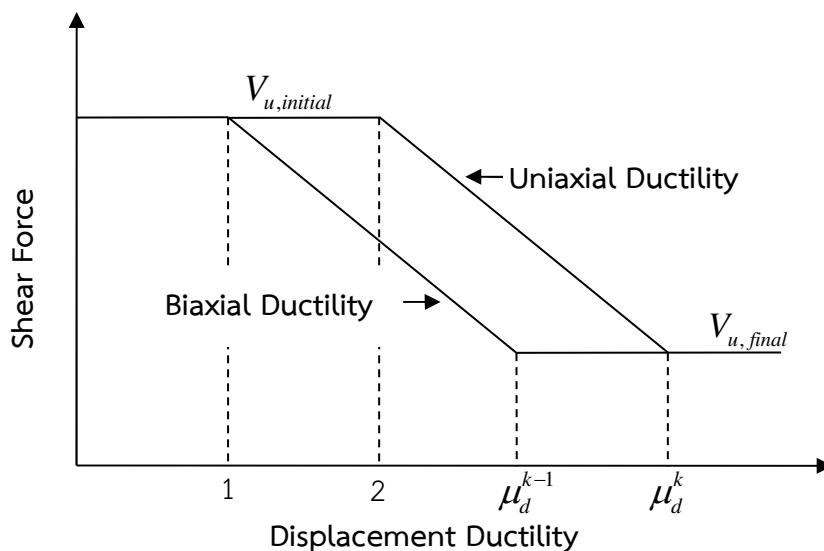


Figure 2-7 Shear force versus displacement ductility of Ang and Wong model

[Ang et al., 1989]

2.3.4 Watanabe and Ichinose (1991)

The shear strength model of Watanabe and Ichinose (1991) is established based on the superposition of arch and truss actions for rectangular column design. The reduced of stress due to the plastic rotation is presented by the concrete compression diagonals in the truss and arch mechanisms. Furthermore, this approach has been applied in the recommendation of Architectural Institute of

Japan. The total initial shear strength is the contributions of the truss mechanism V_s and shear force which is carried by the arch action V_a .

$$V_u = V_s + V_a \quad (2-18)$$

Figure 2-8 (a) shows the Watanabe and Ichinose's assumptions relating to the truss mechanism. The contribution of truss mechanism to shear force is given by

$$V_s = \frac{A_v f_{yv} (jt)}{s} \cot \theta \quad (2-19)$$

where

$$\cot \theta \leq \sqrt{\frac{v_0 f'_c b s - A_v f_{yv}}{A_v f_{yv}}} \leq 2.0 \quad (2-20)$$

$$v_0 = 0.7 - \frac{f'_c}{200} \quad (2-21)$$

Under assumptions compression zone depth of a half the member depth in Figure 2-8 (b), shear force, carried by arch action can be written as:

$$V_a = (v_0 f'_c - f_{ct}) \frac{bh}{2} \tan \psi \quad (2-22)$$

where jt is the distance between upper and lower chords of the analogous truss as shown in Figure 2-8 (a); h is the section height; and f_{ct} is the corresponding diagonal compression stress due to truss action and can be written as:

$$f_{ct} = \frac{A_v f_{yv}}{bs} (1 + \cot^2 \theta) \quad (2-23)$$

It needs to note that the angle ψ is defined in Figure 2-8 (b) and $\cot \theta$ is the minimum of 2.0 [Watanabe and Ichinose, 1991].

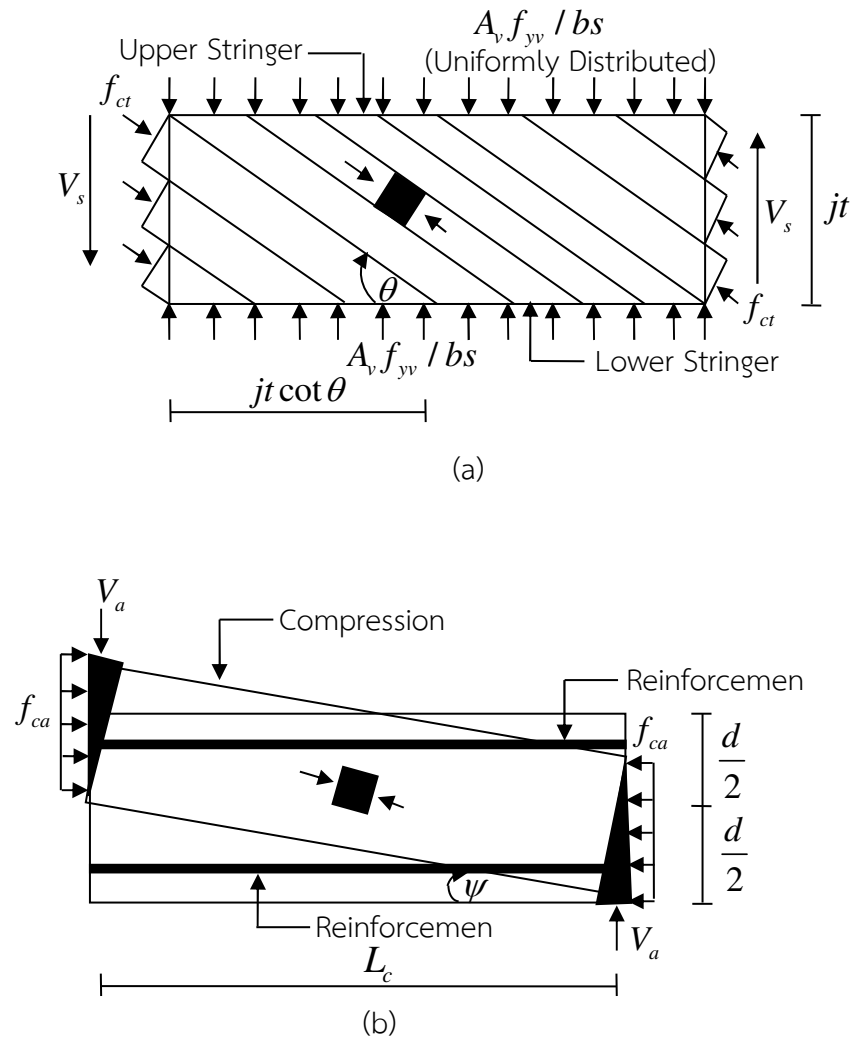


Figure 2-8 Watanabe and Ichinose approach model: (a) truss analogous model and (b) arch mechanism model [Watanabe and Ichinose, 1991]

2.3.5 Priestley et al. (1993)

To develop above shear strength equations, Priestley et al. (1993) modified the shear strength equation by considering the influence of ductility and accounting the axial load component effect. Thus, the shear strength model of Priestley et al. (1993) is able to include the degradation of shear strength due to the influence of increasing curvature ductility demand. The explicit form of the shear strength V_u can be expressed in terms of the summation of contributions from the

concrete mechanism V_c , truss mechanism (Transverse reinforcement) V_s and an arch mechanism associated with axial force V_a as:

$$V_u = V_c + V_s + V_a \quad (2-24)$$

The concrete shear resisting mechanism V_c is defined in Eq. (2-25). It can be observed that the concrete shear strength V_c depends on a parameter k_ϕ associated with the increasing curvature ductility demand μ_ϕ . According to the relation between k_ϕ and μ_ϕ as shown in Figure 2-9, the concrete shear strength V_c becomes lower when the value of curvature ductility demand μ_ϕ exceeds 3 [Mergos and Kappos, 2012].

$$V_c = k_\phi \sqrt{f'_c} (0.80 A_g) \quad (2-25)$$

The shear strength contributed by the transverse reinforcement V_s is derived by the truss mechanism [Park and Paulay, 1975]. For rectangular section, the transverse reinforcement shear resisting mechanism can be written as:

$$V_s = \frac{A_v f_{yv} D'}{s} \cot 30^\circ \quad (2-26)$$

where D' is the distance measured parallel to the applied shear between the centres of transverse reinforcement as shows in Figure 2-10.

The arch mechanism contribution is caused by the inclined strut in beam when considers the axial force of column as shown in Figure 2-11. Figure 2-11 (a) shows the inclination of strut for the specimen with double bending while Figure 2-11 (b) presents the inclination of strut for the specimen with single bending. It is important to note that axial-load component V_a is not degraded with increasing ductility [Priestley et al., 1993] and can calculate from Eq. (2-27).

$$V_a = N \tan \beta = \frac{d-c}{2L_a} N \quad (2-27)$$

where c is the neutral axis depth; L_a is the shear span; and β is the angle between the column axis and the line joining the centres of the flexural compression zones at the top and bottom of the column ends as shown in Figure 2-11 (a) and (b).

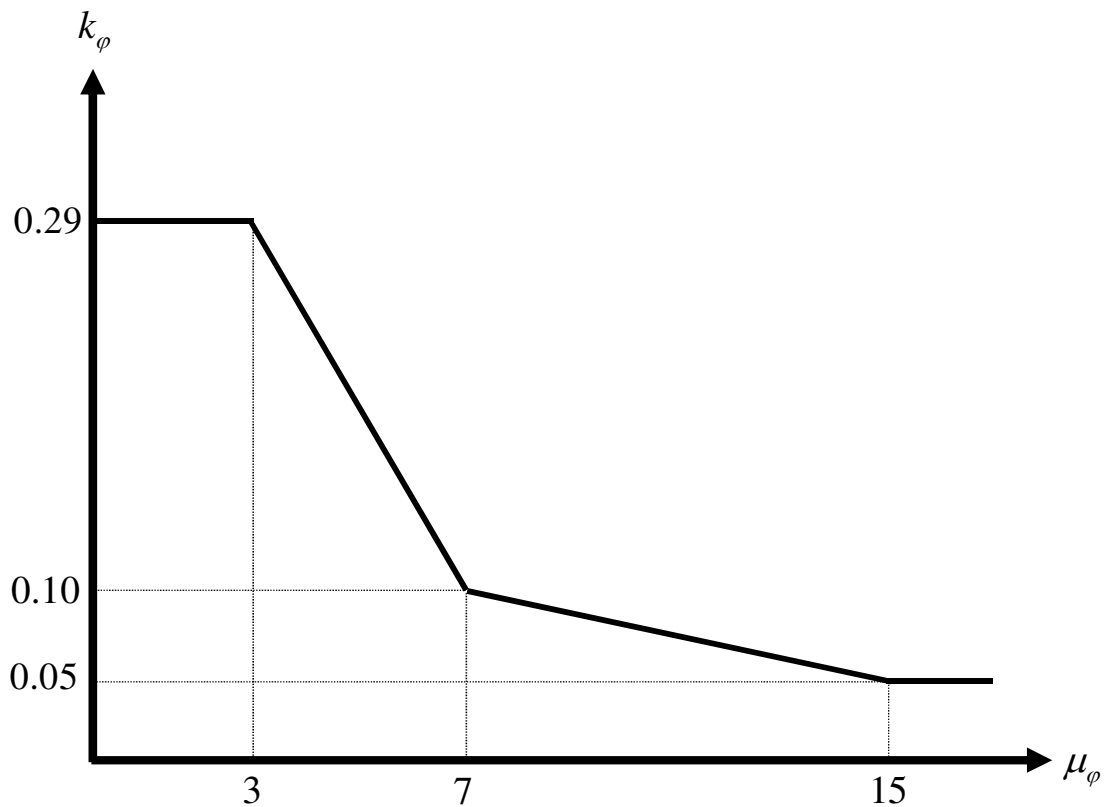


Figure 2-9 Strength of concrete shear resistant versus curvature ductility demand
[Mergos and Kappos, 2012]

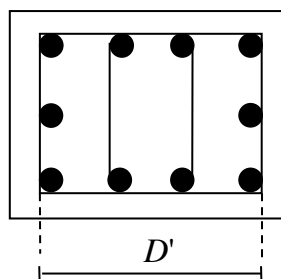


Figure 2-10 Definition of D' for transverse reinforcement contribution [Sezen, 2002]

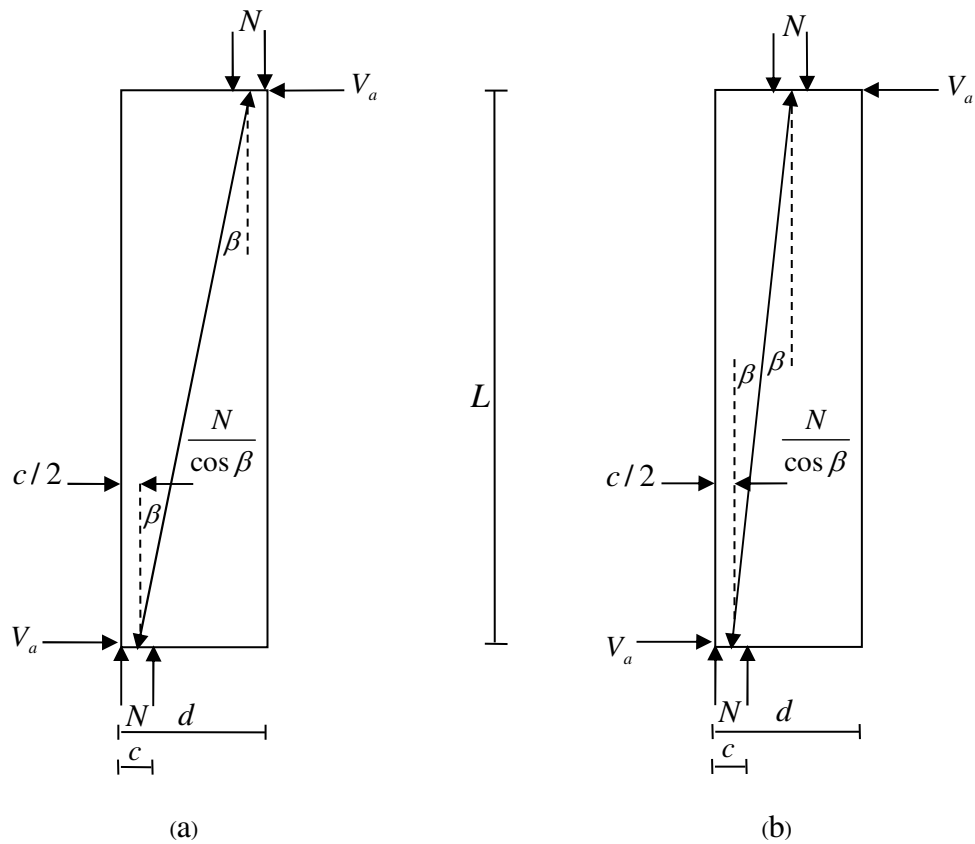


Figure 2-11 Axial load component of shear strength: (a) Double bending and (b) Single bending [Sezen, 2002]

2.3.6 FEMA-273 Seismic Rehabilitation Guidelines (1997)

The shear strength model introduced by FEMA-273 is established based on a review of the available experimental data of the existing column tests under the constant axial load and cyclic lateral displacement. The concrete shear resisting mechanism V_c of the FEMA-273 model can be calculated from Eq. (2-28) while the truss mechanism of shear resisting V_s for FEMA-273 model is similar to the ACI 318-02 code and can calculate from Eq. (2-12).

$$V_c = 0.29 \lambda_{FEMA} \left(k_{FEMA} + \frac{N}{13.8 A_g} \right) \sqrt{f'_c} b d \quad (2-28)$$

where k_{FEMA} is a ductile factor for FEMA-273 model; and λ_{FEMA} is a coefficient of the concrete shear resisting mechanism for FEMA-273 model. NEHRP Guidelines for the Seismic Rehabilitation of Buildings (1997) suggested that k_{FEMA} is equal to 1.0 for low ductility demand and 0.0 for moderate and high ductility demand while λ_{FEMA} is equal to 1.0 for normal weight concrete. The low ductility demand is defined by a demand-to-capacity ratio of 2.0 for the linear analysis or a displacement ductility of less than 2.0.

2.3.7 Sezen and Moehle (2004)

Sezen and Moehle (2004) proposed the maximum shear strength equation with the influence of many factors such as axial load ratio, shear span ratio, and displacement ductility. It can be observed from Eqs. (2-29) and (2-30) that both concrete and transverse reinforcement contributions for shear resisting force are depended on the factor depending on the influence of displacement ductility demand k_d although the shear strength equation is similar approaches in the above equation as shown in Eq. (2-10). The concrete and transverse reinforcement contributions are given as:

$$V_c = k_d \left(\frac{0.5\sqrt{f'_c}}{L_a/d} \sqrt{1 + \frac{N}{0.5\sqrt{f'_c}A_g}} \right) 0.8A_g \quad (2-29)$$

$$V_s = k_d \frac{A_v f_{yv} d}{s} \quad (2-30)$$

In addition to all above shear strength models, the shear strength equations of Priestley et al. (1993) is very attractive and suited to the development of RC frame element including the shear-flexure interaction effects in this study because this model is able to include the degradation of shear strength due to the influence of increasing curvature ductility demand. Therefore, the author uses the Priestley et al. model (1993) to predict the ultimate shear force of the non-ductile RC columns. Furthermore, the author calls the shear strength model proposed by Priestley et al. (1993) as the “UCSD Shear-Strength Model”. This name comes from

the University of California, San Diego (UCSD), where is used to develop this shear strength model.

2.4 Beam Theories

The classical beam theories, which have been widely using in engineering, are Timoshenko and Euler-Bernoulli beam theory. A difference between both beam theories is the deformation hypothesis. The Timoshenko beam theory considers the shear deformation effect as shown in Figure 2-12 while the Euler-Bernoulli beam theory neglects it (See in appendix A). For the RC frame structure analysis, the frame element considers among the axial, flexure, and shear actions under the complex distributed loads. Thus, the Timoshenko beam theory is also more reasonable than the Euler-Bernoulli beam theory in this study.

Timoshenko beam theory has the fundamental hypothesis that “*Plane sections remain plan but lose normality to the longitudinal beam axis due to the shear deformation*” [Limkatanyu, 2008]. From this deformation hypothesis, the displacement fields depend on the sectional displacements as shown in Eq. (2-31) and Eq. (2-32). The variation of strain distributions are shown in Figure 2-13. It needs to note that the variation of the shear strain along the frame cross-section is assumed to be constant, according to the research work of Marini and Spacone (2006) because the effect of variation of the shear strain along the frame cross-section can be replaced with a constant value that more detail will be discussed in the material constitutive laws in Chapter 5.

The displacement fields at any point along beam axis are expressed as:

$$u(x) = u_0(x) - y\theta(x) \quad (2-31)$$

$$v(x) = v_0(x) \quad (2-32)$$

where $u(x)$ and $v(x)$ are the displacements of any point along beam axis in x and y directions, respectively; $u_0(x)$ and $v_0(x)$ are the displacements of beam section along the x and y directions, respectively; y is the distance from the reference axis x ; and $\theta(x)$ is the beam rotation around the z axis.

The axial strain $\varepsilon_{xx}(x)$ and shear strain $\gamma_{xy}(x)$ at any fiber section can be written as [Oñate, 2013]:

$$\varepsilon_{xx}(x) = \frac{du(x)}{dx} = \frac{du_0(x)}{dx} - y \frac{d\theta(x)}{dx} = \varepsilon_0(x) - y\varphi(x) \quad (2-33)$$

$$\gamma_{xy}(x) = \frac{du(x)}{dy} + \frac{dv(x)}{dx} = -\theta(x) + \frac{dv_0(x)}{dx} = \gamma(x) \quad (2-34)$$

where $\varepsilon_0(x)$ is the sectional axial strain at reference axis; $\varphi(x)$ is the sectional bending curvature; and $\gamma(x)$ is the sectional shear strain.

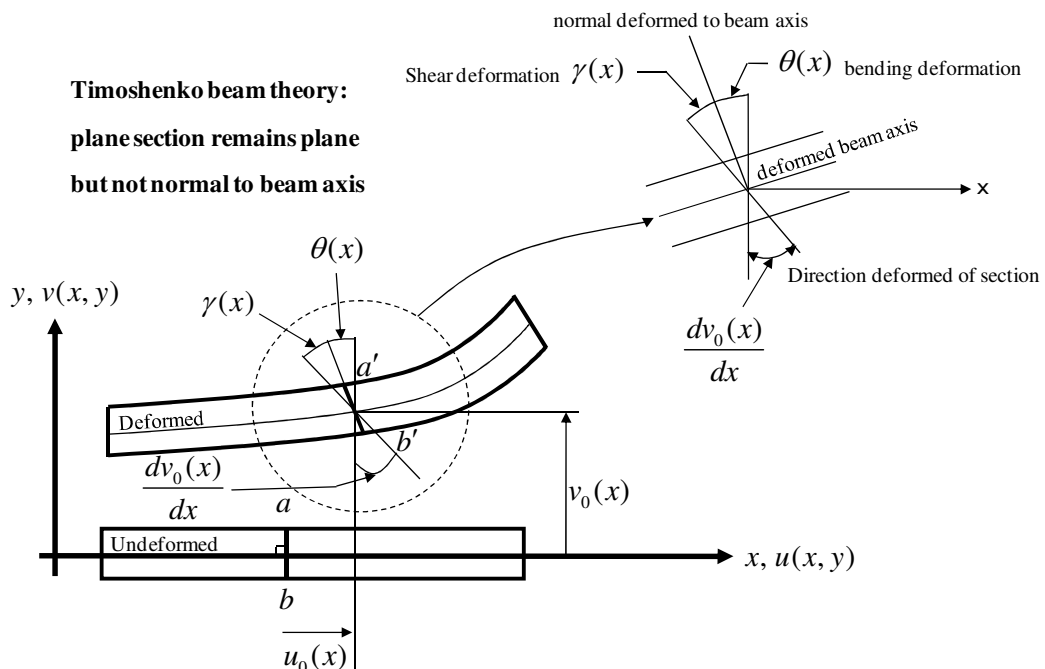


Figure 2-12 Kinematics description of the Timoshenko beam element before deformation and after deformation [Limkatanyu, 2008]

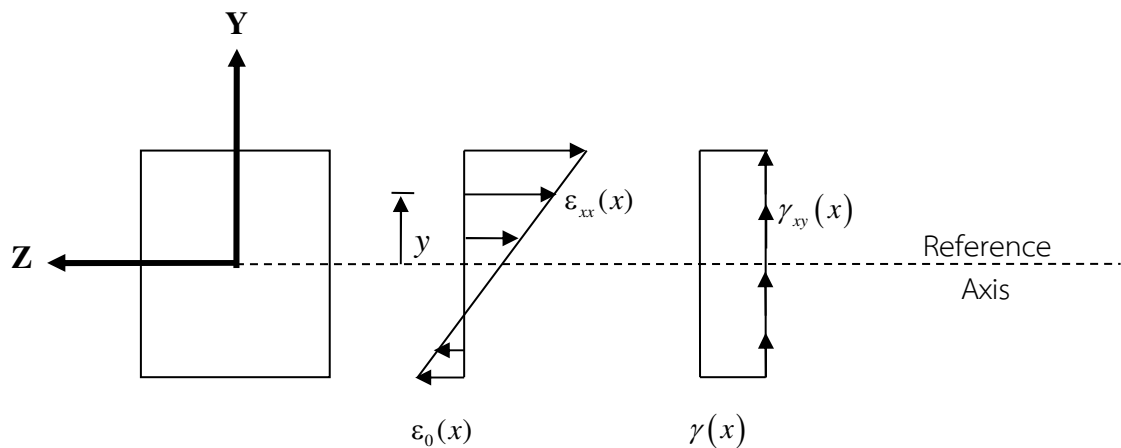


Figure 2-13 Strain distributions of Timoshenko element [Marini and Spacone, 2006]

2.5 General Finite Element Formulation of Reinforced Concrete Frame Element Including Shear Responses and Shear-Flexure Interaction Effects

Nowadays, several research works for the reinforced concrete structure analysis (e.g. Giberson, 1967; Chan, 1982; Cervenka, 1985; Vecchio and Collins, 1986; Bazant and Prat, 1988; Hsu, 1988; Mander et al., 1988; Issa, 1989; Saatcioglu and Ozcebe, 1989; Moehle and Mahin, 1991; Garstka et al., 1993; Spacone et al., 1996; Ranzo and Petrangeli, 1998; Ricles et al., 1998; Petrangeli et al., 1999; Pincheira et al., 1999; Palermo and Vecchio, 2003; Bairan, 2005; Kotronis et al., 2005; Recuperero et al., 2005; Marini and Spacone, 2006; Ceresa et al., 2007; Mullapudi and Ayoub, 2013; Feng et al., 2016; Feng and Xu, 2018a; Feng et al. 2018b) have been proposed. Among those numerical models, the fiber-section model is the most favorite one for the seismic analysis of RC structures under cyclic load. This approach has been developed in the past forty years [Chan, 1982; Scordelis, 1984; Zeris and Mahin, 1991; Spacone et al., 1996; Limkatanyu, 2002; Barbato, 2009; Ceresa et al., 2009; Ning et al., 2013; Li et al., 2016; Panto et al., 2017]. The fiber model is based on the discretization of the cross-section into the layers (in the 2D model) or fibers (in the 3D model). The axial-flexure relation is coupled in the section level as well as

the interaction between concrete and reinforcing steel in the section. According to the original fiber-section model, the shear deformation is neglected due to the element based on the Euler-Bernoulli beam theory resulting in the failed prediction of the dissipated hysteretic energy and the initial/unloading stiffness in the short columns, coupling beams, and beam-column connections etc. [Feng and Xu, 2018a]. Later, the fiber-section model is modified by taking into of the shear deformation following the Timoshenko beam theory. There are many assumptions on the shear strain variation along the fiber-section depth. For example, some research group (e.g. Ranzo and Petrangeli, 1998; Marini and Spacone, 2006; Ceresa et al. 2009; Ning et al., 2013; Feng and Xu, 2018a) assumed shear strain uniformly distributed along the cross-section while some research group (e.g. Vecchio and Collins, 1988; Petrangeli et al., 1999; Kagermanov and Ceresa, 2017) assumed shear strain vary following the shear strain profile. In this research, the shear strain distribution is based on the uniform distribution along the cross-section because this approach is simple and gives similar performance when comparing with the variation of shear strain profile approach.

The benefits of the fiber-section model are mentioned in the several research works (e.g. Spacone et al., 1996; Spacone and Limkatanyu, 2000; Limkatanyu, 2002; Li et al., 2016; Feng and Xu, 2018a) that fiber-section approach can present the accuracy responses, consider with the uni-axial material models, and shows smaller computational cost comparing with 2D and 3D material models. Thus, this study uses this approach to apply with the RC column analysis.

In addition to the state-of-the-art review on the frame element models with accounting the shear responses and considering the shear-flexure interaction effects, this study focuses on the review of a series of fiber frame element models based on Timoshenko beam theory as well as the discussion in the research works of Ceresa et al. (2007) and Ceresa et al. (2008). Based on the different modeling strategies for accounting the shear responses, this study categorizes those models into the two general groups. The first group represents a series of models using the concept of truss analogy with uniaxial material constitutive models [e.g. Guedes et al., 1994; Martinelli, 1988; Ranzo and Petrangeli, 1998; Marini and Spacone,

2006; Mergos and Kappos, 2008 and 2012] while the second group presents the models based on the 2D or 3D suitable constitutive models [e.g. Vecchio and Collins, 1988; Petrangeli et al., 1999; Bentz, 2000; Kotronis, 2000; Remino, 2004; Bairan, 2005; Saritas, 2006; Kagermanov and Ceresa, 2017]. Both groups can be summarized and expressed as follow:

2.5.1 Models based on the concept of truss analogy with uniaxial material constitutive models

In the approach of the first group, the shear responses are introduced with an equivalent truss model. As the result, the relation between shear and axial stresses is only partial interacted. The material constitutive models of this group are based on uniaxial behavior for concrete and reinforcing steel. Some modeling approaches in this group are summarized and expressed as:

2.5.1.1 Guedes's Modelling Approach

The formulation of Guedes's model [Guedes et al., 1994; Guedes and Pinto 1997] is derived through principal stress analysis under displacement-based method and the shear responses can determine from a strut-and-tie model (Figure 2-14). The force system is composed of two diagonal concrete struts and steel ties in longitudinal and transversal directions. These systems are enforced following the compatibility and equilibrium conditions as shown in Figure 2-15. Moreover, the interaction between the fiber and truss model are presented by the average axial strain ε_i which can calculate from Eq. (2-35).

$$\varepsilon_i = \frac{\Delta_i}{l / (\cos \phi)} = \varepsilon_{oe} (\cos \phi)^2 + \varepsilon_{wy} (\sin \phi)^2 \pm \frac{\tan \gamma}{2} (\sin 2\phi) \quad (i=1,2) \quad (2-35)$$

where $\varepsilon_{oe} = l_{oe} / l$ and γ are derived from Timoshenko beam kinematics and the strain of stirrups $\varepsilon_{wy} = \Delta_{wy} / h$ is computed form cross-section equilibrium by iterative method.

The concrete strut forces F_{ci} and the transversal steel tie forces F_{wy} are described in the equilibrium equation terms and given by

$$F_{ci} = f_c(\varepsilon_i)A_{strut} = \sigma_c(\varepsilon_i)(1 - D_i)bh \cot \phi \quad (i=1,2) \quad (2-36)$$

$$F_{wy} = f_{sw}(\varepsilon_{wy}) \frac{h / \tan \phi}{s} (2A_w) \quad (2-37)$$

where $A_{strut} = bh$ is the truss area; $D_i = \varepsilon_{i,max} / \varepsilon_{ult}$ is a damage parameter; and ε_{ult} is the ultimate strain of the concrete. The more details are fully discussed in the research works of Guedes and Pinto (1997).

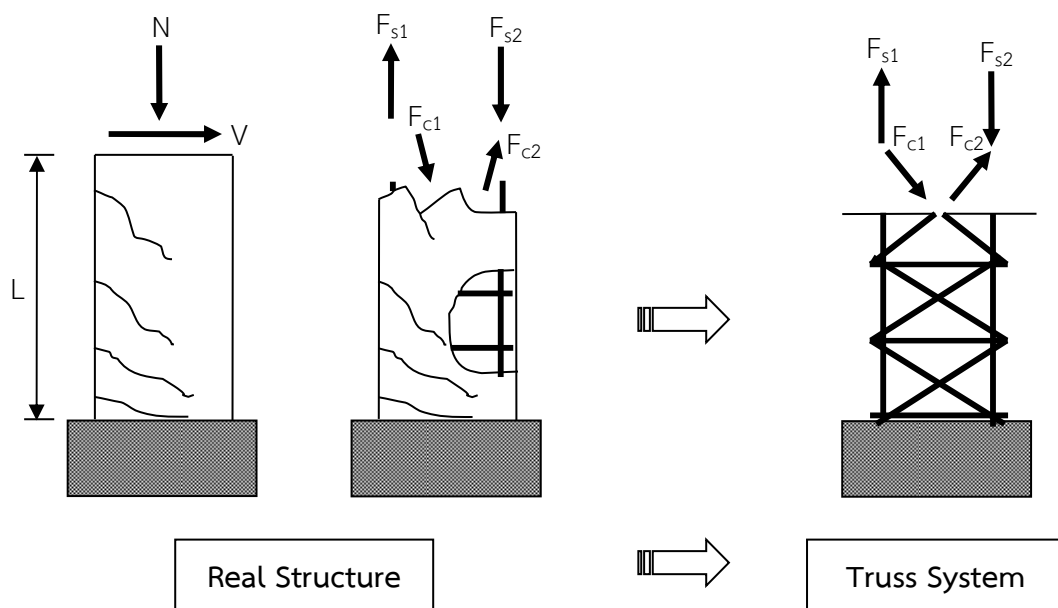


Figure 2-14 Truss analogy of Guedes and Pinto model [Guedes and Pinto, 1997]

Although this method can account shear components into the formulation, this model cannot present the physical basis of responses (Not fully coupling between shear and flexural responses), the crack-closing phenomenon of reinforced concrete under loading, and the pinching effect.

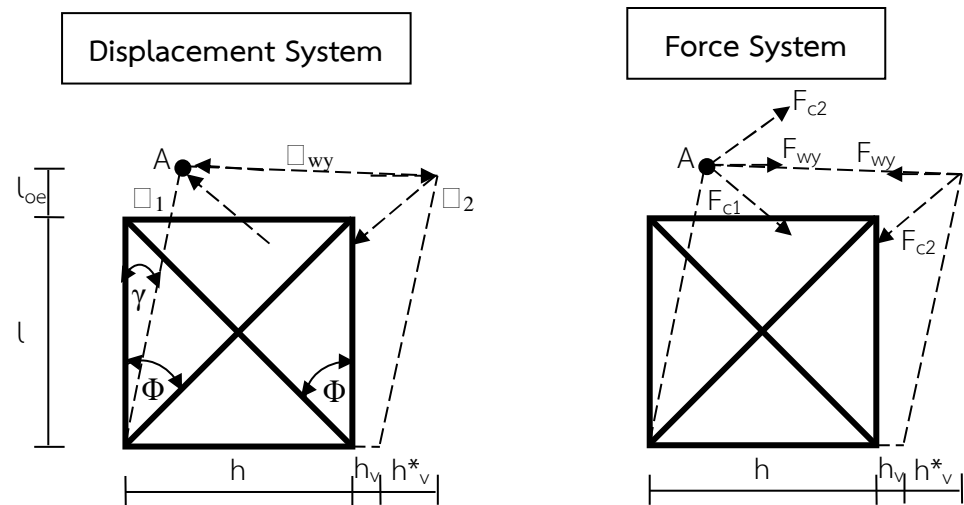


Figure 2-15 Compatibility and Equilibrium of structure system

[Guedes and Pinto, 1997]

2.5.1.2 Martinelli's Modelling Approach

Martinelli (1998) proposed the displacement-based fiber column element based on the Garstka et al. model [Garstka et al., 1993]. In this model, the axial and flexure are coupled through a 3D multifiber model based on the uniaxial constitutive relationship for the material models. The truss model is established from transverse reinforcement and the concrete properties in the tensile and compressive zones. The resisting shear force is derived from the different resisting mechanisms, such as the truss mechanism, arch action, aggregate interlock, and the compression concrete over the neutral axis. The arch action mechanism is similar the concept of Watanabe and Ichinose (1991) and Priestley et al. (1993) as above discussed while truss mechanism is derived from the x-y plane structure as shown in Figure 2-16. The truss deformation determines from the shear deformation based on the Timoshenko kinematic assumptions. Then, the Mohr's circle is applied to determine the principal stress and strain by enforcing the equilibrium in y-direction ($\sigma_{yy} = 0$). It can observe that the shear contribution depends on ε_{xx} that governs on the flexural response of the element. In other words, the shear responses are coupled with the flexural responses through the strut mechanism even if it does not exist in the stiffness matrix terms.

However, although the Martinelli's approach is able to capture the different shear resisting mechanics, such as truss mechanism, arch action, aggregate interlock, and the compression concrete, this approach cannot full couple the axial, flexure and shear forces in the element. Moreover, the numerical model as derived from this approach lacks the detection of specimen collapse [Ceresa et al., 2008].

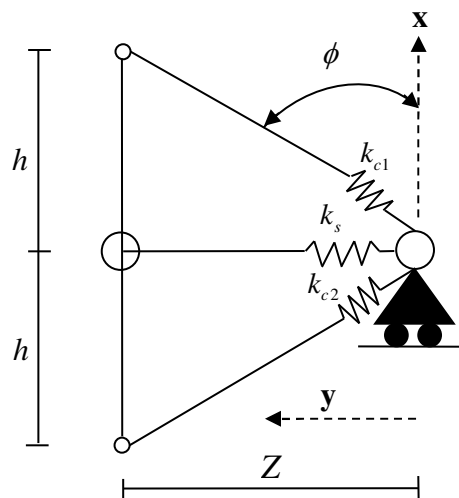


Figure 2-16 Planer structural assemblage for truss mechanism [Martinelli, 1998]

2.5.1.3 Ranzo and Petrangeli's Modelling Approach

Ranzo and Petrangeli (1998) presented a 2-node force-based beam element for seismic analysis of RC structures. The uniaxial constitutive laws for concrete and steel are employed in their work. Based on the fiber model and Timoshenko kinematic assumption, the axial and flexure responses are coupled at the section level while the shear responses uncouple with axial and flexure responses directly as well as the previous approaches. The interaction between flexure and shear is different from the previous approaches that the coupling between flexure and shear is presented by a damage of shear force-shear strain curve $V - \gamma$ by using the shear strength prediction introduced by Priestly et al. (1994). The shear constitutive relationship depends on the sectional shear strain γ and the discrete variable ϵ_{\max} (Maximum value of tensile axial deformation during each cycle) as shown in Figure 2-17.

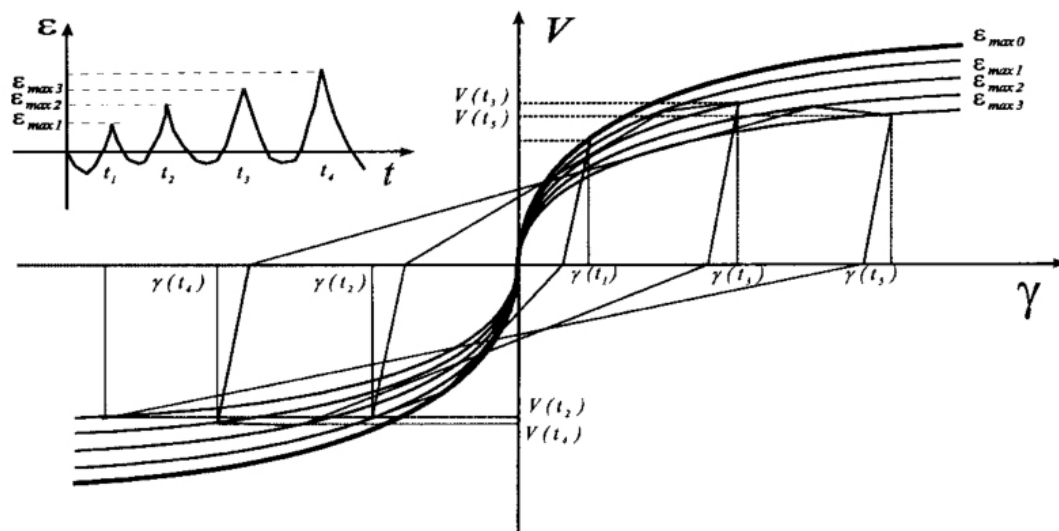


Figure 2-17 Hysteretic shear force-shear strain response of Ranzo and Petrangeli model [Ranzo and Petrangeli, 1998]

From the Ranzo and Petrangeli's approach, the modeling strategy is similar to the previous models based on strut-and-tie analogies that the shear responses interact with the flexural one but without full coupling among axial, flexure, and shear forces directly. Moreover, the shear constitutive relationship of Ranzo and Petrangeli's approach is limited for the employment in the general applications because the primary curve of the shear hysteretic model is required to calibrate for each analysis case [Ceresa et al., 2007].

2.5.1.4 Marini and Spacone's Modelling Approach

Marini and Spacone (2006) proposed a force-based two-dimensional (2D) element based on the Timoshenko beam theory for analysis of reinforced concrete. In this approach, the interaction between axial and flexural responses is represented through the fiber section model based on Timoshenko beam theory while the shear response is independent of the axial and flexural responses. However, the equilibrium equations must be satisfied point-wise along the element based on the force-based formulation so the interaction among axial-flexural and shear responses are enforced at the element level. The material models for concrete and reinforcing steel are based on the uniaxial relationship proposed by Filippou et al. (1983a).

The shear responses are modeled by the hysteretic law and the shear resisting force and tangent shear stiffness can determine in this law. The possible primary curves are defined as a function of the shear capacity V_{Rd} , suggested by Eurocode 2 (1991) and contributed of the force of steel stirrups V_{Rds} , the force of the concrete member under zero axial load V_{Rdc}^* , and the contribution of the concrete member capacity enhancement $V(N)$ that is induced by the axial compression N as shown in Figure 2-18 (a). Under cyclic loading, the shear response must follow by the hysteretic rule in Figure 2-18 (b).

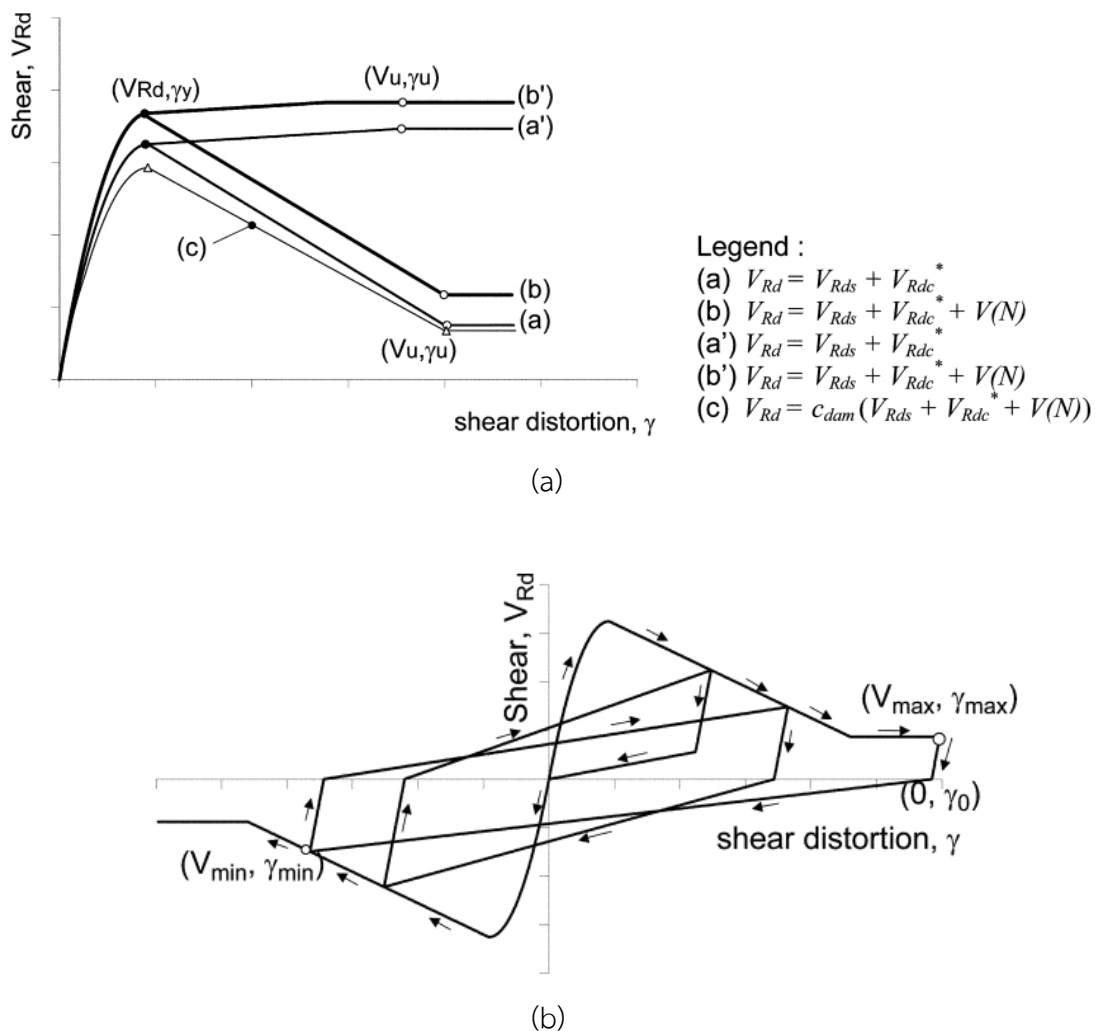


Figure 2-18 Section shear law of Marini and Spacone: (a) possible primary curves and (b) hysteretic of shear law [Marini and Spacone, 2006]

From the analysis results of Marini and Spacone model (2006), the shear capacity V_{Rd} model suggested by Eurocode 2 (1991) underestimates for the shear strength prediction because this model does not account for the aspect ratio. For this reason, the model needs improvement of shear strength capacity prediction that accounts for the aspect ratio and shear span ratio [Ceresa et al. 2008].

2.5.1.5 Mergos and Kappos's Modelling Approach

Mergos and Kappos (2008 and 2012) proposed the beam-column element with the gradual spread inelastic sub-elements based on the concept of Soleimani (1978), which represented the flexural and shear responses at the end of a member. The bond slip effect was presented through the fixed-end rotational spring as shown in Figure 2-19. Moreover, Mergos and Kappos (2008 and 2012) proposed the shear hysteretic model of reinforced concrete. Shear hysteresis was adapted and improved from the proposals by Ozcebe and Saatcioglu (1989). The hysteretic model was verified with experimental results.

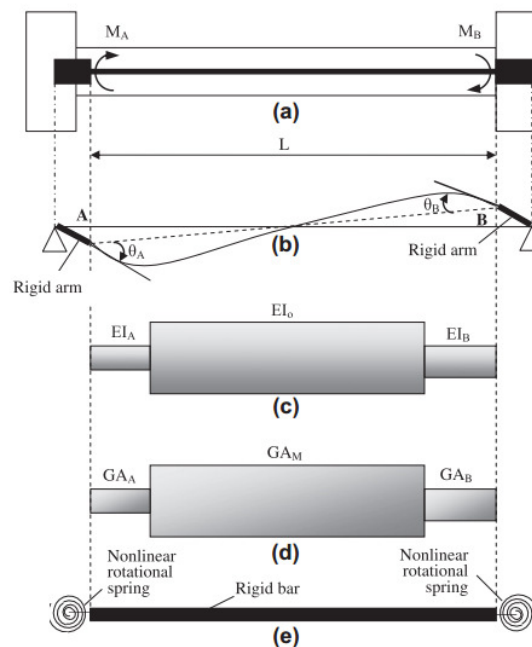


Figure 2-19 Mergos and Kappos element model [Mergos and Kappos, 2012]

The relation between shear force and shear strain starts from the primary curve without shear-flexural interaction as shown in Figure 2-20. The curve

consists of four branches but has only three different slopes. The first branches present the uncracked concrete interval. The second and third branches illustrate the pre-flexural yielding and post-flexural yielding, respectively, while the last branches present the post-transverse yielding.

The concept of the interaction between shear and flexural responses of Mergos and Kappos's approach (2008 and 2012) is rather similar to the Ranzo and Petrangeli's approach (1998) as above discussed. The coupling between shear and flexure occurs after the plastic hinge rotation has formed (After the second branches in Figure 2-20). The influence of the inelastic flexure deformation leads to the degradation of the shear strength in the concrete contribution ΔV_c^{deg} that can estimate from the shear strength models (e.g. Priestley et al.'s model, 1993; and Sezen and Moehle's model, 2004)

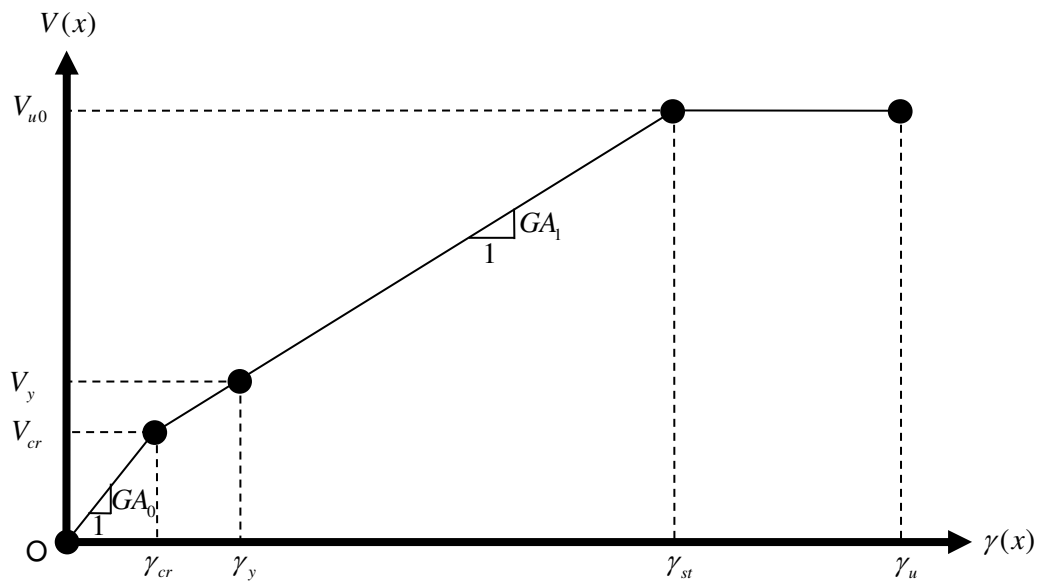


Figure 2-20 The initial shear force-shear strain primary curve without shear-flexural interaction [Mergos and Kappos, 2012]

The procedure for the sectional shear stiffness approximation after plastic hinge rotation forming GA_{eff} is proposed by Mergos and Kappos (2012). This procedure includes the shear-flexural interaction effects and can estimate from the

relationship between incremental shear force ΔV and shear strain $\Delta\gamma$ as shown in Figure 2-21 and Eq. (2-38).

$$\Delta\gamma = \frac{\Delta V}{GA_{eff}} = \frac{\Delta V + \Delta V_c^{deg}}{GA_1} \quad (2-38)$$

where GA_1 is the cracked shear stiffness. The sectional shear stiffness after plastic hinge rotation forming can calculate by solving the Eq. (2-38). The following equation is obtained.

$$GA_{eff} = \frac{\Delta V}{\Delta V + \Delta V_c^{deg}} GA_1 \quad (2-39)$$

However, although the idea for the coupling between shear and flexural responses of Mergos and Kappos's approach (2008 and 2012) is attractive for the development of RC element with considering the shear-flexure interaction effects, this models require the formation of an ad-hoc curve of moment-curvature law that doesn't naturally take into account the axial-flexural interaction. Moreover, the procedure for the sectional shear stiffness approximation of Mergos and Kappos (2012) is derived based on the constant stiffness as shown in Eq. (2-39) that doesn't cover all the possible events of the shear strength degradation. The clear detail will discuss in Chapter 5.

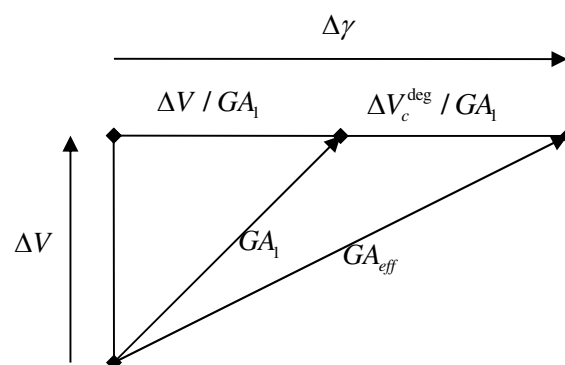


Figure 2-21 Definition of GA_{eff} [Mergos and Kappos, 2012]

2.5.2 Models based on the 2D or 3D suitable constitutive model

The second group for accounting the shear responses and coupling interaction between axial force, shear force, and bending moment is the modeling strategies to attempt capture the mechanics of reinforced concrete members by using a family of the 2D and 3D suitable constitutive models, such as Microplane model [Bazant and Prat, 1988; Brocca and Bazant, 2001; Park and Kim, 2003; Ismail et al., 2016], smeared crack model [Vecchio and Collins, 1986; Bentz, 2000; Remino, 2004; Bairan, 2006a and 2006b; Ceresa et al., 2009; Stramandinoli and Rovere, 2012; Biscaia et al., 2013; Mullapudi and Ayoub, 2013; Li et al., 2016], and damage models [Ju, 1989; Faria et al., 1998; Lee and Fenves, 1998; Kotronis, 2000; Kotronis et al. 2005; Saritas, 2006; Wu et al., 2006; Long et al., 2014; Wu 2017 and 2018]. Some modeling strategies to account interaction between axial, flexure, and shear in this group are summarized and expressed as:

2.5.2.1 Petrangeli's Modelling Approach

Petrangeli et al. (1996 and 1999) proposed the 2D fiber beam element based on flexibility-based formulation for RC beam and column analysis. A biaxial constitutive law is employed to represent the behavior of concrete based on the Microplane approach (Ozbolt and Bazant, 1992) while the stress-strain relation of reinforcing steel is described by Menegotto and Pinto model (1977). The variation of sectional stresses along the cross-section in the research works of Petrangeli et al. (1996 and 1999) is shown in Figure 2-22. The shear strain variation is assumed with the constant value or a parabolic distribution. The interaction among axial, flexure, and shear are presented through the concrete model directly at each fiber as shown in Eq. (2-40).

$$\begin{Bmatrix} d\sigma_{xx}^m \\ d\sigma_{xy}^m \end{Bmatrix} = \begin{bmatrix} K_a^m & K_{as}^m \\ K_{sa}^m & K_s^m \end{bmatrix} \begin{Bmatrix} d\varepsilon_{xx}^m \\ d\varepsilon_{xy}^m \end{Bmatrix} \quad (2-40)$$

where K_a^m and K_s^m are the axial and shear stiffness coefficients of the m -th fiber respectively, K_{as}^m and K_{sa}^m are the coupling axial-shear components. All the value of

K_a^m , K_s^m , K_{as}^m , and K_{sa}^m can determine from the coefficients of the material matrix of the m -th fiber D_{ab}^m and transversal reinforcement ratio ρ^m as shown in Eq. (2-41).

$$\begin{aligned} K_a^m &= (D_{11}^m - D_{12}^m D_{21}^m \rho^m), & K_s^m &= (D_{33}^m - D_{23}^m D_{32}^m \rho^m) \\ K_{as}^m &= (D_{13}^m - D_{12}^m D_{23}^m \rho^m), & K_{sa}^m &= (D_{31}^m - D_{32}^m D_{21}^m \rho^m) \end{aligned} \quad (2-41)$$

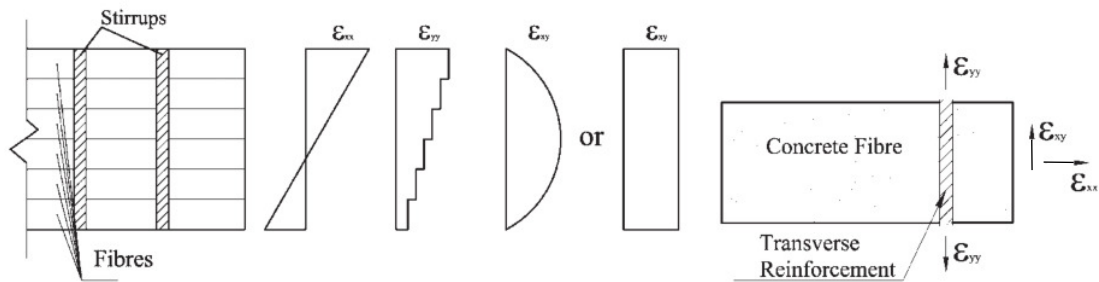


Figure 2-22 Fiber section mechanics [Petrangeli et al., 1999]

Although the model of Petrangeli et al. (1999) is able to capture well the behavior of RC members due to the use of a biaxial constitutive law for concrete model, the considering and accounting of the different mechanisms (e.g. the contribution of shear resistance forces) in this model are slightly more difficult as noted by Ceresa et al. 2008. As the result, the underestimation of the shear capacity may occur at the significant portion, especially the plastic-hinge portion, when the shear responses are considered.

2.5.2.2 Vecchio and Collins's Modelling Approach

Vecchio and Collins (1988) proposed the method for the estimation of RC beam under shear action and shear deformation. This method is the so-called as "Dual-section" approach. Under this method, the shear stress $\tau_{xy}(x)$ can determine from the normal stress value on each side of a finite-length layer through the finite difference method as shown in Figure 2-23 and Eq. (2-42).

$$\tau_{xy}(x) = -\frac{1}{b(y)} \int_{-y}^y \frac{\partial \sigma_{xx}}{\partial x} b(y) dy \quad (2-42)$$

where b is the section width; y is the distance from the bottom layer; and $\frac{\partial \sigma_{xx}}{\partial x}$ is the difference of the normal stress value and can approximate from Eq. (2-43).

$$\frac{\partial \sigma_{xx}}{\partial x} \approx \frac{\sigma_{xx}(x_2) - \sigma_{xx}(x_1)}{S} \quad (2-43)$$

where $\sigma_{xx}(x_1)$ and $\sigma_{xx}(x_2)$ are the normal stresses at both side of analysed fiber section; and S is the distance that can estimate about 1/6 of the section depth.

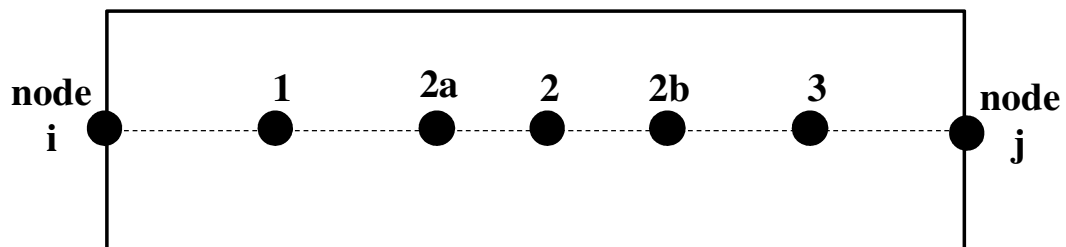


Figure 2-23 Dual-section approach of Vecchio and Collins [Vecchio and Collins, 1988]

The Modified Compression Field Theory (MCFT) is applied in the constitutive laws of the research work of Vecchio and Collins (1988). The MCFT method, was developed from the Disturbed Stress Field model (DSFM) at the University of Toronto, describes the behavior of the cracked reinforced concrete. The interaction between the concrete and steel are represented through the principal stress analysis at the section level as shown in Figure 2-24. The constitutive law of the cracked concrete is proved by the experimental data and represented in terms of the average stresses and strains (Principal axis 1, 2). This first MCFT method was used to analyze only the monotonic loading proposed by Vecchio and Collins (1986). Later, this method was adopted in the cyclic loading by Vecchio (1999) and Palermo and Vecchio (2002).

According to the dual-section approach, this method may lead to the unstable responses because this method requires the information from the two section sides to evaluate the shear strain value as shown in Eq. (2-42). Moreover, the

discontinuities of shear strain profile could be happened in the different depth of the cracking of the two analyzed cross-section because of the different moments.

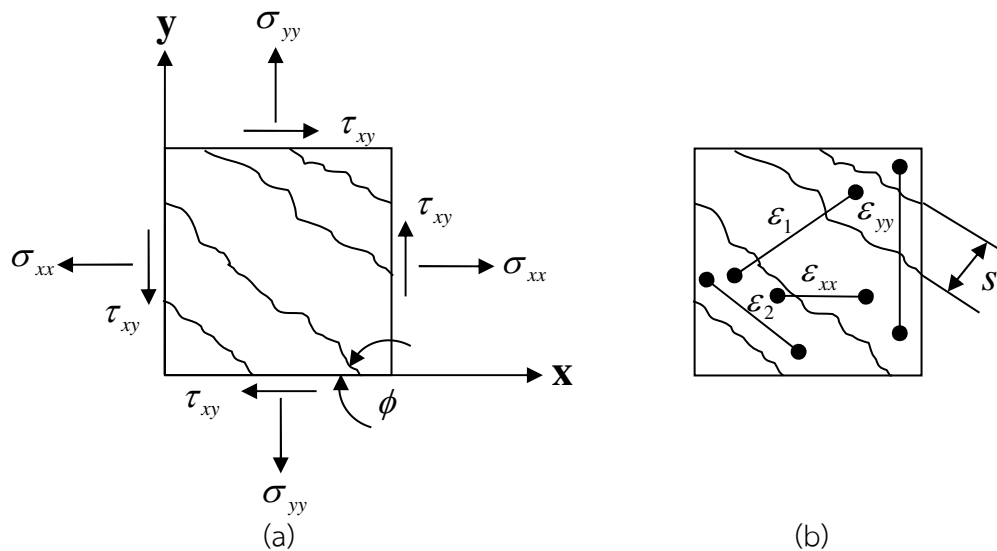


Figure 2-24 The Modified Compression Field Theory of smeared cracks: (a) stress and (b) strain [Vecchio and Collins, 1988]

2.5.2.3 Bentz's Modelling Approach

To overcome the limitations of the dual-section approach of Vecchio and Collins (1988) as described above, Bentz (2000) presented the so-called as “*Longitudinal Stiffness Method*”. This method can overcome the inaccuracy and numerical instabilities in the dual-section approach. The gradient of the normal stress in this method is determined from the derivative of stress with respect to the axis of the element based on the chain rule. The fundamental assumption of the Bentz's model follows the classical beam theory that the plane sections remain plane but the variation of the shear stress across the section is governed by the flexural stress. An initial shear strain profile is assumed as a function of the mean sectional shear deformation and the iteration is employed until the assumed and calculated shear strain profile are matchable within an acceptable tolerance. The MCFT is used to couple the interaction of axial force, shear force, and bending moment in the constitutive model each fiber layer.

Although the Bentz's approach is interesting in that each inter-fiber equilibrium is satisfied and the model can capture the forces and deformations of the RC element subjected to axial, shear, and bending loads, the local effects exist along the element. For example, the concrete and reinforcing steel forces must be in equilibrium at each integration point along the length of the element but both forces in some distance from the support and the load positions are not in equilibrium as noted by Ceresa et al. (2008).

2.5.2.4 Remino's Modelling Approach

Remino (2004) proposed the 2D force-based beam-column element based on Timoshenko beam theory following the research work of Spacone et al. (1996). The fiber-section model is used to discretize the RC cross-section as shown in Figure 2-25. The section stiffness matrix is calculated based on the finite difference formula. The Rose-Shing model [Rose, 2001] is used to represent the fiber constitutive laws. The Rose-Shing model is adapted from the framework of the Modified Compression Field Theory (MCFT) but it differs in terms of material constitutive laws, the kinematic of crack, and the relation of aggregate-interlock.

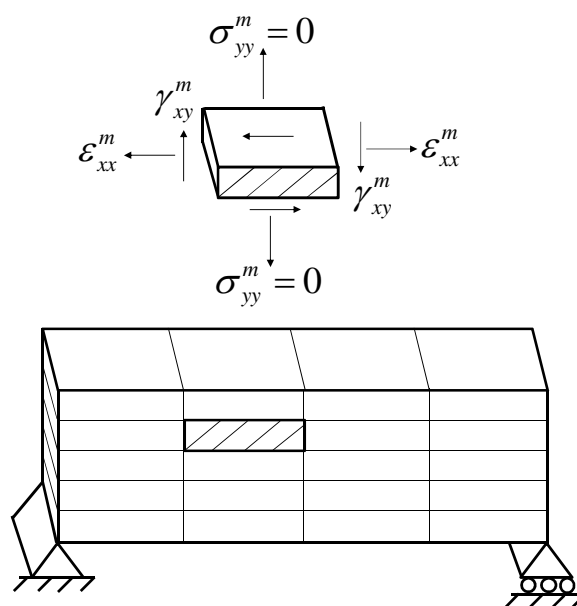


Figure 2-25 The fiber stress and strain conditions of Rose-Shing model

[Remino, 2004]

Although Remino's model (2004) is able to account for the interaction of axial force, shear force, and bending moment in the element formulation through a smeared crack approach as similar the Vecchio and Collins's approach, the numerical responses of this model are not always satisfactory, especially in the cyclic analysis, when compared with the experimental data. Moreover, the strain localization effects exist in this method observed from a parametric study as noted by Ceresa et al. (2008).

2.5.2.5 Bairan's Modelling Approach

Bairan (2006a and 2006b) proposed a 3D nonlinear fiber sectional model for the reinforced concrete analysis under axial, shear, bending, and torsion forces. This model is capable of simulating the total interaction among axial, shear, bending, and torsion forces. The equilibrium along entirely element at the structural and sectional levels are still maintained by the superposition of the plane section displacement field based on Euler Bernoulli beam theory $u_{ps}(x)$ and the imposing distortion-warping displacement field $u_w(x)$ as shown in Figure 2-26. Thus, the displacement field $u(x)$ can be written as

$$u(x) = u_{ps}(x) + u_w(x) \quad (2-44)$$

The rotating smeared-crack approach is employed to couple the axial, shear, bending, and torsion forces through constitutive relation for concrete. In the research works of Bairan (2006a and 2006b), the concrete model in compression is based on the concrete model introduced by Vecchio and Selby (1991) while the concrete model in tension follows the research work of Cervenka (1985). For the reinforcing steel model, the elastoplastic uniaxial stress-strain is employed for simulating the behavior of reinforcing steel.

Although Bairan's model (2006a and 2006b) success to couple the total interaction among axial, shear, bending, and torsion forces with arbitrarily shaped cross-section, this model still requires the improved approximation of the

distortion displacement field, its variation along the element, and material behavior at section level to develop this model as discussed by Ceresa et al. (2008).

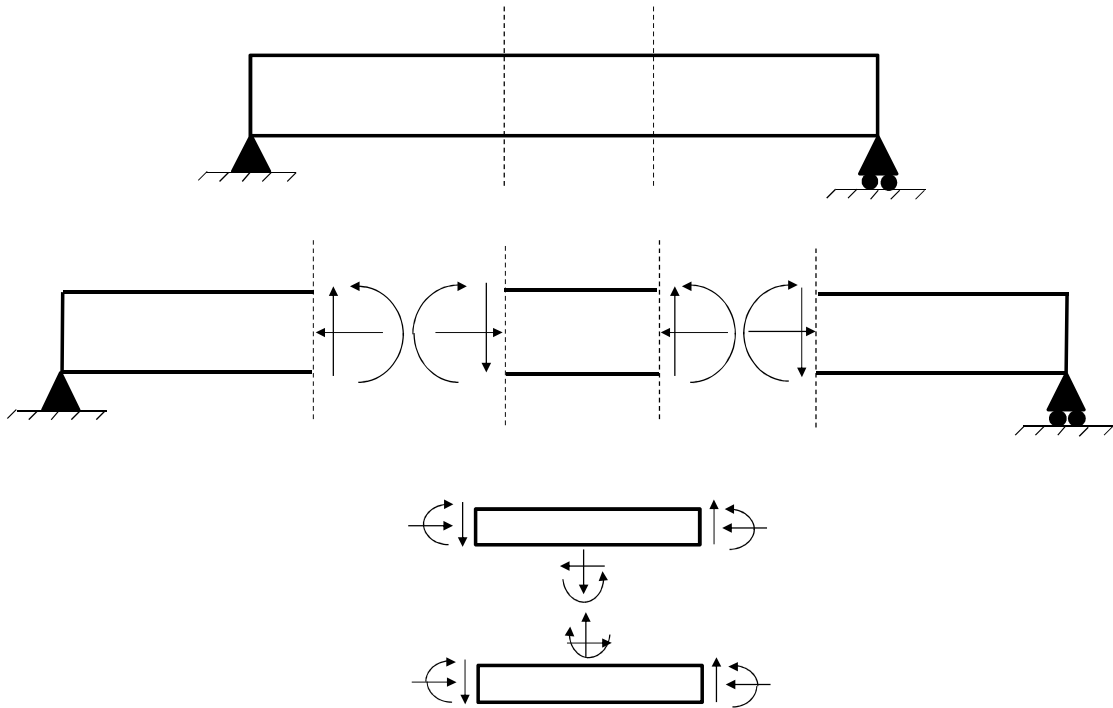


Figure 2-26 The equilibrium conditions of Bairen's model [Bairan, 2005]

2.5.2.6 Kagermanov and Ceresa's Modelling Approach

Kagermanov and Cereasa (2017) proposed the force-based frame element model for nonlinear analysis of shear-critical reinforced concrete frames. This model consolidates a procedure for the computation of an exact shear strain profile and corresponding shear stress distribution over cross-section (Satisfy the internal fiber equilibrium conditions in Figure 2-27 (a)) at the section level. The interaction between axial and shear response in this model is presented at the fiber level that based on a smeared-crack orthotropic constitutive model, presented in Kagermanov and Cereasa (2016).

Moreover, this model approximates the shear strain γ_{xy} at the section level by linear shape functions as shown in figure 2-27 (b). To receive the convergence responses under force-based formulation, the iterative state

determination procedure is invoked at the element level to find the corresponding section strains at each integration point that proposed by Spacone et al. (1996).

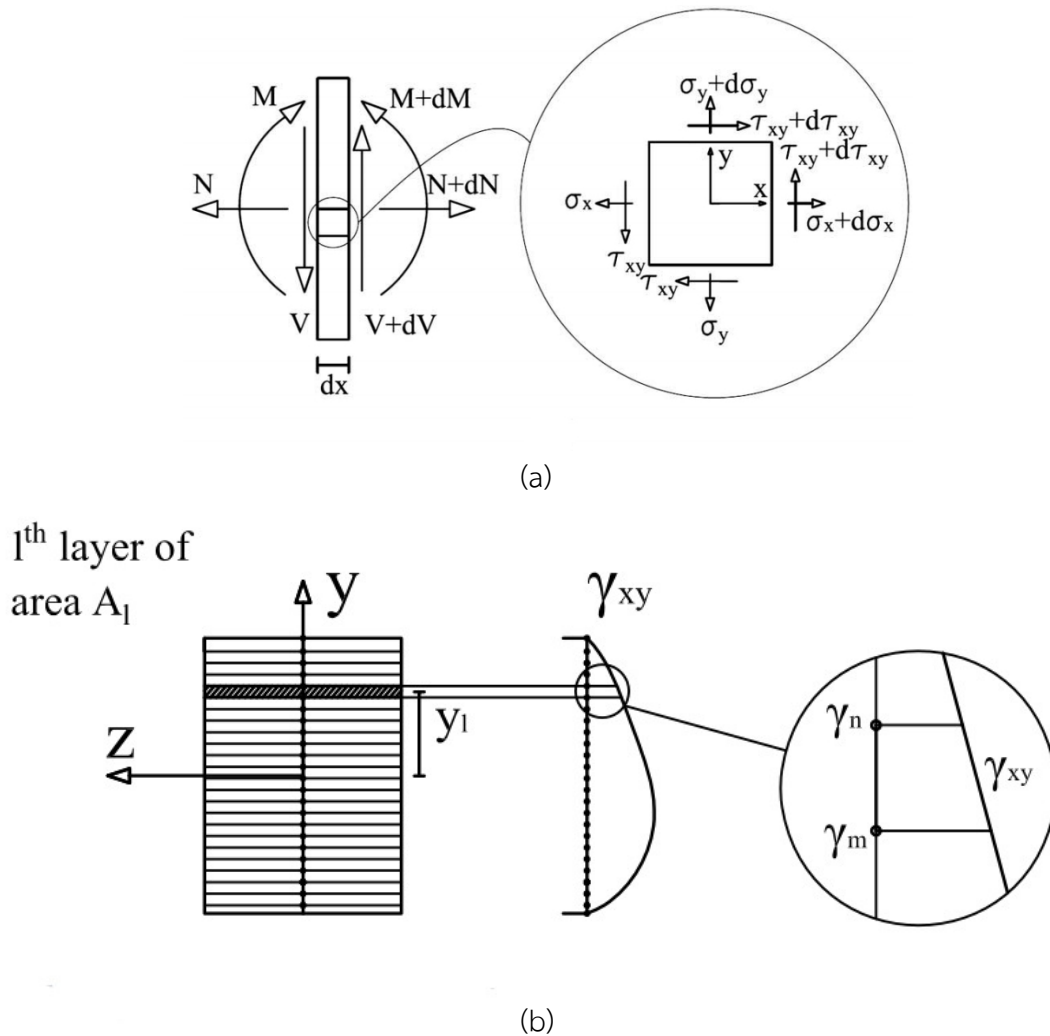


Figure 2-27 State of art of Kagermanov and Ceresa model: (a) internal fiber equilibrium and (b) shear strain profile [Kagermanov and Ceresa, 2017]

From the concept interaction between axial, shear, and flexure of Vecchio and Collins (1988), Bentz (2000), Remino (2004), Bairan (2006), and Kagermanov and Ceresa (2017), all those approaches can be categorized into the same group as the fiber beam-column element using the smeared crack models as well as the research works of Ceresa et al. (2007 and 2008).

2.5.2.7 Kotronis's Modelling Approach

Kotronis et al. (2000 and 2005) presented a 3D multifiber beam element including shear response based on Timoshenko beam theory. Their element is based on the displacement-based formulation and the displacement interpolation functions depend on the material properties (e.g. Young's modulus and shear modulus). The concrete constitutive law of this model considers the shear effect (Shear is considered in the linear behavior), damage due to crack in concrete and permanent effect under cyclic loading as shown in Figure 2-28. Although this model is capable of simulating quite well the global behavior of experimental test, the linear shear assumption does not seem to allow the accurate of an anisotropic response of reinforced concrete section when the crack occurs at the section introduced by shear [Ceresa et al., 2008].

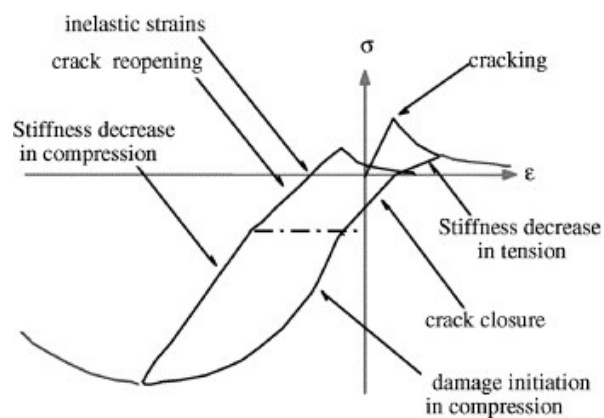


Figure 2-28 La Bordiere damage model of concrete [Kotronic et al., 2005]

2.5.2.8 Saritas's Modelling Approach

Saritas (2006) proposed a 2D Timoshenko beam-column element based on mixed formulation, introduced the axial-shear-bending interaction. At section level, the shear profile was distributed by the sectional interpolation function $\phi(y)$. The deformation at any point along the cross-section $\boldsymbol{\varepsilon}$ is given by

$$\boldsymbol{\varepsilon} = \begin{Bmatrix} \varepsilon_{xx}(x) \\ \gamma_{xy}(x) \end{Bmatrix} = \begin{Bmatrix} \varepsilon_0(x) - y_m \phi(x) \\ \phi(y) \gamma(x) \end{Bmatrix} \quad (2-45)$$

$$\phi(y_m) = \left(1 + 4 \left(\frac{bt_f}{dt_w} \right) \right) - 4 \frac{y_m^2}{d^2} \quad (2-46)$$

where $\varepsilon_{xx}(x)$ is the axial strain at any cross-section; $\gamma_{xy}(x)$ is the shear strain at any cross-section; $\varepsilon_0(x)$ is the sectional axial strain; $\phi(x)$ is the sectional curvature; $\gamma(x)$ is the sectional shear strain; b is the width of the flange; t_f is the thickness of the flange; t_w is the thickness of the web; and d is the depth of the cross-section. Moreover, the section forces \mathbf{D} are obtained from the summation of the stresses which satisfy the material constitutive laws and written as:

$$\mathbf{D} = \begin{Bmatrix} N(x) \\ M(x) \\ V(x) \end{Bmatrix} \approx \sum_{m=1}^{nfib} \begin{Bmatrix} \sigma_m A_m \\ -y_m \sigma_m A_m \\ \psi(y_m) \tau_m A_m \end{Bmatrix} \quad (2-47)$$

$$\psi(y_m) = \frac{\phi(y_m)}{\beta} \quad (2-48)$$

$$\beta = \frac{\int_A [\phi(y)]^2 dA}{\int_A [\phi(y)] dA} = \frac{\left(1 + 4 \left(\frac{bt_f}{dt_w} \right) \right)^2 - \frac{2}{3} \left(1 + 4 \left(\frac{bt_f}{dt_w} \right) \right) + \frac{1}{5}}{\frac{2}{3} \left(1 + 6 \left(\frac{bt_f}{dt_w} \right) \right)} \quad (2-49)$$

where $N(x)$ is the sectional axial force; $V(x)$ is the sectional shear force; $M(x)$ is the sectional bending moment; $\psi(y_m)$ is the modified shear strain profile; β is a parameter; m represents the generic fiber and $nfib$ represents the number of fibers in the section. y_m , σ_m , τ_m and A_m represent the distance from the reference axis x , the normal stress, the shear stress, and the cross-section area, respectively.

Saritas's modeling strategy assumed the perfect bond between concrete and steel, neglecting the buckling of longitudinal steel, neglecting dowel action of steel bar at the cracks, and neglecting the tension stiffening effect in the

concrete material model. From this limitation of Saritas's modeling strategy, the model needs improvement as suggested by Ceresa et al. (2007).

According to Kotronis et al. (2000 and 2005) and Saritas (2006) approach as discussed above, the shear responses in both approaches are considered through the damaged constitutive model for concrete (e.g. Armstrong and Frederick, 1966; Lee and Fenves, 1998). In the recent year, this concept has been developed and used in the several research works (e.g. Wu et al., 2006; Hafezolghorani et al., 2017; Wu 2017 and 2018).

All of the state-of-the-art reviews on the frame element models with accounting the shear responses and considering the shear-flexure interaction as above discussed, this thesis is aimed at the development of finite frame element with including shear-flexure interaction based on the concept of Ranzo and Petrangeli (1998) and the shear-flexure interaction procedure is adopted and modified from the Mergos and Kappos (2008 and 2012) within the framework of the UCSD shear-strength model proposed by Priestley et al. (1993). This concept corresponds well with the convenience of using in the engineering practice that the input parameters in the proposed model are closely related to the engineering properties. Moreover, the developed frame element is simple but accurate for using in the non-ductile RC column analysis under cyclic loading.

CHAPTER 3

Element Formulation

3.1 Introduction

This chapter presents the frame element formulation for seismic analysis of non-ductile RC column with shear-flexure interaction. The element is derived from the principle of virtual displacement under the small-deformation hypothesis. A set of governing differential equations of the frame element (strong form) are first derived. Then, the displacement-based frame element based on Timoshenko beam theory is formulated following the virtual displacement principle. Linked displacement interpolation functions are used to remedy the shear-locking problematic phenomenon that is discussed here. Next, the fiber-section model is employed to derive the nonlinear relations between forces and deformations of the uniaxial stress-strain of material constitutive laws. Among the compatibility, constitutive and equilibrium equations of the element formulation, the Tonti's diagram is used to conveniently represent both the strong and weak forms of the frame element formulations.

3.2 A Set of Governing Equations of Timoshenko Frame Element (Strong Form)

3.2.1 Equilibrium

The free body diagram of an infinitesimal segment dx of a frame member subjected to the transverse distributed load $P_y(x)$ is shown in Figure 3-1. Based on the small-deformation hypothesis, all equilibrium equations are considered in the undeformed configuration. Axial, moment, and vertical equilibriums of the infinitesimal segment dx of a frame member can be written as follow:

$$\frac{dN(x)}{dx} = 0 \quad (3-1)$$

$$\frac{dM(x)}{dx} - V(x) = 0 \quad (3-2)$$

$$\frac{dV(x)}{dx} - P_y(x) = 0 \quad (3-3)$$

where $N(x)$ is the frame sectional axial force; $V(x)$ is the frame sectional shear force; and $M(x)$ is the frame sectional bending moment. Eqs. (3-1), (3-2), and (3-3) establish a set of governing equilibrium equations of a Timoshenko frame element and can be written in the matrix form as follow:

$$\mathbf{L}_{TB}^T \mathbf{D}(x) - \mathbf{p}(x) = \mathbf{0} \quad (3-4)$$

where $\mathbf{D}(x) = \{N(x) \ M(x) \ V(x)\}^T$ represents the element sectional force vector; $\mathbf{p}(x) = \{0 \ 0 \ P_y(x)\}^T$ represents the element distributed load vector; and \mathbf{L}_{TB} denotes the Timoshenko frame differential operator and can define as:

$$\mathbf{L}_{TB} = \begin{bmatrix} \frac{d}{dx} & 0 & 0 \\ 0 & \frac{d}{dx} & 0 \\ 0 & -1 & \frac{d}{dx} \end{bmatrix} \quad (3-5)$$

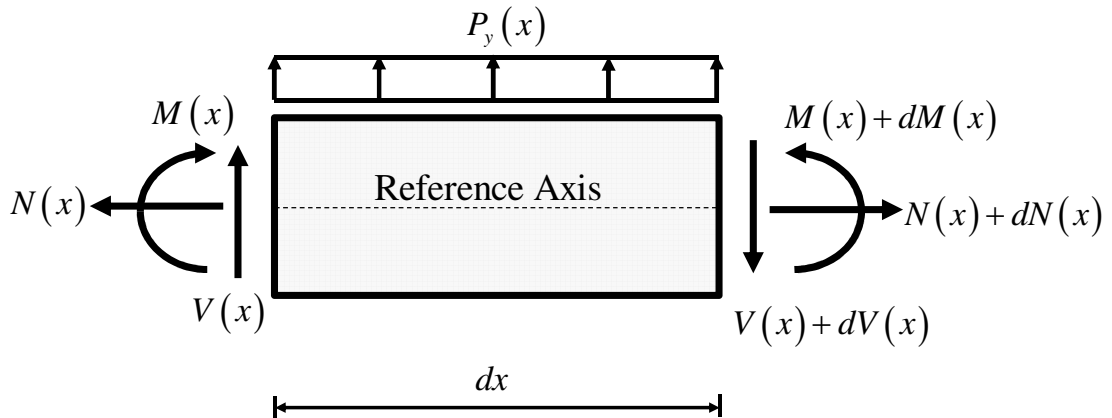


Figure 3-1 A differential segment of frame element

3.2.2 Compatibility

The element deformations at any section are related to the element sectional displacement fields through compatibility conditions. The element sectional deformation vector $\mathbf{d}(x)$ work conjugate of the element sectional force vector $\mathbf{D}(x)$ can be defined as:

$$\mathbf{d}(x) = \{\varepsilon_0(x) \quad \varphi(x) \quad \gamma(x)\}^T \quad (3-6)$$

where $\varepsilon_0(x)$ is the sectional axial strain at reference axis; $\varphi(x)$ is the sectional curvature; and $\gamma(x)$ is the sectional shear strain. The sectional displacement fields of frame element can be expressed in the following matrix form:

$$\mathbf{u}(x) = \{u_0(x) \quad \theta(x) \quad v_0(x)\}^T \quad (3-7)$$

where $u_0(x)$ is the sectional axial displacement at reference axis; $\theta(x)$ is the sectional rotation; and $v_0(x)$ is the sectional transverse displacement. Based on the Timoshenko kinematic assumptions as shown in Figure 2-12 and the small-deformation hypothesis, the element sectional deformations can be expressed in terms of the element sectional displacement fields through the compatibility conditions [Onate, 2013] as follow:

$$\varepsilon_0(x) = \frac{du_0(x)}{dx} \quad (3-8)$$

$$\varphi(x) = \frac{d\theta(x)}{dx} \quad (3-9)$$

$$\gamma(x) = -\theta(x) + \frac{dv_0(x)}{dx} \quad (3-10)$$

Eqs. (3-8), (3-9), and (3-10) represent a set of governing compatibility equations of a Timoshenko frame element. For the convenience of finite element model implementation, a set of governing compatibility equations can be expressed in the following matrix form as:

$$\mathbf{d}(x) = \mathbf{L}_{TB} \mathbf{u}(x) \quad (3-11)$$

It is noteworthy to emphasize that a set of governing compatibility equations in Eqs. (3-8), (3-9), and (3-10) are associated with a set of governing equilibrium equations in Eqs. (3-1), (3-2), and (3-3). It is clear that the statical and kinematical transformations are contragradient [Limkatanyu et al., 2014].

3.2.3 Section Force-Deformation Relations

The nonlinear nature of RC frame element in this study is presented through the nonlinear displacement-based constitutive model that can be defined as:

$$\mathbf{D}(x) = \Psi[\mathbf{d}(x)] \quad (3-12)$$

In order to perform the nonlinear analysis of RC frame element, the incremental-step solution requires the linear incremental forms of the force-deformation relation. Thus, the nonlinear relation of Eq. (3-12) can be written in consistent linearized forms as:

$$\mathbf{D}(x) = \mathbf{D}^0(x) + \mathbf{k}^0(x) \Delta \mathbf{d}(x) \quad (3-13)$$

where $\mathbf{D}^0(x)$ and $\mathbf{k}^0(x)$ are the sectional force vector and stiffness matrix at the initial point, respectively. It needs to notice that the superscript 0 denotes to the value of a vector or matrix at the initial point of the incremental-iterative solution procedure.

In order to compute the nonlinear force-deformation of Eq. (3-13), the fiber-section model with nonlinear uniaxial laws for RC sections [Spacone and Limkatanyu, 2000] is used to derive in this study. The fiber-section model is a common technique to subdivide the frame cross-section into the fibers (layers) as shown in Figure 3-2, moreover, this technique can automatically take into account the coupling between axial and bending responses. Thus, the sectional axial force $N(x)$ and sectional bending moment $M(x)$ are defined as:

$$N(x) = \sum_{m=1}^{nfib} \sigma_m A_m \quad \text{and} \quad M(x) = - \sum_{m=1}^{nfib} y_m \sigma_m A_m \quad (3-14)$$

where m represents the generic fiber and $nfib$ represents the number of fibers in the section. y_m , σ_m , and A_m represent the distance from the reference axis x (in Figure 3-2), the normal stress, and the cross-section area, respectively, of the m^{th} fiber in the section. Based on Eq. (3-14), the element sectional force vector $\mathbf{D}(x)$ can be rewritten as:

$$\mathbf{D}(x) = \left\{ \sum_{m=1}^{nfib} \sigma_m A_m \quad - \sum_{m=1}^{nfib} y_m \sigma_m A_m \quad V(x) \right\}^T \quad (3-15)$$

It is interesting to observe from Eq. (3-15) that the axial and bending actions need the number of fibers in the section $nfib$ to represent the variation of the normal stress σ_m along the section depth while shear actions doesn't require the fiber-section discretization because of the constant shear stress along the section depth based on the Timoshenko beam theory [Onate, 2013]. In other words, the fiber-section discretization for shear action is analogous to the one-fiber discretization.

The sectional stiffness matrix $\mathbf{k}(x)$ can be expressed via the fiber-section model as:

$$\mathbf{k}(x) = \begin{bmatrix} \sum_{m=1}^{n_{fib}} E_m A_m & -\sum_{m=1}^{n_{fib}} y_m E_m A_m & 0 \\ -\sum_{m=1}^{n_{fib}} y_m E_m A_m & -\sum_{m=1}^{n_{fib}} y_m^2 E_m A_m & 0 \\ 0 & 0 & GA_s(x) \end{bmatrix} \quad (3-16)$$

where E_m is the modulus of the m^{th} fiber in the section and $GA_s(x)$ is the sectional shear stiffness. It can be observed that there is no coupling between shear and flexure actions through fiber-section model for Timoshenko frame element as shown in Eq. (3-16). However, the interaction between shear and flexure can be accounted for via shear strength model proposed by Priestley et al. (1993) and will be cleared later in the Chapter 5.

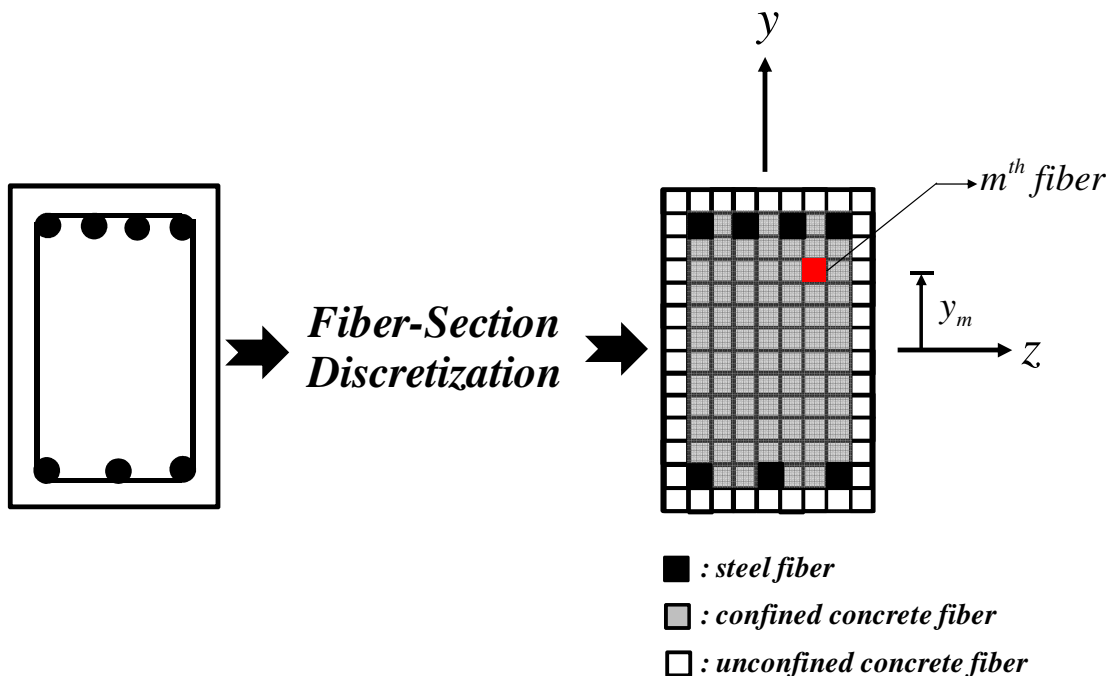


Figure 3-2 Fiber discretization of RC frame cross-section

In this study, the uniaxial cyclic constitutive laws of concrete, steel, and shear are schematically shown in Figure 3-3. Concrete model follows by the Kent and Park (1971) law; the reinforcing steel follows by the Menegotto and Pinto (1973); and the tri-linear envelope curve proposed by Mergos and Kappos (2012) is used for the shear response. The more detail of those used constitutive laws are discussed in the Chapter 5.

According to the equilibrium, compatibility, and sectional constitutive laws discussed above for the RC frame element, it can be conveniently presented in the classical Tonti's diagram of Figure 3-4 [Tonti, 1977]. This diagram will be modified subsequently to demonstrate the displacement-based formulation of the proposed RC frame element.

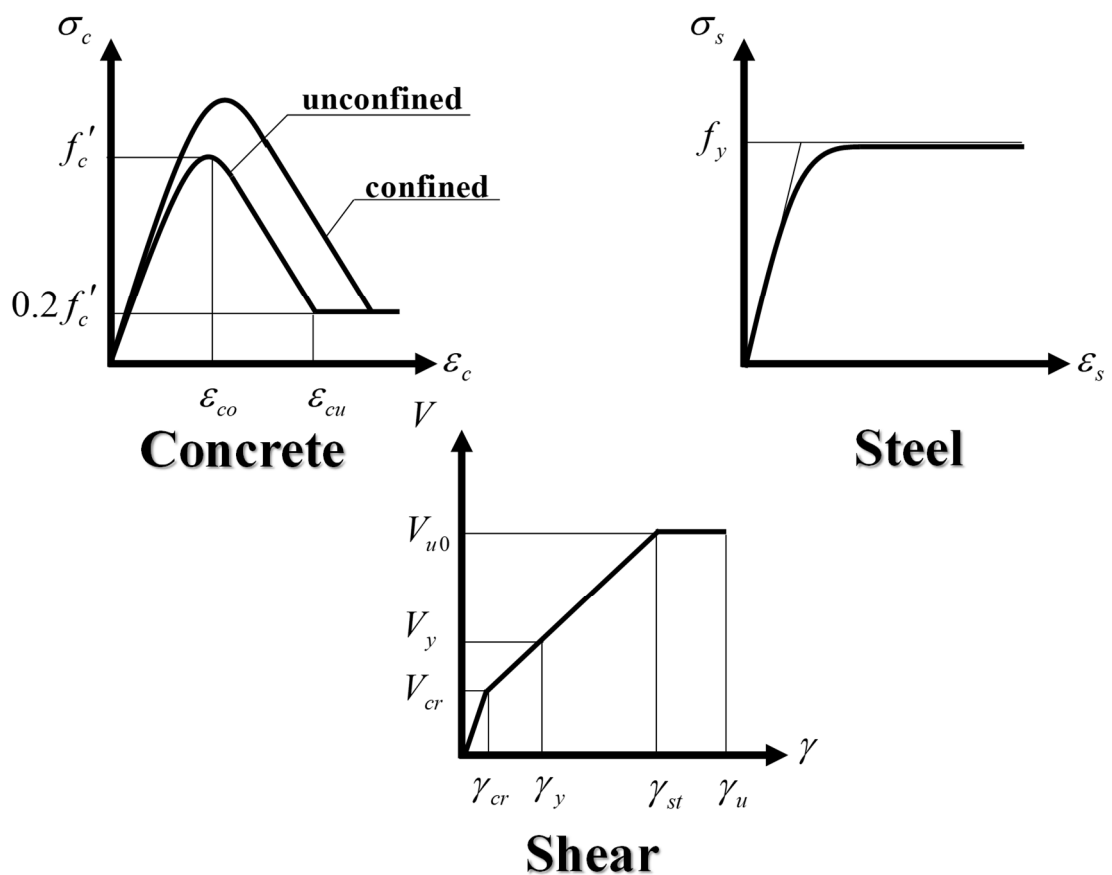


Figure 3-3 Uniaxial cyclic constitutive laws of concrete, steel, and shear

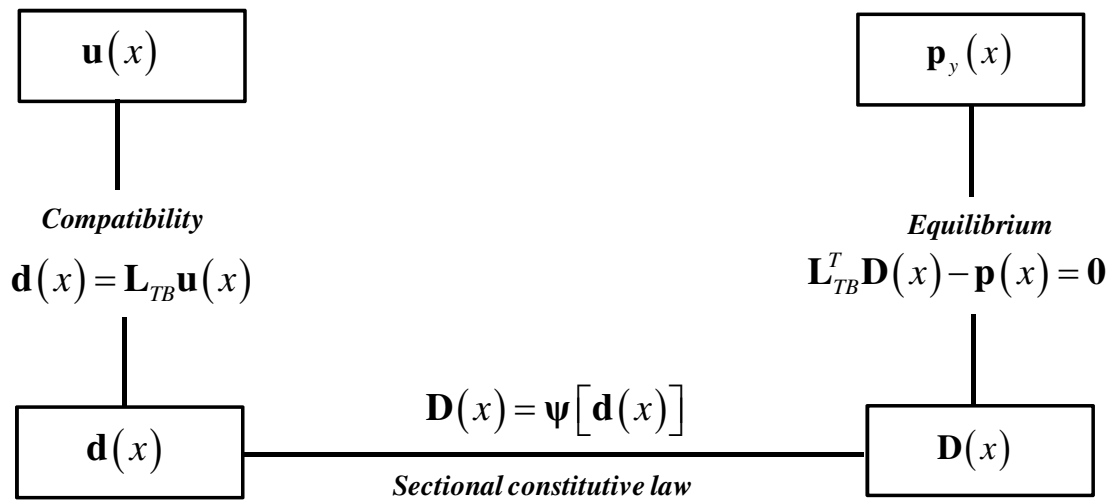


Figure 3-4 Tonti's diagram for Timoshenko frame element: differential equations (Strong form) [Tonti, 1977]

3.3 Displacement-Based Formulation of Timoshenko Frame Element (Weak Form)

3.3.1 Formulation

In the present work, the proposed RC frame element is derived based on the displacement-based finite element formulation. The element nodal displacements \mathbf{U} are treated as the primary variables of the element. The sectional displacement fields $u_0(x)$, $\theta(x)$, and $v_0(x)$ are expressed in terms of the element nodal displacements \mathbf{U} through the displacement interpolation functions. The element deformations $\mathbf{d}(x)$ are determined by enforcing the compatibility conditions of Eqs. (3-8), (3-9), and (3-10). Based on this reason, the compatibility conditions are satisfied point-wise along the element (Strong sense). On the other hand, the section equilibrium conditions are only enforced to satisfy in the weighted integral form (Weak sense) through the virtual displacement principle. The general framework of the proposed frame element model can be summarized in the modified Tonti's diagram of Figure 3-5.

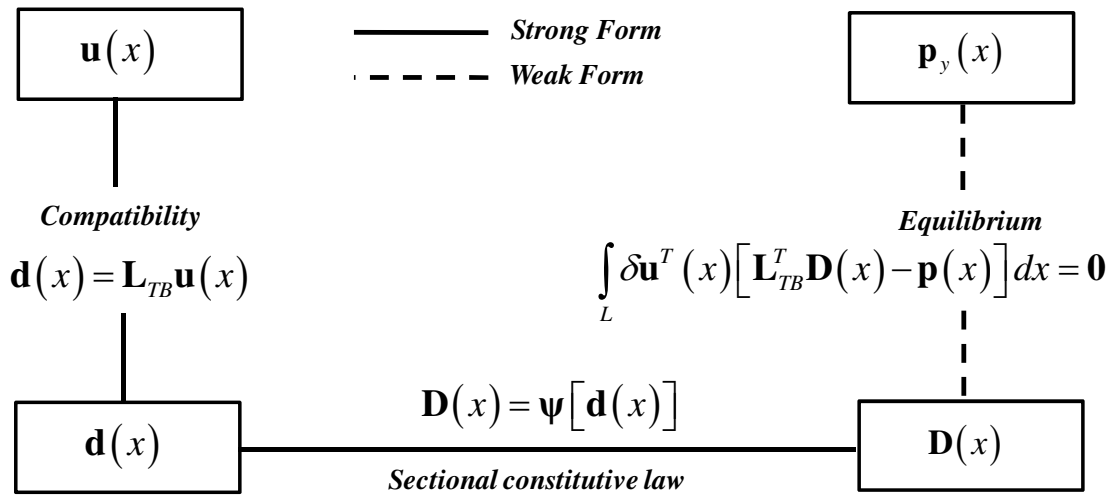


Figure 3-5 The modified Tonti's diagram for Timoshenko frame element: displacement-based formulation (Weak form)

The weighted residual form of a set of governing equilibrium equations in Eq. (3-4) can be written as:

$$\int_L \delta \mathbf{u}^T(x) [\mathbf{L}_{TB}^T \mathbf{D}(x) - \mathbf{p}(x)] dx = 0 \quad (3-17)$$

where $\delta \mathbf{u}(x)$ is a vector collecting compatible virtual displacement fields. Substituting Eqs. (3-13) into (3-17) and enforcing compatibility of Eq. (3-11) lead to:

$$\int_L \delta \mathbf{u}^T(x) [\mathbf{L}_{TB}^T (\mathbf{D}^0(x) + \mathbf{k}^0(x) \mathbf{L}_{TB} \Delta \mathbf{u}(x)) - \mathbf{p}(x)] dx = 0 \quad (3-18)$$

Integration by parts is applied to move order the differential operator \mathbf{L}_{TB} from the section force vector $\mathbf{D}(x)$ to the virtual displacement vector $\delta \mathbf{u}(x)$, thus leading to:

$$\begin{aligned} & \int_L (\mathbf{L}_{TB} \delta \mathbf{u}(x))^T \mathbf{k}^0(x) (\mathbf{L}_{TB} \Delta \mathbf{u}(x)) dx \\ & = \delta \mathbf{U}^T \mathbf{P} + \int_L \delta \mathbf{u}^T(x) \mathbf{p}(x) dx - \int_L (\mathbf{L}_{TB} \delta \mathbf{u}(x))^T \mathbf{D}^0(x) dx \end{aligned} \quad (3-19)$$

where $\delta \mathbf{U}^T \mathbf{P}$ represents the boundary terms that can be obtained during the integration by parts, moreover, $\delta \mathbf{U}^T \mathbf{P}$ refers to the external virtual work done by

$\delta\mathbf{U}^T$ (The virtual element nodal displacements) on the element nodal forces \mathbf{P} . It needs to note that Eq. (3-19) demonstrates the fundamental equation for the displacement-based finite element formulation of the RC frame element proposed in this study.

The element sectional displacements $\mathbf{u}(x)$ are related to the element nodal displacement \mathbf{U} through the displacement interpolation function matrix $\mathbf{N}_{TB}(x)$.

$$\mathbf{u}(x) = \mathbf{N}_{TB}(x)\mathbf{U} \quad (3-20)$$

According to the selection of displacement interpolation functions for the Timoshenko frame element, it must be made with care and is to be discussed in the subsequent section. Substituting Eq. (3-20) into (3-19) and accounting for the arbitrariness of $\delta\mathbf{U}$ lead to:

$$\left[\int_L \mathbf{B}_{TB}^T(x) \mathbf{k}^0(x) \mathbf{B}_{TB}(x) dx \right] \Delta\mathbf{U} = \mathbf{P} + \int_L \mathbf{N}_{TB}^T(x) \mathbf{p}(x) dx - \int_L \mathbf{B}_{TB}^T(x) \mathbf{D}^0(x) dx \quad (3-21)$$

where $\mathbf{B}_{TB}(x) = \mathbf{L}_{TB} \mathbf{N}_{TB}(x)$ is the sectional deformation-displacement matrix. Eq. (3-21) can be expressed in the compact form as:

$$\mathbf{K}^0 \Delta\mathbf{U} = (\mathbf{P} + \mathbf{P}_p) - \mathbf{Q}^0 \quad (3-22)$$

where

$\mathbf{K}^0 = \int_L \mathbf{B}_{TB}^T(x) \mathbf{k}^0 \mathbf{B}_{TB}(x) dx$ is the frame element stiffness matrix;

$\mathbf{P}_p = \int_L \mathbf{N}_{TB}^T(x) \mathbf{p}(x) dx$ is the equivalent load vector due to the distributed load $\mathbf{p}(x)$;

$\mathbf{Q}^0 = \int_L \mathbf{B}_{TB}^T(x) \mathbf{D}^0(x) dx$ is the element resisting force vector.

It is noteworthy to point out that the right-hand side vector $(\mathbf{P} + \mathbf{P}_p) - \mathbf{Q}^0$ of the discrete form of the stiffness equation in Eq. (3-22) refers to the residual force vector associated with the weak statement of equilibrium equations of

Eqs. (3-1), (3-2), and (3-3). It becomes vanish when the equilibrium configuration is reached during the incremental-iterative solution procedure.

3.3.2 Linked displacement interpolation functions

Based on the Timoshenko beam theory, the sectional rotation field $\theta(x)$ is independent of the sectional transverse displacement field $v_0(x)$. It can be observed that the sectional rotation field $\theta(x)$ is not subjected to a kinematic constraint of being equal to the first derivative of the sectional transverse displacement field $v_0(x)$ as in case of Euler-Bernoulli beam theory. Therefore, the sectional rotation $\theta(x)$ and sectional transverse displacement $v_0(x)$ can be interpolated independently to their nodal values in the displacement-based formulation of Timoshenko frame model. Although the Timoshenko frame element belongs to the class of C^0 -continuity elements and is simple than the class of C^1 -continuity as Euler-Bernoulli frame element, the selection of independent interpolation functions for the sectional transverse displacement $v_0(x)$ and sectional rotation $\theta(x)$ must be careful due to leading to the problematic phenomenon known as “*shear-locking*”. Shear-locking phenomenon causes the resulting Timoshenko frame model to suffer the unrealistic displacement solution for slender beam analysis. More details on the diagnosis of the shear-locking phenomenon are discussed in Onate (2013). To overcome the shear-locking problem, several approaches have been proposed such as, the reduced integration method [Prathap and Bhashyam, 1982], the consistent interpolation method [Reddy, 1997], mixed and force-based formulations [Erguven and Gediki, 2003; and Marini and Spacone, 2006].

In the present study, the consistent interpolation approach is used to remedy the shear-locking problem. The consistent interpolation approach requires that the choice of interpolation functions for the sectional transverse displacement $v_0(x)$ and sectional rotation $\theta(x)$ fields has to be such that $dv_0(x)/dx$ and $\theta(x)$ are polynomials of the same order. In other words, the interpolation function for the sectional transverse displacement field $v_0(x)$ must be one-degree higher than that for the sectional rotation field $\theta(x)$. Therefore, a standard linear Timoshenko frame

element shown in Figure 3-6 is to be improved with a quadratic (Bubble) term for the sectional transverse displacement field $v_0(x)$. The resulting interpolation functions are:

$$u_0(x) = \left(1 - \frac{x}{L}\right)U_1 + \frac{x}{L}U_4 \quad (3-23)$$

$$v_0(x) = \left(1 - \frac{x}{L}\right)U_2 + \frac{x}{L}U_5 + \underbrace{\alpha_b x(x-L)}_{\text{Enhanced Bubble Function}} \quad (3-24)$$

$$\theta(x) = \left(1 - \frac{x}{L}\right)U_3 + \frac{x}{L}U_6 \quad (3-25)$$

where $\mathbf{U} = \{U_1 \ U_2 \ U_3 \ U_4 \ U_5 \ U_6\}^T$ is a vector containing element nodal displacements and α_b represents a parameter to be determined from the limit Euler-Bernoulli condition of vanishing shear strain ($\gamma(x)=0$) for slender beams.

Following Eqs. (3-10), (3-24), and (3-25), the sectional shear strain can be expressed as:

$$\gamma(x) = \left(\frac{U_2 - U_5}{L}\right) + U_3 + \alpha_b L + x \left(\frac{U_6 - U_3}{L} - 2\alpha_b\right) \quad (3-26)$$

To satisfy the limit Euler-Bernoulli condition of vanishing shear strain ($\gamma(x)=0$) for slender beams, Eq. (3-26) should be independent of the coordinate x , thus the parameter α_b can be written as:

$$\alpha_b = \left(\frac{U_6 - U_3}{2L}\right) \quad (3-27)$$

Substituting Eq. (3-27) into (3-24), the sectional transverse displacement field $v_0(x)$ can be expressed as:

$$v_0(x) = \left(1 - \frac{x}{L}\right)U_2 + \frac{x}{L}U_5 + \left(\frac{x}{2} - \frac{x^2}{2L}\right)U_3 + \left(-\frac{x}{2} + \frac{x^2}{2L}\right)U_6 \quad (3-28)$$

Eq. (3-28) is clear that the sectional transverse displacement field $v(x)$ is interpolated not only in terms of nodal displacements associated the transverse degrees of freedom (U_2 and U_5) but also in terms of displacements associated the rotation degrees of freedom (U_3 and U_6). Consequently, the authors refer to this displacement interpolation functions as the so-called “*linked*” displacement interpolation functions. This concept to remedy the shear-locking problem in the beam analysis as discussed above is perhaps from the research work of de Veubeke (1965) and extends in the several research works [Tessler and Dong, 1981; Reddy, 1997].

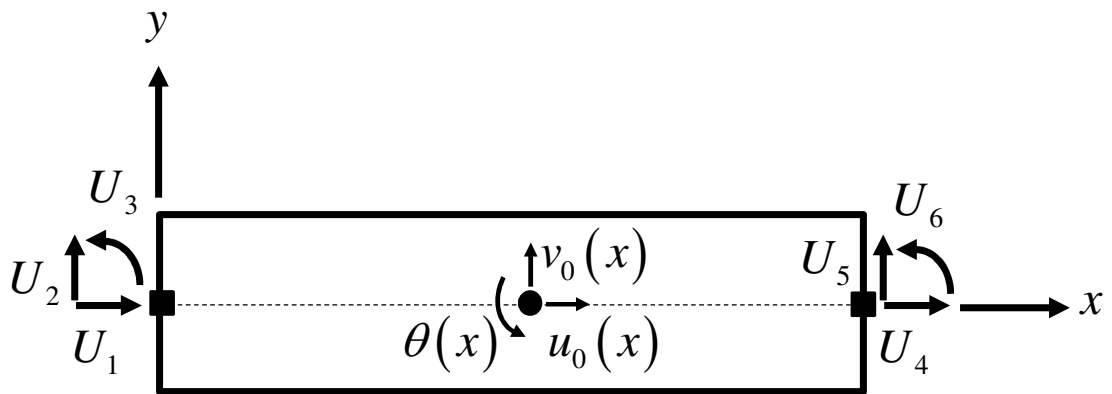
Following the displacement fields of Eqs. (3-23), (3-25), and (3-28), the displacement interpolation function matrix $\mathbf{N}_{TB}(x)$ can be written as:

$$\mathbf{N}_{TB}(x) = \begin{bmatrix} 1 - \frac{x}{L} & 0 & 0 & \frac{x}{L} & 0 & 0 \\ 0 & 0 & 1 - \frac{x}{L} & 0 & 0 & \frac{x}{L} \\ 0 & 1 - \frac{x}{L} & \frac{x}{2} - \frac{x^2}{2L} & 0 & \frac{x}{L} & -\frac{x}{2} + \frac{x^2}{2L} \end{bmatrix} \quad (3-29)$$

The sectional deformation-displacement matrix $\mathbf{B}_{TB}(x)$ is:

$$\mathbf{B}_{TB}(x) = \mathbf{L}_{TB} \mathbf{N}_{TB}(x) = \begin{bmatrix} -\frac{1}{L} & 0 & 0 & \frac{1}{L} & 0 & 0 \\ 0 & 0 & -\frac{1}{L} & 0 & 0 & \frac{1}{L} \\ 0 & -\frac{1}{L} & \frac{1}{2} & 0 & \frac{1}{L} & \frac{1}{2} \end{bmatrix} \quad (3-30)$$

All symbolic calculations of this thesis are performed by using the computer software Mathematica (Wolfram, 1992).



$$\mathbf{u}(x) = \{u_0(x) \quad \theta(x) \quad v(x)\}^T$$

$$\mathbf{U} = \{U_1 \quad U_2 \quad U_3 \quad U_4 \quad U_5 \quad U_6\}^T$$

Figure 3-6 A standard linear Timoshenko frame element

CHAPTER 4

Element State Determination

4.1 Introduction

This chapter presents the structural state determination and the element state determination for the RC frame element based on the displacement-based formulation of Chapter 3. The structural state determination is the iterative step to compute the structural resisting forces and the structural stiffness matrix corresponding to the given structural nodal displacements while the element state determination is the procedure to determine the element resisting forces and the element stiffness matrix corresponding to the given element nodal displacements. This chapter focuses on the element state determination that is the essential procedure to determine the structural responses. Next, the brief discussion of the used convergent criterion is presented herein. The element convergence follows the same rules of the general-purpose finite element program, i.e. FEAP (Taylor, 2000). Finally, the numerical integration scheme is discussed here.

4.2 Structure State Determination

The nonlinear material properties in the finite element discretization of the structural system may lead to the nonlinear algebraic equations. To find those converged solutions, the iterative Newton-Raphson method is applied. The structural stiffness matrix is treated as a predictor while the structure resisting forces are selected as a convergent checker. The converged solutions are obtained when the difference between the externally applied nodal forces and the structural resisting forces are smaller than an acceptable tolerance. The process to compute the stiffness matrix and resisting forces by the given nodal displacements is often called as “*state determination*”. The state determination can be divided into two phases. The first phase is the structure state determination which is the process to assemble

the stiffness matrix and the resisting forces at the structural level by the given structural nodal displacements. The second phase is the element state determination which is the process to find the stiffness matrix and the resisting forces at element level by the given element nodal displacements. The rule of both the stiffness matrix and the resisting forces assembling at the structural and element levels bases on the direct stiffness method.

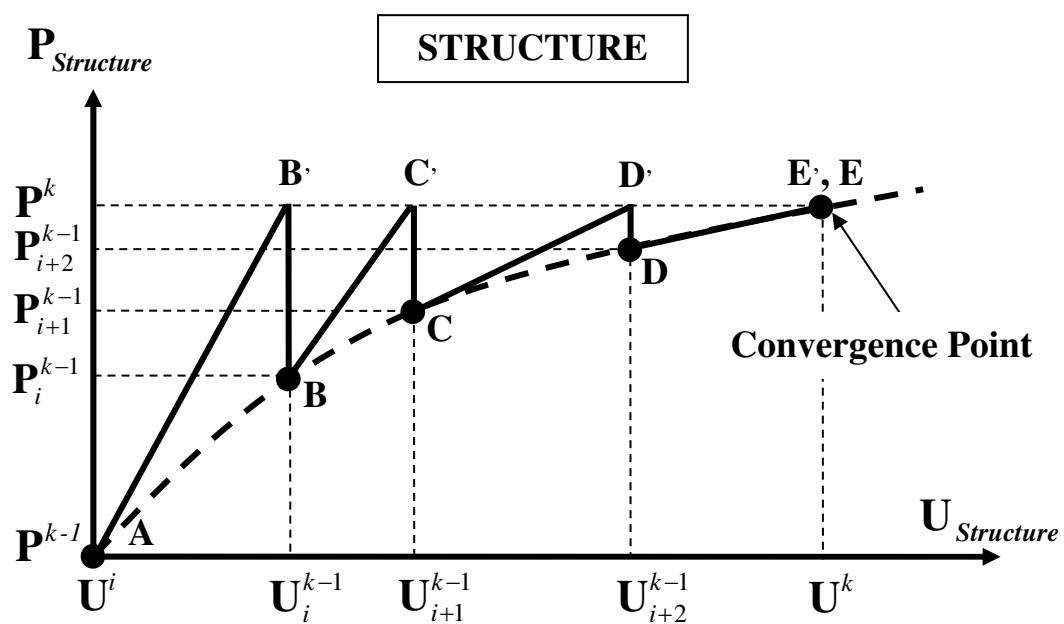


Figure 4-1 Structure state determination by Newton-Raphson solution at load step k
[Limkatanyu, 2002]

Figure 4-1 shows the Newton-Raphson solution scheme for load step k . Based on the applied structural load vector \mathbf{P}^k and the current tangent stiffness matrix, points B', C', D', and E' represent the predictor points while point B, C, D, and E represent the convergent points. Moreover, the nodal forces at point B, C, D, and E must equilibrium with the structural resisting forces which correspond to the current structural nodal displacements. Finally, the solution converges at the displacement vector \mathbf{U}_k when the superscripted index k denotes the incremental load step at the structural level and the subscripted index i denotes the Newton-

Raphson iterative step at the structural level. The details of the structure state determination as described above are a part of the total state determination procedures which are commonly found in the nonlinear analysis programs. The more details of the structure state determination are discussed by Limkatanyu (2002).

4.3 Element State Determination

In the element state determination, this process is performed to determine the resisting forces \mathbf{Q} and element stiffness matrix \mathbf{K} corresponding with the element nodal displacements \mathbf{U} which are extracted from the imposed structure nodal displacements. Following the displacement-based finite element method, the element formulation both linear and nonlinear algorithms is based on the displacements of the structural degrees of freedom or the element nodal displacements. Therefore, the displacement-based formulation is also simple and as straightforward for the implement of finite element analysis. In addition, the summarized the steps in the implementation of the RC frame based on displacement-based formulation are presented in Table 4.1.

Figure 4-2 presents the general scheme for the procedures in the element state determination. It can be observed that point B, C, D, and E in Figure 4-2 correspond to those points in Figure 4-1. The current sectional deformations $\mathbf{d}(x)$ are first computed from the current nodal displacements \mathbf{U} through the sectional deformation-displacement matrix $\mathbf{B}_{TB}(x)$ (Step a in Table 4.1). Then, the sectional resisting forces $\mathbf{D}_R(x)$ and the sectional stiffness matrix $\mathbf{k}(x)$ are determined from the sectional state determination based on the current sectional deformations $\mathbf{d}(x)$ (Step b in Table 4.1). Next, the element stiffness \mathbf{K} is computed from the sectional stiffness matrix $\mathbf{k}(x)$ (Step c in Table 4.1). Finally, the element resisting force \mathbf{Q} is obtained from the sectional resisting forces $\mathbf{D}_R(x)$ (Step d in Table 4.1). The step-by-step algorithm for element state determination procedure as above described is presented as follows:

1. Compute the element nodal displacement increments $\Delta\mathbf{U}$ from Eq. (3-21).

2. Determine the sectional deformation increments $\Delta \mathbf{d}(x)$ from the element nodal displacement increments $\Delta \mathbf{U}$ through the sectional deformation-displacement matrix $\mathbf{B}_{TB}(x)$ from Eq. (3-30).

$$\Delta \mathbf{d}(x) = \mathbf{B}_{TB}(x) \Delta \mathbf{U} \quad (4-1)$$

3. Update the sectional deformations $\mathbf{d}(x)$.

$$\mathbf{d}(x) = \mathbf{d}^0(x) + \Delta \mathbf{d}(x) \quad (4-2)$$

4. Determine the sectional resisting forces $\mathbf{D}_R(x)$ and the sectional stiffness matrix $\mathbf{k}(x)$ with corresponding of the sectional deformations $\mathbf{d}(x)$ in step 3 from the section state determination as described in the next chapter.

5. Compute the element stiffness \mathbf{K} .

$$\mathbf{K} = \int_L \mathbf{B}_{TB}^T(x) \mathbf{k} \mathbf{B}_{TB}(x) dx \quad (4-3)$$

6. Calculate the element resisting force \mathbf{Q} .

$$\mathbf{Q} = \int_L \mathbf{B}_{TB}^T(x) \mathbf{D}_R(x) dx \quad (4-4)$$

Table 4-1 Step in element state determination for RC frame element analysis based on displacement-based formulation

Step	Displacement-Based Algorithm
a) Sectional Deformations	$\mathbf{d} = \mathbf{B}_{TB} \mathbf{U}$
b) Sectional State Determination	$\mathbf{k} = \mathbf{k}(\mathbf{d}), \mathbf{D}_R = \mathbf{D}_R(\mathbf{d})$
c) Element Stiffness	$\mathbf{K} = \int_L \mathbf{B}_{TB}^T \mathbf{k} \mathbf{B}_{TB} dx$
d) Element Forces	$\mathbf{Q} = \int_L \mathbf{B}_{TB}^T \mathbf{D}_R dx$

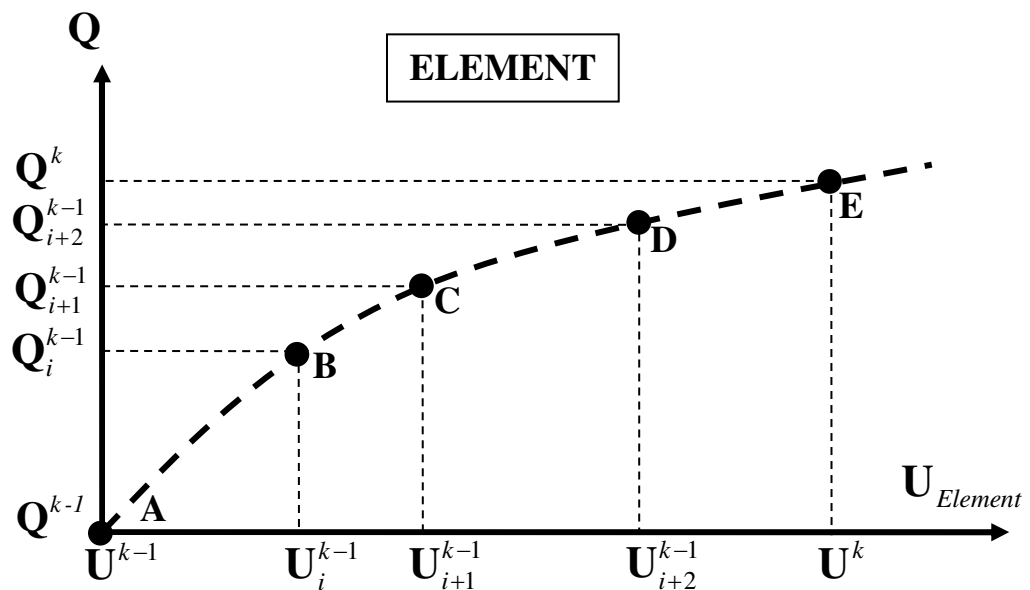


Figure 4-2 Element state determination at load step k

[Limkatanyu, 2002]

It is noteworthy that the characteristic of the convergence in the section state determination of the axial and bending actions as shown in Figure 4-3 (a) is very similar in the structure and element state determinations. However, it can be observed that characteristic of the convergence in the section state determination of the shear action as shown in Figure 4-3 (b) differs from the section state determination of the axial and bending actions and there is the iterative procedure within the i^{th} Newton-Raphson iterative step especially. The more detail and the iterative procedure are not discussed here and will be described in the next chapter.

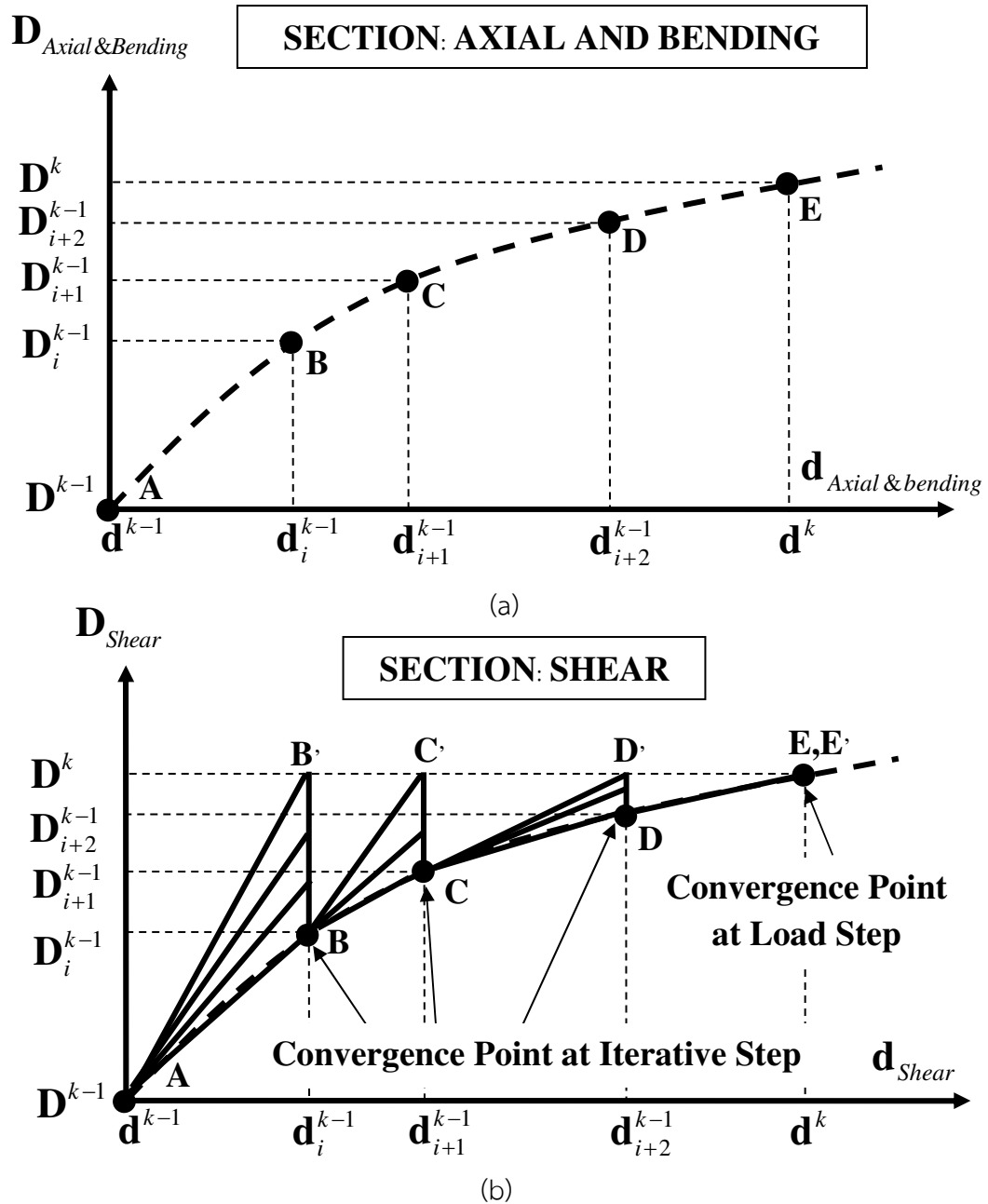


Figure 4-3 Section state determination at load step k : (a) axial and bending actions and (b) shear action

4.4 Convergence Criterion

From the state determination as discussed above, the nonlinear algorithms are based on a set of linear matrix equations. Those equations are

repeatedly applied until the convergence is reached. In other words, this procedure is repeatedly applied until the element residual forces corresponding to the element residual deformations are identically zero. In practice, the perfect balance between the applied forces and the occurred forces is either impossible or too expensive to attain. In nonlinear analysis, it is normally accepted that convergence is achieved when some control parameters, such as the residual forces, are smaller than an acceptable tolerance. The control parameters selection has been studied up to date and have been discussed. There are many choices to select the control parameters, such as norms or absolute values of these variables etc.

In this study, the finite element formulation is implemented in the general-purpose finite element platform FEAP (Taylor, 2000). Fortunately, the convergence criterion selected for the element iterations in the state determination is very similar in FEAP to check the convergence at the global level. For the convergence criterion in FEAP, the work (Energy) increment at the global level is selected as the control parameter. The convergent condition of the Newton-Raphson iteration algorithm is achieved when the value of the ratio between the current work increment and the initial work increment is lesser than an acceptable tolerance. The work (Energy) at the i^{th} Newton-Raphson iterative step W_{str}^i can be expressed as:

$$W_{str}^i = [\Delta U_{str}^i]^T \Delta P_{str}^i \quad (4-5)$$

It needs to note that the subscript str indicates the values at the structural level. The convergence of Newton-Raphson iterative step is reached upon the following expression:

$$\frac{|W_{str}^i|}{|W_{str}^{i-1}|} < Tolerance \quad (4-6)$$

The convergence scheme as shown above is part of FEAP and can adopt with the other iterative scheme. The more discussion detail is presented by Zienkiewicz and Taylor (1991).

4.5 Numerical Integration

According to the assessment of the integral terms in the implement of the finite element formulation, the classical Gauss integration scheme has been extensively used in the research works (e.g. Monegato, 1994; Pelekasis and Tsamopoulos, 1995; and Xucheng and Xiaoning, 1995). However, the first and last integration points of the classical Gauss integration scheme are not evaluated at the end-sections. Thus, the classical Gauss integration scheme cannot be used to present the behaviors of the model in the end-sections even though the number of integration points is increased. In the distributed plasticity model, the end sectional responses of the model are essential especially when the element experiences with the maximum responses at the end-section. To overcome this limitation, this study is performed based on the Gauss-Labatto integration scheme. The Gauss-Labatto integration scheme is extended the classical Gauss integration scheme domain to evaluate at the end-sections as shown in Eq. (4-7).

$$I = w_1 g(\xi_1 = -1) + \sum_{i=2}^{N_G-1} w_i g(\xi) + w_{N_G} g(\xi_{N_G} = 1) \quad (4-7)$$

where the index i denotes the monitored section; w_i represents the corresponding weight factor [Stroud and Secrest, 1966]; ξ is the natural coordinate. Gauss-Lobatto integration scheme with N_G integration points provides that the exact integration of polynomial of degree up to $(2 N_G - 3)$.

The classical Gauss integration scheme with N_G integration points provides that the exact integration of polynomial of degree up to $(2 N_G - 1)$ and is based on the following equation:

$$I = \sum_{i=1}^{N_G} w_i g(\xi) \quad (4-8)$$

CHAPTER 5

Material Constitutive Laws

5.1 Introduction

This chapter presents the constitutive models for concrete, reinforcing steel, and shear. All of the material constitutive models are based on uniaxial behaviors. The nonlinear behaviors between stress and strain of material models under monotonic or cyclic loading are expressed in term of the strain (Deformation). This procedure in the implement of finite element analysis to determine the sectional stress (Forces) and sectional stiffness is called as “*section state determination*” and is discussed herein. In the first material constitutive models of this research, the used concrete model was proposed by Kent and Park (1971). Then, Scott et al. (1982) modified the Kent and Park concrete model to account the confinement and Yassin (1994) modified the Kent and Park concrete model to include tensile strength and tensile damage. As for the plain reinforcing steel model, Menegotto and Pinto (1973) were proposed the stress-strain relation of reinforcing steel. Then, the reinforcing steel model was modified by Filippou (1983b) to include the isotropic hardening effects. Finally, the used shear model follows the envelope curve originally proposed by Mergos and Kappos (2008 and 2012) and is modified in this study.

5.2 Concrete Constitutive Model

The concrete constitutive model in this research is based on the modified Kent-Park model. In 1971, Kent and Park proposed the original concrete model. The model was simple but accurate. However, Kent and Park model didn't include the confinement and tensile effect. Then, the concrete model was modified by Scott et al. (1982) to accounts the confinement effect and by Yassin (1994) to include the tensile stiffening and tensile damage. It was the so-called as “*modified Kent-Park concrete model*”. Due to the computationally efficient and well

prediction, this model has been extensively employed to model the concrete behavior in the several research works (e.g. Spacone et al. 1996; Spacone and Limkatanyu, 2000; Limkatanyu, 2002; Limkatanyu and Spacone, 2002; Marini and Spacone, 2006). It needs the note that the tensile effects of the concrete are neglected in this research for the reinforced concrete structure analysis. In other words, only the concrete in the compressive zone is considered. However, the tensile effects of concrete are great essential in the analysis of the reinforced concrete structure, especially the prediction of the monotonic responses.

The main features of the modified Kent-Park concrete model can be divided as following:

- The concrete stress-strain relation in the compressive zone
- The hysteretic response of concrete model under cyclic loading

5.2.1 Stress-strain relation for concrete in compressive zone

The stress-strain relation for concrete in compressive zone is shown in Figure 5-1. This model is a simplicity and accuracy under cyclic loading. Moreover, the previous research works (e.g. Sinha et al., 1964 and Karsan et al., 1969) indicated that the envelope curve under cyclic loading is very close to the envelope curve under monotonic loading. Therefore, the cyclic damage of concrete model in the compressive zone is not taken into account in this study. From Figure 5-1, Kent and Park model (1971) can describe into the three regions based on the monotonic envelope curve. The monotonic concrete stress-strain relation $\sigma_c - \varepsilon_c$ and the corresponding tangent stiffness E_t , during each region are given by the following expressions:

Region OA: $\varepsilon_c \leq \varepsilon_{c0}$

$$\sigma_c = Kf'_c \left[2 \left(\frac{\varepsilon_c}{\varepsilon_{c0}} \right) - \left(\frac{\varepsilon_c}{\varepsilon_{c0}} \right)^2 \right] \quad (5-1)$$

$$E_t = \frac{Kf'_c}{\varepsilon_{c0}} \left[1 - \left(\frac{\varepsilon_c}{\varepsilon_{c0}} \right) \right] \quad (5-2)$$

Region AB: $\varepsilon_{c0} \leq \varepsilon_c \leq \varepsilon_{cu}$

$$\sigma_c = Kf'_c [1 - Z(\varepsilon_c - \varepsilon_{c0})] \quad (5-3)$$

$$E_t = -ZKf'_c \quad (5-4)$$

Region BC: $\varepsilon_{cu} \leq \varepsilon_c$

$$\sigma_c = 0.2Kf'_c \quad (5-5)$$

$$E_t = 0 \quad (5-6)$$

where

$$\varepsilon_{c0} = 0.002K \quad (5-7)$$

$$K = 1 + \frac{\rho_v f_{yv}}{f'_c} \quad (5-8)$$

$$Z = \frac{0.5}{\frac{3 + 0.29f'_c}{145f'_c - 1000} + 0.75\rho_v \sqrt{\frac{h'}{s_h}} - 0.002K} \quad (5-9)$$

where f'_c is the concrete compressive cylinder strength (MPa); ε_{c0} is the concrete strain at maximum stress in compression; K is a parameter which accounts the strength increase because of the confinement; Z is the slope of the softening branch; f_{yv} is yield strength of the stirrups (MPa); ρ_v is the volumetric ratio of the hoop reinforcement; h' is the width of concrete core; and s_h is the center to center spacing of stirrups or hoop set. The parameter K and Z as above equations are obtained from the empirical data which are given by Scott et al. (1982).

The strain at concrete crushing ε_{cu} , accounts the reducing of the strength in concrete to $0.2f'_c$, is suggested by Scott et al. (1982) and can be written as:

$$\varepsilon_{cu} = 0.004 + 0.9\rho_v \left(\frac{f_{yv}}{300} \right) \quad (5-10)$$

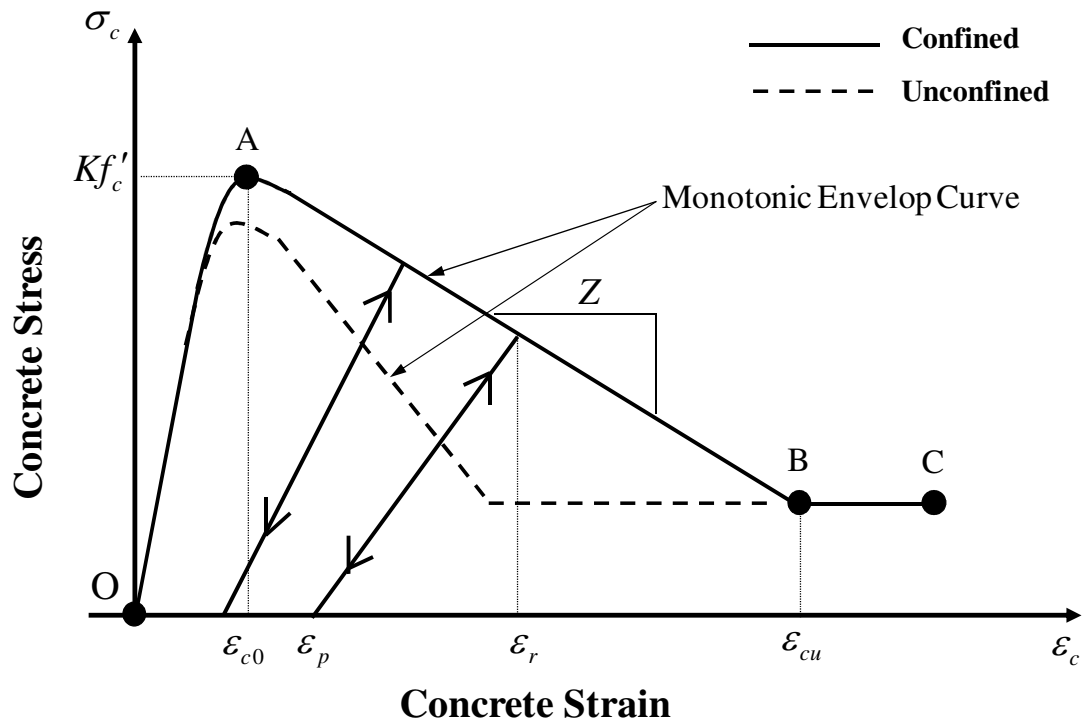


Figure 5-1 Constitutive model of concrete under cyclic loading in compression

[Limkatanyu, 2002]

5.2.2 The hysteretic response of concrete model under cyclic loading

The hysteretic behavior of the concrete stress-strain relation under cyclic loading is shown in Figure 5-1. The rules of the concrete model in the compressive zone during cyclic loading can be expressed as following:

1. The unload state on the envelope curve occurs along a straight line between the point ε_r at which unloading starts and the point ε_p on the strain axis. These relations can be given by the following equations:

$$\frac{\varepsilon_r}{\varepsilon_{c0}} < 2: \quad \frac{\varepsilon_p}{\varepsilon_{c0}} = 0.145 \left(\frac{\varepsilon_r}{\varepsilon_{c0}} \right)^2 + 0.13 \left(\frac{\varepsilon_r}{\varepsilon_{c0}} \right) \quad (5-11)$$

$$\frac{\varepsilon_r}{\varepsilon_{c0}} \geq 2: \quad \frac{\varepsilon_p}{\varepsilon_{c0}} = 0.707 \left(\frac{\varepsilon_r}{\varepsilon_{c0}} - 2 \right) + 0.834 \quad (5-12)$$

Eq. (5-11) corresponds to the normalized strain on the envelop curve with the strains at the completion of unloading through a quadratic formula proposed by Karsan and Jirsa (1969). However, this equation demonstrates the unrealistic prediction of behavior of concrete in case of the high compressive strain conditions. Thus, Eq. (5-12) is introduced to the concrete model so that the unloading modulus of elasticity remains positive under high compressive strains.

2. Due to the neglect of the tensile resistance of concrete model, the concrete stress is equal to zero for the concrete strain smaller than the concrete strain at complete unloading (Crack opening) as shown in Figure 5-1.

3. In the reloading state in the compressive zone, the concrete behavior is in tension as long as the strain is smaller than the concrete strain at complete unloading (Crack opening). If the concrete strain exceeds that value, the reloading path follows the previous unloading path.

It is worth to note that the unloading and reloading path in the reality follow the nonlinear paths. However, both paths are considered in the linear straight line for the sake of simplicity.

5.3 Reinforcing Steel Constitutive Model

The relation between stress-strain of reinforcing steel was modeled by Menegotto and Pinto (1973) as shown in Figure 5-2. Although the original reinforcing steel model of Menegotto and Pinto (1973) was simple and computationally efficient, the model didn't account taking into the isotropic hardening effects. Later, Filippou et al. (1983b) modified the Menegotto and Pinto model to include the isotropic hardening effects. From their research work of Filippou et al. (1983b), the modified reinforcing steel model is computationally efficient and can closely represent experimental results from cyclic tests on reinforcing bars.

is towards the reversal point with the slope E_1 . The tangent modulus E_t of this transition curve can be obtained by differentiating Eqs. (5-13), (5-14), and (5.15) and can be written by

$$E_t = \frac{d\sigma}{d\varepsilon} = \left(\frac{\sigma_0 - \sigma_r}{\varepsilon_0 - \varepsilon_r} \right) \left(b + \left(\frac{1-b}{(1+(\varepsilon^*)^R)^{1/R}} \right) \left(1 - \frac{(\varepsilon^*)^R}{1+(\varepsilon^*)^R} \right) \right) \quad (5-16)$$

where σ_r and ε_r define the stress and strain at the point of strain reversal (Point A in Figure 5-2), that is also the origin of the asymptote with slope E_0 (Line (a) in Figure 5-2). σ_0 and ε_0 define the stress and strain at the point of intersection of the two asymptotes (Point B in Figure 5-2). The parameter b is the strain-hardening ratio. In other words, b is the ratio between slope E_1 and E_0 . The parameter R is introduced to control the shape of the transition curve between the asymptotes and permit a good representation of the Bauschinger effect. Finally, $(\varepsilon_r, \sigma_r)$ and $(\varepsilon_0, \sigma_0)$ are updated after each strain reversal as shown in Figure 5-2.

The parameter for controlling shape of the transition curve R is governed by the absolute strain difference between the current asymptote intersection point (Point B in Figure 5-3) and the previous maximum or minimum strain reversal point (Point C in Figure 5-3) depending on whether the current strain increases or decreases, respectively. The parameter for controlling shape of the transition curve R introduced by Menegotto and Pinto (1973) can express as:

$$R(\xi) = R_0 - \frac{a_1 \xi}{a_2 + \xi} \quad (5-17)$$

where R_0 is the value of the parameter R during first loading and a_1 and a_2 are parameters which determine from the experimental test.

5.3.2 The hysteretic response of reinforcing steel model under cyclic loading

The rules for the hysteretic stress-strain relation of reinforcing steel, which are implied by using Eq. (5-13) to (5-17), can be briefly described as follows:

The section is loaded first along the monotonic and then is unloaded with the tangent modulus E_t until it reaches the abscissa point. An unloading is changed into the reloading state. The reloading continues in the opposite direction until it reaches the monotonic envelope on the opposite side and continues loading until it encounters with the unloading state. After unloading is changed into the reloading state, the reloading continues in the opposite direction with the pinching response. More details on the hysteresis law of reinforcing steel model can be found in Filippou et al. (1983b).

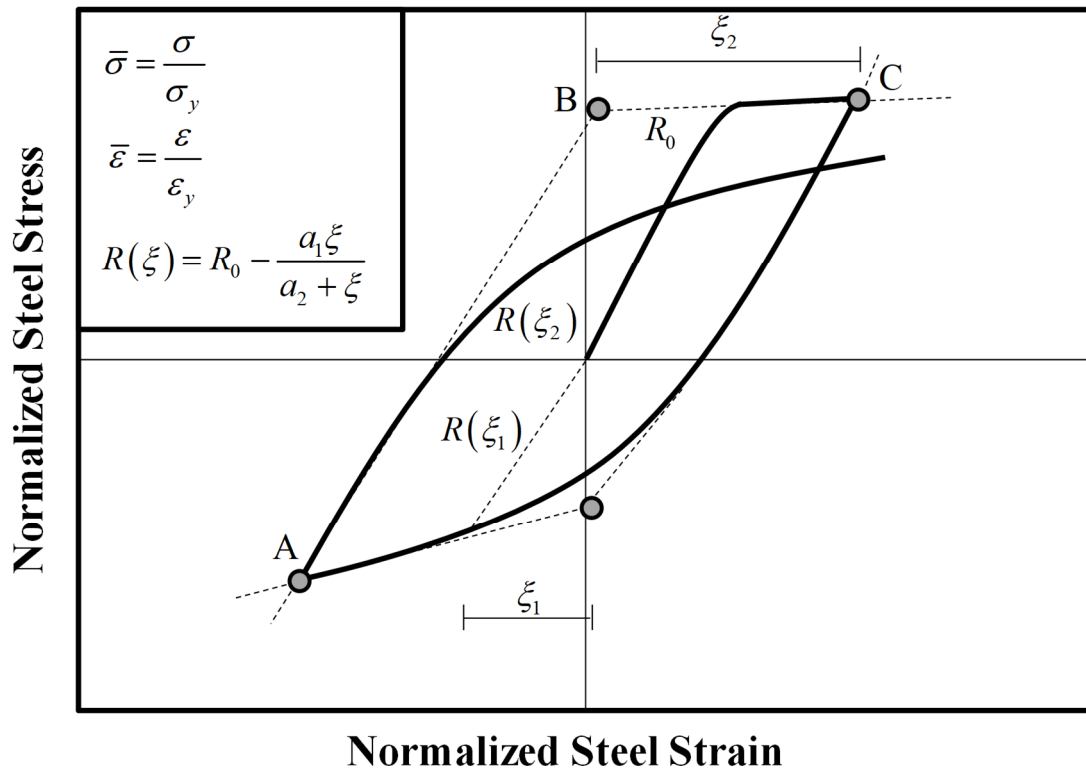


Figure 5-3 Definition of curvature parameter R in Menegotto-Pinto reinforcing steel model [Limkatanyu, 2002]

Due to the drawback of the isotropic hardening effect in the capable of reproducing experimental results, Filippou et al. (1983b) suggested a stress shift in the linear yield asymptote σ_{st} as follows:

$$\sigma_{st} = a_3 \left(\frac{\varepsilon_{\max}}{\varepsilon_y} - a_4 \right) \sigma_y \quad (5-18)$$

where ε_{\max} is the absolute strain at the maximum/minimum strain reversal point which corresponds to the direction of applied stress. ε_y and σ_y are the strain and stress at yield point, respectively, and a_3 and a_4 are the experimental determined parameters. Although the reinforcing steel model in this study accounts the isotropic hardening effect, this feature isn't used in the model implement because the study of Filippou et al. (1983b) discussed the effect of isotropic hardening that the steel model with and without isotropic hardening yield almost identical results. Therefore, the used parameter are: $R_0 = 20$, $a_1 = 18.5$, $a_2 = 0.15$, and $a_3 = a_4 = 0.0$. It can be observed that parameter a_3 and a_4 are equal to zero based on the original model of Menegotto and Pinto (1973).

5.4 Shear Constitutive Model

Based on the concrete and reinforcing steel constitutive models at above demonstration, both models don't include the shear effect in those models so this study introduces the shear constitutive law which is adapted and modified from Mergos and Kappos model [Mergos and Kappos, 2008 and 2012] for the explanation of shear force-shear strain relation of reinforced concrete. Furthermore, the model accounts the shear-flexure interaction effects that lead to the degradation of shear strength and shear stiffness at the plastic hinge regions. The main features of the shear constitutive model in this study are as follows:

- The undamaged primary curve
- The modified Mergos and Kappos shear-flexure interaction procedure
- The hysteretic shear force-shear strain responses

5.4.1 The Undamaged Primary Curve

The shear model starts from the undamaged primary curve to define the monotonically increasing deformation response for the shear hysteretic model. The undamaged primary curve is first derived without the degradation of shear strength and shear stiffness due to the shear-flexure interaction effects as shown in Figure 5-4. The original envelope curve of the shear model was proposed by Mergos and Kappos (2008) and subsequently modified by Mergos and Kappos (2012). As shown in Figure 5-4, the undamaged primary curve is composed of four branches but has only three different slopes.

The first linear portion **oa** with uncracked slope $(GA)_0$ represents the elastic behavior of the uncracked section in shear. As shown in Figure 5-4, the origin point **o** links to the cracking point **a** (V_{cr}, γ_{cr}). The cracking shear force V_{cr} is defined as the point at which the nominal tensile stress exceeds the tensile strength of concrete [Mergos and Kappos, 2008]. As suggested by Sezen and Moehle (2004), the cracking shear force V_{cr} can be expressed as:

$$V_{cr} = \frac{f'_t}{L_u / h} \sqrt{1 + \frac{N}{f'_t A_g}} 0.80 A_g \quad (5-19)$$

where f'_t is the nominal tensile strength of concrete; L_u / h is the shear span ratio; N is the compressive axial force; and A_g is the gross cross section. The uncracked slope $(GA)_0$ is defined in Eq. (5-20), accounted a parabolic shear stress distribution along the cross-section depth.

$$(GA)_0 = 0.80 GA_g \quad (5-20)$$

From the cracking shear force in Eq. (5-19) and the uncracked slope in Eq. (5-20), the cracking shear strain γ_{cr} is simple determined as following:

$$\gamma_{cr} = \frac{V_{cr}}{(GA)_0} \quad (5-21)$$

According to the second linear **ab** and third linear **bc** portions, both linear portions have the same slope of $(GA)_1$. The second linear portion ab connects the cracking point **a** (V_{cr}, γ_{cr}) to the flexure-yielding point **b** (V_y, γ_y) at which the longitudinal reinforced steel reaches to a yielding state for the first time. The yielding information of the longitudinal reinforced steel is provided by the fiber-section model. The third linear portions **bc** attaches the flexure-yielding point **b** (V_y, γ_y) to the shear-yielding point **c** (V_{u0}, γ_{st}). This study defines the shear-yielding point **c** (V_{u0}, γ_{st}) at which the shear strain reaches to the shear strain at the onset of transverse reinforcement yielding γ_{st} while the shear force reaches to its ultimate value V_{u0} .

The shear strain at the onset of transverse reinforcement yielding γ_{truss} can simply approximated by using the truss analogy approach [Park and Paulay, 1975]. Although their approach was based on a rational approach and calibration studies, but it was not accurately due to the axial load and aspect ratio effects. Later, Mergos and Kappos (2012) used the regression analyses to improve the shear strain at the onset of transverse reinforcement yielding equation by two modification factors when one accounts the axial load effect κ and other includes aspect ratio effect λ . Therefore, the shear strain at the onset of transverse reinforcement yielding with modification factors γ_{st} is given by the following equation.

$$\gamma_{st} = \kappa \lambda \gamma_{truss} \quad (5-22)$$

where $\kappa = 1 - 1.07 \left(\frac{N}{f_c' A_g} \right)$ is the modification factor accounting for the axial load effect; $\lambda = 5.37 - 1.59 \min \left(2.5, \frac{L_d}{h} \right)$ is the modification factor accounting for the aspect ratio effect; and γ_{truss} is the shear strain associated with the yielding of transverse reinforcement based on the truss analogy approach [Park and Paulay, 1975] and can be written as following:

$$\gamma_{truss} = \frac{V_{cr}}{(GA)_0} + \frac{A_v f_{yv} \left[\sin^4 \phi + \frac{E_s}{E_c} \rho_v \right]}{s E_s b \rho_v \sin^4 \phi \cot \phi} \quad (5-23)$$

where A_v is the transverse reinforcement area with a spacing s ; b is the section width; E_s is the elastic modulus of steel; E_c is the elastic modulus of concrete; and ϕ represents the angle characterized by the member axis and the direction of diagonal struts. In the research work of Mergos and Kappos (2012), an optimal value of angle ϕ was obtained from the regression analyses between experimental and analytical results. Mergos and Kappos (2012) suggested the optimal value of angle ϕ was 45 degree. Moreover, the cracked slope $(GA)_1$ can simply determine from the geometric of the undamaged primary as:

$$(GA)_1 = \frac{V_{u0} - V_{cr}}{\gamma_{st} - \gamma_{cr}} \quad (5-24)$$

where V_{u0} is the non-degraded sectional shear force at initial state and can simply calculate based on the UCSD shear-strength model in Eq. (2-24) by setting the curvature ductility value ≤ 3 .

The last linear portion **cd** represents the plastic behavior of shear response and links the shear-yielding point **c** (V_{u0}, γ_{st}) to the shear-ultimate point **d** (V_{u0}, γ_u) at which the shear strain reaches to its ultimate γ_u while the shear force reaches to its ultimate value V_{u0} as well as the shear-yielding point **c**. Moreover, the last linear portion **cd** is defined from the experimental observation that shear-critical members can experience additional shear deformation under sustained shear force before the onset of shear failure [Ma et al., 1976; and Aboutaha et al., 1999]. Therefore, the shear strain at ultimate state γ_u may be considerably larger than the shear strain at the onset of transverse reinforcement yielding γ_{st} observed from several research works [Gerin and Adebar, 2004; Sezen, 2008; and Mergos and Kappos, 2012]. Based on the regression analysis in research work of Mergos and Kappos (2012), the shear strain at ultimate point γ_u was approximated among the experimental results for 25 RC members eventually failing in shear with three

modification factors (λ_1 to λ_3). The shear strain at ultimate γ_u can be written by the following equation:

$$\gamma_u = \lambda_1 \lambda_2 \lambda_3 \gamma_{st} \geq \gamma_{st} \quad (5-25)$$

where $\lambda_1 = 1.0 - 2.5 \min(0.40, \frac{N}{f'_c A_g})$ is the parameter accounting for the axial load;

$\lambda_2 = \min(6.25, \frac{L_a^2}{h^2})$ is the parameter accounting for the member aspect ratio; and

$\lambda_3 = 0.31 + 17.8 \min(\frac{A_v f_{yv}}{b s f'_c}, 0.08)$ is the parameter accounting for the amount of

transverse reinforcement. It is important to note that the Mergos and Kappos formula (2012) for γ_{st} and γ_u suggests the criteria: $1.11 \leq \frac{L_a}{h} \leq 3.91$, $0 \leq \frac{N}{f'_c A_g} \leq 0.61$ and

$$0.47\% \leq \frac{A_v f_{yv}}{b s f'_c} \leq 8.13\% .$$

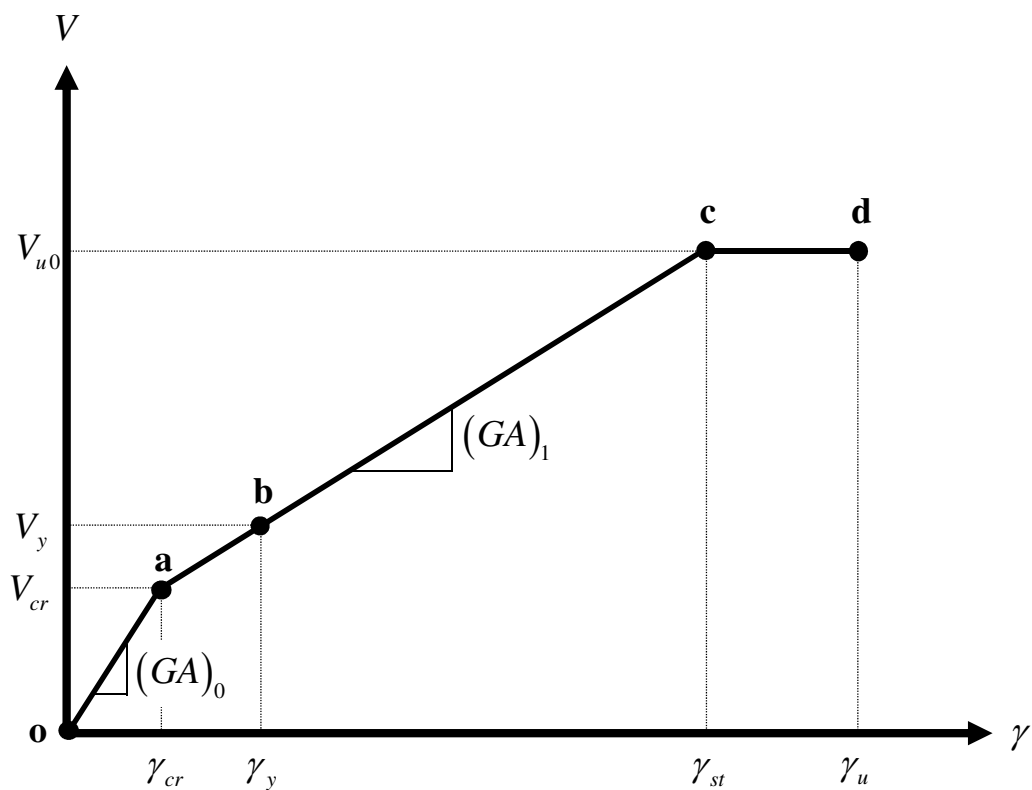


Figure 5-4 The undamaged primary curve of shear constitutive model

[Mergos and Kappos, 2012]

5.4.2 Modified Mergos-Kappos Shear-Flexure Interaction Procedure

The interaction between shear and flexural action has long been recognized in the research community. From the previous research works (e.g. Ghee et al., 1989; Watanabe and Ichinose, 1991; Priestley et al., 1993; and Sezen, 2002), they demonstrated that the inelastic flexural deformation influences on the shear resistance. In other words, the shear strength of a RC section in the plastic hinge region decreases with increasing inelastic flexural deformation. The degradation of shear strength is caused by the concrete damage associated with the inelastic flexural deformation (Plastic-hinge formation). Moreover, the several experimental results (e.g. Lynn, 2001; and Sezen, 2002) were observed that the sectional shear strain in the plastic hinge region increases drastically following the inelastic flexural deformation while shear force is constant. Both phenomena results as above discussion are caused by the influences of the shear-flexure interaction effects. To include these two phenomena results due the shear-flexure interaction in the implement of finite element analysis, Mergos and Kappos (2008 and 2012) introduced the interaction procedure that consider together by combining the UCSD shear-strength model [Priestley et al., 1993] and the truss analogy approach [Park and Pauley, 1975] for the analysis of the RC members with the shear-flexure interaction.

In this research, the interaction method introduced by Mergos and Kappos (2008 and 2012) is adopted and modified to include the sectional shear force-bending moment interaction as discussed here. Figure 5-5 presents the general scheme for the interaction between shear and flexural procedure and the development of the degraded shear envelope curve with increasing curvature ductility demand μ_ϕ . The reduced shear strength is associated with the degradation of the concrete shear-strength component V_c as defined by the UCSD shear-strength model (In Chapter 2) and is influenced to the ordinate of the undamaged shear envelope curve. In other word, the sectional shear response starts to deviate from the undamaged envelope curve when there is the shear strength degradation. The damaged (Reduced) envelope curve is kept updating with the evolution of the

degraded shear strength and the resulting envelope curve is along the path $o-a-b-e-f'-g'-c^s-d^s$ as shown in Figure 5-5. Due to the degraded shear strength, there are three possible cases to be encountered when the shear strain is larger than the shear strain at the flexure-yielding point γ_y at point **b**. It can be expressed as:

The first case (Case I) defines the non-degradation of shear strength case. In other words, the sectional curvature ductility is lesser than 3 ($\mu_\phi \leq 3$). Based on the UCSD shear-strength model, there is no the shear strength degradation. In this case, It can be observed that the sectional shear response points at the start and end of load increment step both locate on the undamaged shear envelope curve with the cracked sectional shear stiffness $(GA)_i$ as shown in Figure 5-5 and 5-6.

The second case (Case II) presents the initial degradation of shear strength case. In this presented case can simply describe that after the curvature ductility exceeds 3 ($\mu_\phi > 3$) for the first time, there is the degradation of shear strength based on the UCSD shear-strength model. The sectional shear response point at the start of load increment step locates on the undamaged primary curve while the end of load increment step lies on the damaged (Reduced) shear envelope curve with the effective sectional shear stiffness $(GA)_{eff}$.

The last case (Case III) represents the post-degradation of shear strength case. After the curvature ductility exceeds 3 ($\mu_\phi > 3$) for the first time (Case II), the sectional shear response points at the start and end of load increment step both locate on the damaged (Reduced) shear envelope curve with the effective sectional shear stiffness $(GA)_{eff}$.

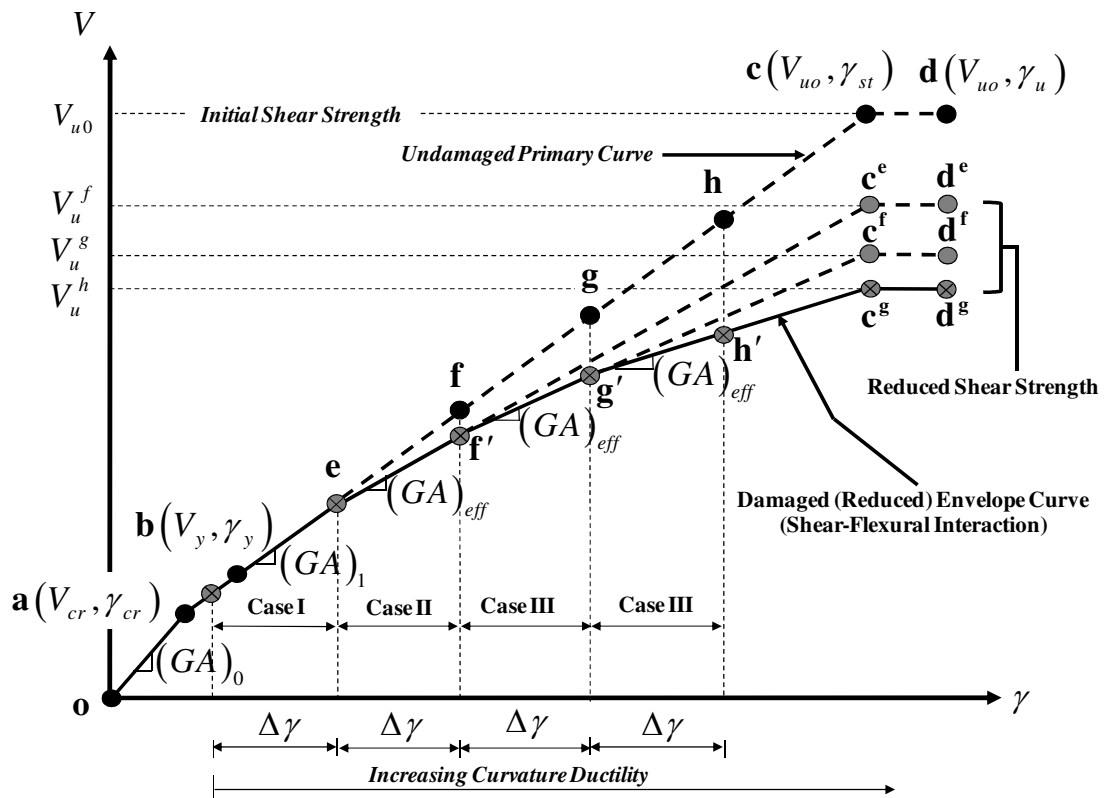


Figure 5-5 The damaged primary curve of shear constitutive model

According to the original research works of Mergos and Kappos (2008 and 2012), their interaction procedure was derived by considering only case I and case II as above discussed. Therefore, Mergos-Kappos interaction procedure is modified in this study to determine the incremental shear force ΔV and the effective sectional shear stiffness $(GA)_{eff}$ by giving the incremental shear strain $\Delta\gamma$ for all above-mentioned cases. The authors refer to this procedure as “*modified Mergos-Kappos*” shear-flexure interaction procedure. In the modified Mergos-Kappos shear-flexure interaction procedure, this study presents the so-called reference shear stiffness $(GA_{ref})_i^k$ which is used to refer the sectional shear response point at end of load increment step on the undamaged shear envelope curve and predict the effective sectional shear stiffness $(GA)_{eff}$. The reference shear stiffness $(GA_{ref})_i^k$ is defined as following:

$$\left(GA_{ref}\right)_i^k = \frac{V_{0,i}^k - V^k}{\Delta\gamma_i^k} \quad (5-26)$$

where $V_{0,i}^k$ is the non-degraded sectional shear force corresponding to the sectional shear strain $\gamma_i^{k+1} = \gamma^k + \Delta\gamma_i^k$ and can be determined as follows:

$$V_{0,i}^k = V_{cr} + (GA)_1 (\gamma_i^{k+1} - \gamma_{cr}) \quad (5-27)$$

It needs to note that the reference shear stiffness $\left(GA_{ref}\right)_i^k$ in case I and II is also equal to the cracked sectional shear stiffness $(GA)_1$ as shown in Figure 5-6. The general representing of the shear-flexure interaction procedure is derived from the relation between incremental shear force ΔV and shear strain $\Delta\gamma$ of the three cases as shown in Figure 5-6. Form the geometric of Figure 5-6, the relation between incremental shear force ΔV and shear strain $\Delta\gamma$ can be expressed as:

$$\Delta\gamma_i^k = \frac{\Delta V_i^k}{\left(GA_{eff}\right)_i^k} = \frac{\Delta V_i^k + \left(\Delta V_c^{deg}\right)_i^k}{\left(GA_{ref}\right)_i^k} \quad (5-28)$$

where ΔV_i^k is the incremental shear force; and $\left(\Delta V_c^{deg}\right)_i^k$ is the degradation of the shear strength associated with the concrete shear strength degradation based on the UCSD shear-strength model and can be determined as following:

$$\left(\Delta V_c^{deg}\right)_i^k = \left(GA_{ref}\right)_i^k \Delta\gamma_i^k - \left(\frac{V_{ui}^k - V^k}{\gamma_{st} - \gamma^k}\right) \Delta\gamma_i^k \quad (5-29)$$

where V_{ui}^k is the degraded shear strength dictated by the variation of the concrete contribution coefficient k_ϕ with the sectional curvature ductility μ_ϕ in Figure 2-9. Based on Eq. (5-28), the effective sectional shear stiffness $\left(GA_{eff}\right)_i^k$ can be rewritten by solving the Eq. (5-28). The new relation can be expressed as:

$$(GA_{eff})_i^k = \frac{\Delta V_i^k}{\Delta V_i^k + (\Delta V_c^{deg})_i^k} (GA_{ref})_i^k \quad (5-30)$$

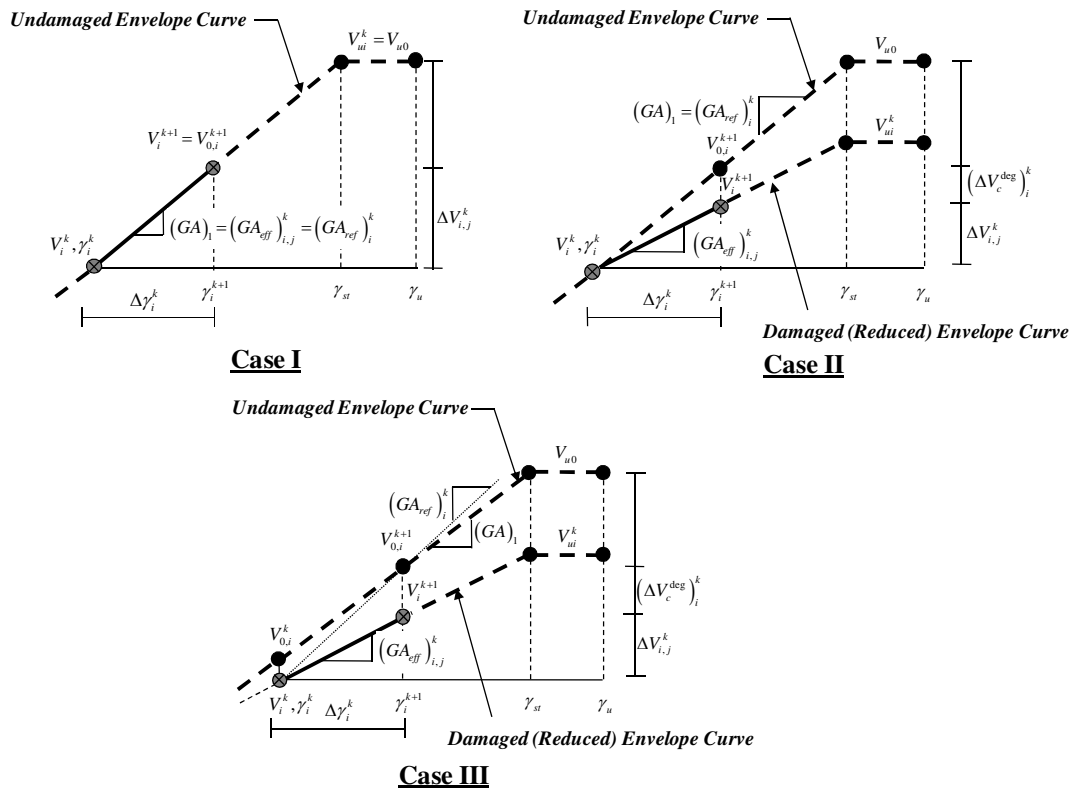


Figure 5-6 Three cases of the incremental shear force-shear strain relation

However, it can be observed from Eq. (5-30) that the effective sectional shear stiffness $(GA_{eff})_i^k$ and the incremental shear force ΔV_i^k are the unknown variables and mutually dependent. To determine these two values, the additional iterative procedure within the element iterative step i of the load increment k is introduced within the modified Mergos-Kappos shear-flexure interaction procedure. It needs to be noted that the following variables $(GA_{ref})_i^k$, $(\Delta V_c^{deg})_i^k$, and $\Delta \gamma_i^k$ are not changed during this additional iterative procedure. Thus, the additional subscript index “ j ” is appended to the effective sectional shear stiffness $(GA_{eff})_i^k$ and the incremental shear force $(\Delta V_{i,j}^k)$ to define the iterative step within the shear-flexure interaction procedure.

Based on Eqs. (5-28) and (5-30), the residual function $\Phi\left((GA_{eff})_{i,j}^k\right)$ can be defined as following:

$$\Phi\left((GA_{eff})_{i,j}^k\right) = (GA_{eff})_{i,j}^k \Delta\gamma_i^k - \frac{(GA_{eff})_{i,j}^k (\Delta V_c^{deg})_i^k}{(GA_{ref})_i^k - (GA_{eff})_{i,j}^k} \quad (5-31)$$

The Newton-Raphson method [Chapra and Canale, 2002] is used to solve the solution of Eq. (5-31). Therefore, the derivative of Eq. (5-31) with respect to the sectional effective shear stiffness $(GA_{eff})_{i,j}^k$ can be written as:

$$\frac{d\Phi\left((GA_{eff})_{i,j}^k\right)}{d(GA_{eff})_{i,j}^k} = \Delta\gamma_i^k - \frac{(\Delta V_c^{deg})_i^k}{(GA_{ref})_i^k - (GA_{eff})_{i,j}^k} - \frac{(GA_{eff})_{i,j}^k (\Delta V_c^{deg})_i^k}{\left((GA_{ref})_i^k - (GA_{eff})_{i,j}^k\right)^2} \quad (5-32)$$

The algorithm of iterative analytical process for the value determinations of the incremental shear force $\Delta V_{i,j}^k$ and the sectional effective shear stiffness $(GA_{eff})_{i,j}^k$ within the element iterative step i of the load increment k is shown in Figure 5-7 and implemented in the following steps:

1. Determine the reference shear stiffness $(GA_{ref})_i^k$ from Eq. (5-26) and the degradation of the shear strength associated with the concrete shear strength degradation $(\Delta V_c^{deg})_i^k$ from Eq. (5-29).
2. Assume the initial the sectional effective shear stiffness value $(GA_{eff})_{i,j=1}^k$. In the presented research, the initial value of $(GA_{eff})_{i,j=1}^k$ is suggested to set $(GA_{eff})_{i,j=1}^k = (GA_{eff})_{i-1}^k$.
3. Start the iterative procedure ($j \geq 1$) for the shear-flexure interaction within the element iterative step i of the load increment k .

(a) Calculate the residual function $\Phi\left((GA_{eff})_{i,j}^k\right)$ based on Eq. (5-31):

$$\Phi\left((GA_{eff})_{i,j}^k\right) = (GA_{eff})_{i,j}^k \Delta\gamma_i^k - \frac{(GA_{eff})_{i,j}^k (\Delta V_c^{deg})_i^k}{(GA_{ref})_i^k - (GA_{eff})_{i,j}^k}$$

(b) Determine the slope of residual function $d\Phi\left((GA_{eff})_{i,j}^k\right) / d(GA_{eff})_{i,j}^k$ based on Eq. (5-32):

$$\frac{d\Phi\left((GA_{eff})_{i,j}^k\right)}{d(GA_{eff})_{i,j}^k} = \Delta\gamma_i^k - \frac{(\Delta V_c^{deg})_i^k}{(GA_{ref})_i^k - (GA_{eff})_{i,j}^k} - \frac{(GA_{eff})_{i,j}^k (\Delta V_c^{deg})_i^k}{\left((GA_{ref})_i^k - (GA_{eff})_{i,j}^k\right)^2}$$

(c) Update the effective sectional shear stiffness $(GA_{eff})_{i,j+1}^k$:

$$(GA_{eff})_{i,j+1}^k = (GA_{eff})_{i,j}^k - \left(\frac{\Phi\left((GA_{eff})_{i,j}^k\right)}{d\Phi\left((GA_{eff})_{i,j}^k\right) / d(GA_{eff})_{i,j}^k} \right)$$

(d) Compute the update residual function $\Phi\left((GA_{eff})_{i,j+1}^k\right)$ based on the effective sectional shear stiffness $(GA_{eff})_{i,j+1}^k$ in step 3 (c).

4. Check if the update residual value in step 3 (d) is lesser than the specified tolerance (ε_{tol}):

(i) If no, set $j = j + 1$ and go to step 3 (a).

(ii) If yes, return the current sectional shear force $V_i^{k+1} = V_i^k + (GA_{eff})_{i,j}^k \Delta\gamma_i^k$ and the current effective sectional shear stiffness $(GA_{eff})_{i,j}^k$

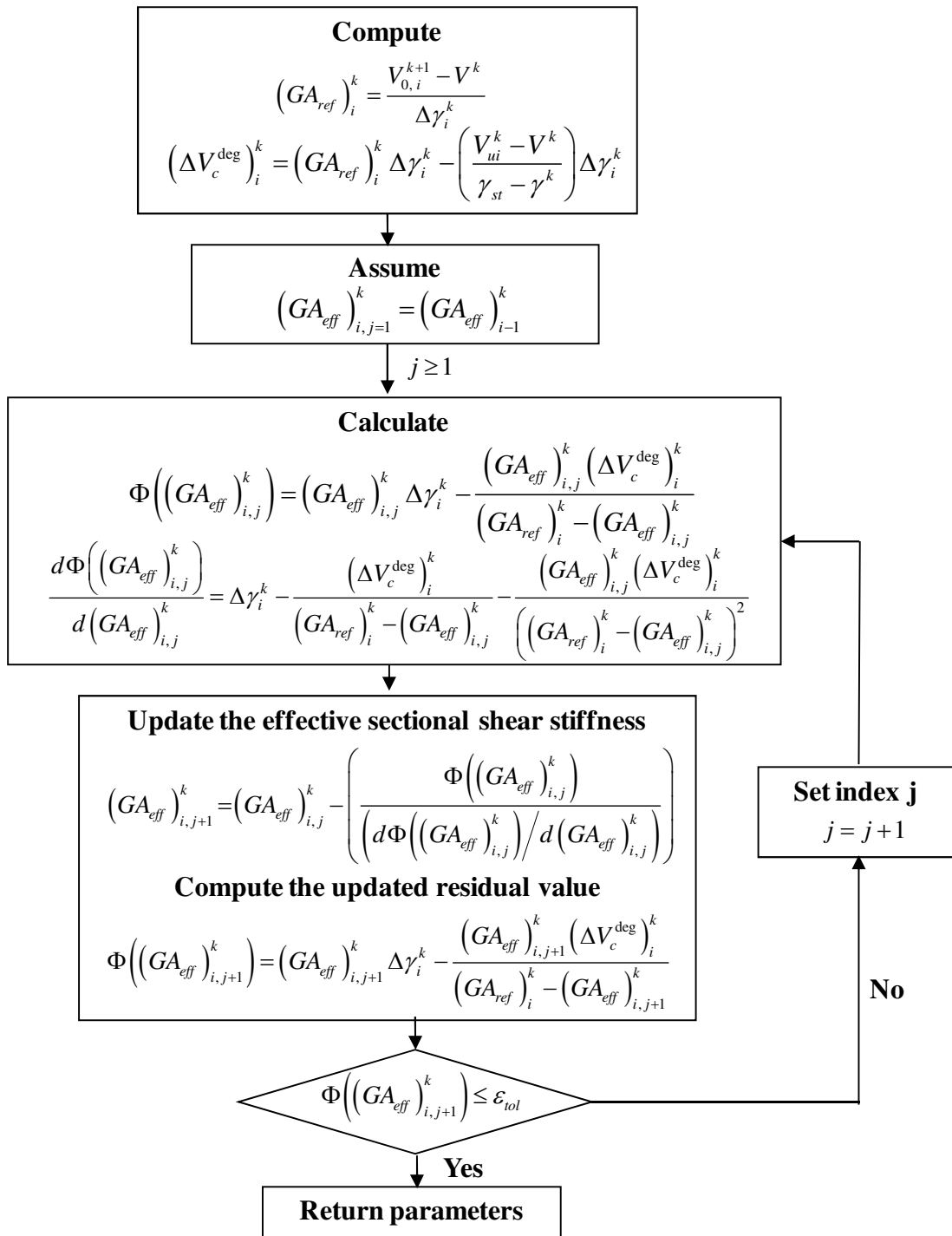


Figure 5-7 The step-by-step algorithm for iterative procedure within the shear-flexure interaction procedure

5.4.3 The Hysteretic Shear Force-Shear Strain Responses

In this study, the sectional shear response under cyclic loading can determine from a hysteretic of shear law as shown in Figure 5-8. The hysteretic of shear force-shear strain relation is based on the uniaxial behaviors and is expressed in term of shear strain. The rule of presented hysteretic model is adopted and modified from the rule of hysteretic moment-rotation relation with pinching and damage proposed by Filippou et al. (1992) and subsequently improved by Martino (1999). Moreover, the presented hysteretic model is attractive since it can represent both damages and pinching effect and cover all the behavior of RC member prior and post-concrete cracking, the flexure-yielding, the transverse reinforcement yielding, and the shear failure. The general shape of the modified hysteretic shear as shown in Figure 5-8 is separated into the four parts as following:

- The monotonic shear force-shear strain relation
- The behavior during unloading state
- The behavior during reloading state
- The reduced shear force-shear strain envelope due to the crack opening

5.4.3.1 The Monotonic Shear Force-Shear Strain Relation

The monotonic envelop curve follows the undamaged envelope curve and the damaged (Reduced) envelope curve due to the shear-flexure interaction effect as above described. The monotonic envelop curve composed of two envelop curves, one in the positive direction and another in the negative direction. During each cycle, the reversal points are updated and used to predict the characteristic shear strain values with damage in the next cycle. The relation between shear force and shear strain can express as:

1. An initial branch (Path $O-A$ and $O-B$)

$$V^{k+1} = (GA)_0 \gamma^{k+1} \quad \text{for} \quad |\gamma^{k+1}| \leq \gamma_{cr} \quad (5-33)$$

2. An post-concrete cracking branch (Path $A-C$)

$$V^{k+1} = V_{cr} + (GA)_1 (\gamma^{k+1} - \gamma_{cr}) \quad \text{for} \quad \gamma_{cr} < |\gamma^{k+1}| \leq \gamma_y \quad (5-34)$$

3. An post-flexural yielding branch (Path $C-D$, $F-G$, and $J-K$)

$$V^{k+1} = V^k + (GA_{eff})_i^k \Delta \gamma^k \quad \text{for} \quad \gamma_y < |\gamma^{k+1}| \leq \gamma_{st} \quad (5-35)$$

4. An ultimate branch (Path $K-L$)

$$V^{k+1} = V_{ui}^k \quad \text{for} \quad \gamma_{st} < |\gamma^{k+1}| \leq \gamma_u \quad (5-36)$$

where the subscribed number index i denotes to the element iterative step of the load increment k .

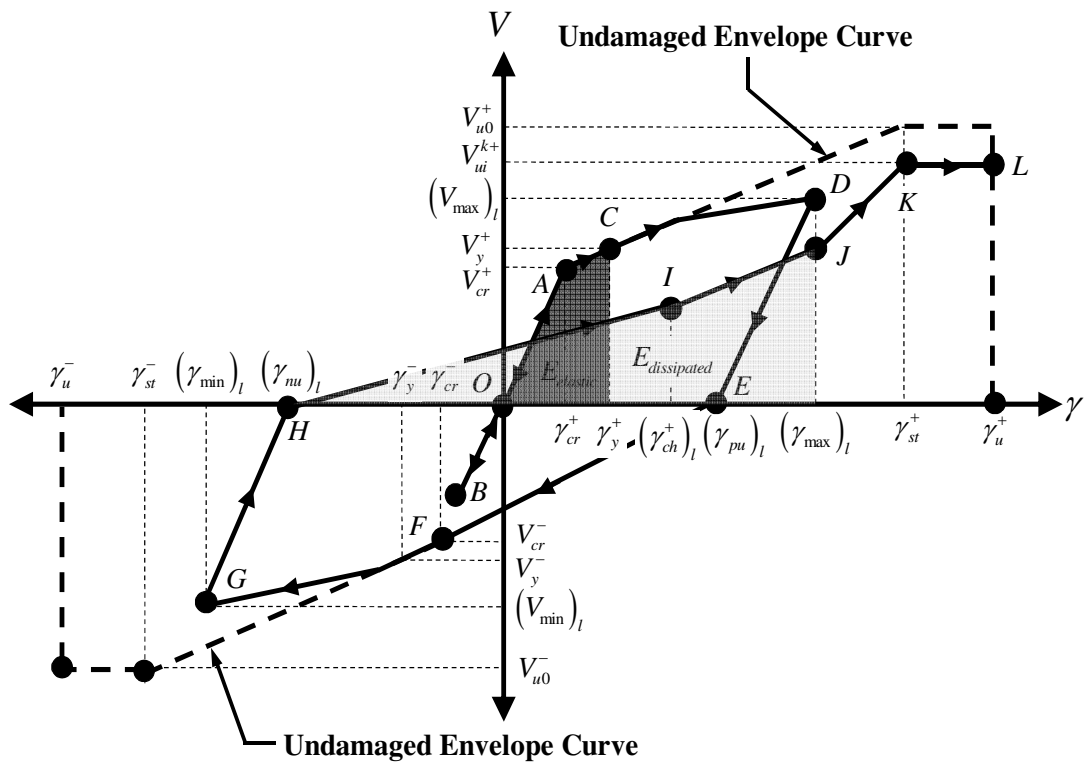


Figure 5-8 The hysteretic of shear model

5.4.3.2 The Behavior During Unloading State

When load reversal occurs, unloading takes place along a straight line with the uncracked slope $(GA)_0$ until the reloading state is reached. The sectional shear response during the unloading state can calculate from Eq. (5-37) for the positive shear strain increment and Eq. (5-38) for the negative shear strain increment, respectively.

1. Unloading state at the positive shear strain increment (Path $G-H$)

$$V^{k+1} = V^k + (GA)_0 \Delta\gamma_i^k \quad \text{for} \quad \gamma^{k+1} < (\gamma_{nu})_l \quad (5-37)$$

2. Unloading state at the negative shear strain increment (Path $D-E$)

$$V^{k+1} = V^k + (GA)_0 \Delta\gamma_i^k \quad \text{for} \quad \gamma^{k+1} > (\gamma_{pu})_l \quad (5-38)$$

where $(\gamma_{nu})_l$ and $(\gamma_{pu})_l$ are the last shear strain for complete negative and positive unloading at cycle l , respectively.

5.4.3.3 The Behavior During Reloading State

The reloading curve is separated into two phases, one in the elastic phase and another one in the post-concrete cracking phase. The reloading in the elastic phase exhibits the elastic behavior of uncracked section in shear. As the result, the sectional shear response can reverse into the original point without damage due to the crack opening on the reinforced concrete section as shown at the path $O-B$ and $O-A$ in Figure 5-8. In the post-concrete cracking phase, the reloading state is composed of two paths. The initial reloading path is directed towards to the so-called as “breakpoint” (Point I) which is a function of the maximum/minimum sectional shear force and shear strain. The breakpoint is defined by the pinching parameters $(\xi_x$ and ξ_y) which use to modify the maximum/minimum shear force and shear strain (Point J). While the initial reloading path reaches to the breakpoint, the opening crack in the opposite reloading direction

must be closed. Finally, the second reloading path is directed towards to the maximum/minimum deformation with damage (Point J) of earlier cycles in the same direction of loading. The sectional shear force at reloading state can calculate following as:

1. Reloading state at the positive shear strain increment ($\Delta\gamma_i^{k+1} > 0$)

1.1. Elastic reloading branch (Path $O - A$)

$$V^{k+1} = (GA)_0 \gamma^{k+1} \quad \text{for} \quad \gamma^{k+1} < \gamma_{cr}^+ \quad (5-39)$$

1.2. First reloading branch (Path $H - I$)

$$V^{k+1} = (\gamma^{k+1} - (\gamma_{nu})_i) (GA_{rel1}^+)_i \quad \text{for} \quad (\gamma_{nu})_i \leq \gamma^{k+1} < (\gamma_{ch}^+)_i \quad (5-40)$$

$$(GA_{rel1}^+)_i = \frac{\xi_y (V_{max})_i}{(\gamma_{ch}^+)_i - (\gamma_{nu})_i} \quad \text{for} \quad (\gamma_{nu})_i \leq \gamma^{k+1} < (\gamma_{ch}^+)_i \quad (5-41)$$

1.3. Second reloading branch (Path $I - J$)

$$V^{k+1} = \xi_y (V_{max})_i (\gamma^{k+1} - (\gamma_{ch}^+)_i) (GA_{rel2}^+)_i \quad \text{for} \quad \gamma^{k+1} \geq (\gamma_{ch}^+)_i \quad (5-42)$$

$$(GA_{rel2}^+)_i = \frac{(1 - \xi_y) (V_{max})_i}{(\gamma_{max})_i - (\gamma_{ch}^+)_i} \quad \text{for} \quad \gamma^{k+1} \geq (\gamma_{ch}^+)_i \quad (5-43)$$

where $(GA_{rel1}^+)_i$ and $(GA_{rel2}^+)_i$ are the reloading sectional shear stiffness of the first and second reloading path in the positive shear strain increment, respectively; ξ_x and ξ_y are the pinching parameters in x and y direction, respectively; and $(\gamma_{ch}^+)_i$ is the shear strain in the positive shear strain increment at the break point of cycle i and can calculate as following:

$$(\gamma_{mp1}^+)_i = (\gamma_{nu})_i + \xi_y ((\gamma_{max})_i - (\gamma_{nu})_i) \quad \text{for} \quad \Delta\gamma_i^k > 0 \quad (5-44)$$

$$\left(\gamma_{mp2}^+\right)_l = \left(\gamma_{\max}\right)_l - \frac{(1-\xi_y)(V_{\max})_l}{(GA)_0} \quad \text{for} \quad \Delta\gamma_i^k > 0 \quad (5-45)$$

$$\left(\gamma_{ch}^+\right)_l = \left(\gamma_{mp1}^+\right)_l + \left(\left(\gamma_{mp2}^+\right)_l - \left(\gamma_{mp1}^+\right)_l\right)\xi_x \quad \text{for} \quad \Delta\gamma_i^k > 0 \quad (5-46)$$

2. Reloading state at the negative shear strain increment ($\Delta\gamma_i^k < 0$)

2.1. Elastic reloading branch (Path $O-B$)

$$V^{k+1} = (GA)_0 \gamma^{k+1} \quad \text{for} \quad \gamma^{k+1} > \gamma_{cr}^- \quad (5-47)$$

2.2. First reloading branch

$$V^{k+1} = \left(\gamma^{k+1} - \left(\gamma_{pu}\right)_l\right) (GA_{rel1}^-)_l \quad \text{for} \quad \left(\gamma_{ch}^-\right)_l < \gamma^{k+1} \leq \left(\gamma_{pu}\right)_l \quad (5-48)$$

$$(GA_{rel1}^-)_l = \frac{\xi_y (V_{\min})_l}{\left(\gamma_{ch}^-\right)_l - \left(\gamma_{pu}\right)_l} \quad \text{for} \quad \left(\gamma_{ch}^-\right)_l < \gamma^{k+1} \leq \left(\gamma_{pu}\right)_l \quad (5-49)$$

2.3. Second reloading branch

$$V^{k+1} = \xi_y (V_{\min})_l \left(\gamma^{k+1} - \left(\gamma_{ch}^-\right)_l\right) (GA_{rel2}^-)_l \quad \text{for} \quad \gamma^{k+1} \leq \left(\gamma_{ch}^-\right)_l \quad (5-50)$$

$$(GA_{rel2}^-)_l = \frac{(1-\xi_y)(V_{\min})_l}{\left(\gamma_{\min}\right)_l - \left(\gamma_{ch}^-\right)_l} \quad \text{for} \quad \gamma^{k+1} \leq \left(\gamma_{ch}^-\right)_l \quad (5-51)$$

where $(GA_{rel1}^-)_l$ and $(GA_{rel2}^-)_l$ are the reloading sectional shear stiffness of the first and second reloading path in the negative shear strain increment, respectively; and $(\gamma_{ch}^-)_l$ is the shear strain in the negative shear strain increment at the break point of cycle l and can calculate as following:

$$\left(\gamma_{mp1}^-\right)_l = \left(\gamma_{pu}\right)_l + \xi_y \left(\left(\gamma_{\min}\right)_l - \left(\gamma_{pu}\right)_l\right) \quad \text{for} \quad \Delta\gamma_i^k < 0 \quad (5-52)$$

$$(\gamma_{mp2}^-)_l = (\gamma_{\min}^-)_l - \frac{(1 - \xi_y)(V_{\min})_l}{(GA)_0} \quad \text{for} \quad \Delta\gamma_i^k < 0 \quad (5-53)$$

$$(\gamma_{ch}^-)_l = (\gamma_{mp1}^-)_l + \left((\gamma_{mp2}^-)_l - (\gamma_{mp1}^-)_l \right) \xi_x \quad \text{for} \quad \Delta\gamma_i^k < 0 \quad (5-54)$$

5.4.3.4 The Reduced Shear Force-Shear Strain Envelope Due to the Crack Opening

In addition to the damages on the envelope curve due to the shear-flexure interaction effects, the presented shear model includes the damages due to the crack opening in the reinforced concrete section. The crack opening leads to lose the ability to achieve the nominal strength (Loss of bond between concrete and reinforcing steel) and the ability of the concrete to dissipate energy in each the shear hysteresis loop. The brief discussion of those damages can be express as follows. First, when the sectional shear response reaches to the reverse points (point *D* and *G*), the unloading will take place and the maximum/minimum shear strain is updated with the damage parameters (d_1 and d_2). It can see in Figure 5-8 that the maximum points (point *J*) or the minimum points in the considering steps aren't higher than the maximum points (point *D*) or the minimum points of the previous cycles due to the hysteretic energy dissipation and the damage of maximum/minimum responses. The reduced characteristic of maximum and minimum shear strain values are defined as:

$$(\gamma_{\min})_l = (\gamma_{\min})_{l-1} \left[1 + \frac{d_1 \left((\gamma_{\min})_l - \gamma_y^- \right)}{\gamma_y^-} + d_2 \left(\frac{E_{dissipated}}{E_{elastic}} \right) \right] \quad \text{for} \quad \begin{array}{l} (\gamma_{\min})_l < \gamma_y^- \\ \text{and} \\ (\gamma^{k+1})_{l-1} = (\gamma_{\min})_l \end{array} \quad (5-55)$$

$$(\gamma_{\max})_l = (\gamma_{\max})_{l-1} \left[1 + \frac{d_1 \left((\gamma_{\max})_l - \gamma_y^+ \right)}{\gamma_y^+} + d_2 \left(\frac{E_{dissipated}}{E_{elastic}} \right) \right] \quad \text{for} \quad \begin{array}{l} (\gamma_{\max})_l > \gamma_y^+ \\ \text{and} \\ (\gamma^{k+1})_{l-1} = (\gamma_{\max})_l \end{array} \quad (5-56)$$

where d_1 is the damage factor which accounts for the loss of section strength; d_2 is the damage factor which accounts for the loss the ability of section to dissipate

energy; $E_{dissipated}$ is the energy absorption (Area under path $H-I-J$ of Figure 5-8); $E_{elastic}$ is the energy absorption at yield (Area under path $O-A-C$ of Figure 5-8); and the superscribed plus and minus symbols refer to the positive and negative considering quadrants, respectively.

CHAPTER 6

Numerical Verification of Model

6.1 Introduction

This chapter presents the analytical results obtained from the presented numerical examples which are performed to assess accuracy and efficiency of the proposed RC frame element under cyclic loading. Furthermore, the importance of including shear-flexure interaction effects is discussed herein. The results from the experimental tests are used to represent the benchmark and to compare with the analytical results obtained from the proposed frame model. The numerical examples are divided into two sets. The first set presents two RC columns which eventually failed in shear following flexural yielding. This type of member is referred to as a “*flexure-shear*” critical member. Furthermore, these numerical examples are used to discuss the effects of interaction between flexure and shear on both global and local responses. Finally, the last set demonstrates the cyclic responses of the RC member which failed in shear before reaching its flexural capacity. This type of member is referred to as a “*shear*” critical member.

6.2 Flexure-Shear critical R/C members

The first and second numerical examples represent the flexure-shear critical members and the characteristic of older existing columns with insufficient transverse reinforcement and poor seismic details (Non-ductile RC columns). Both columns in the first and second numerical examples are selected from the full-scale experimental tests on RC square columns tested by Sezen (2002) and Lynn (2001), respectively. The detail of the numerical analysis results can describe as follows:

6.2.1 Example I: Column 2CLD12 [Sezen, 2002]

The first example used to verify the accuracy and efficiency of the proposed frame element and show the essence of accounting for shear-flexure interaction effects on shear responses is the column 2CLD12 which was one of the experiments on RC square columns representing older existing column with insufficient transverse reinforcement details tested by Sezen (2002). The column was subjected to a constant axial load and cyclic lateral displacements in double bending. According to the recent research work, Mergos and Kappos (2008) used the same column to validate their distributed flexibility frame element with shear-flexure interaction.

The column 2CLD12 geometry is shown in Figure 6-1. The cross section specimen is $457.2 \times 457.2 \text{ mm}^2$ with eight #9 deformed longitudinal reinforcement bars (28.7 mm diameter). Concrete strength is 21 MPa and longitudinal reinforcement yielding strength and transverse reinforcement yielding strength are 434 MPa and 476 MPa, respectively. The transverse reinforcement of this specimen represents by the square hoops of #3 deformed bars (9.5 mm diameter) with 90° hooks and has a spacing of 305 mm. The volumetric ratio of transverse reinforcement is 0.0017 based on the transverse reinforcement details. The clear height of specimen is 2,946 mm and is subjected to lateral load cycles in double bending under a constant axial load of 667 kN (Corresponding to approximately $0.15\% f'_c A_g$). The above properties of the column 2CLD12 were provided by Sezen (2002). Base on the numerical model, the column is discretized into 16 elements with 7 Gauss-Lobatto integration points and the frame cross-section is discretized into 40 fibers to represent the nonlinear responses of this numerical example. The initial shear strength V_{u0} can predict based on the UCSD shear-strength model [Priestley et al., 1993] in Eq. (2-24) about 515.56 kN.

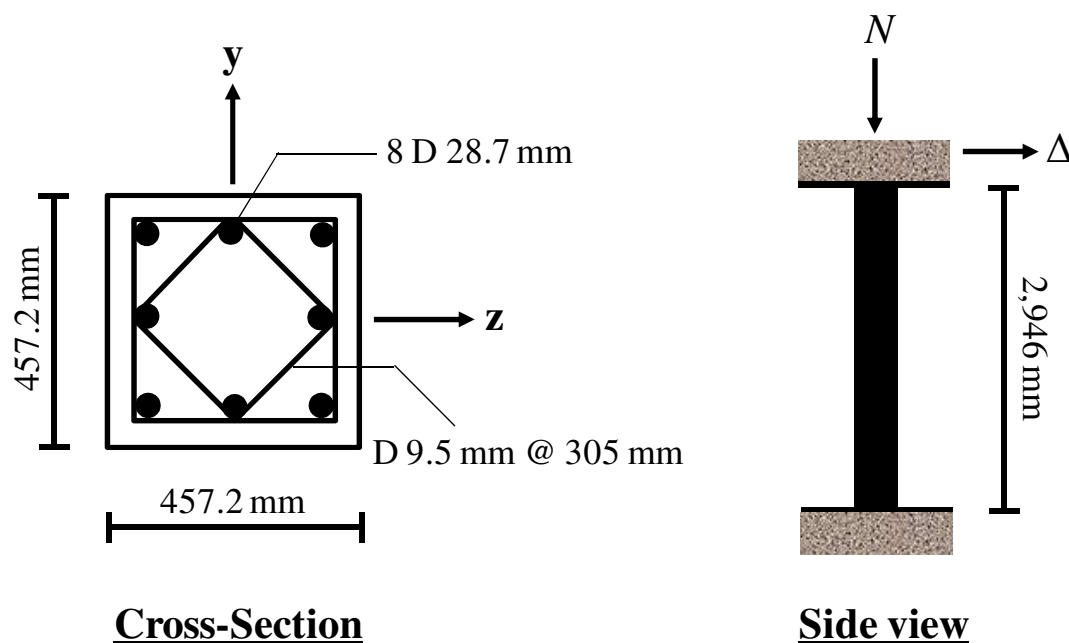
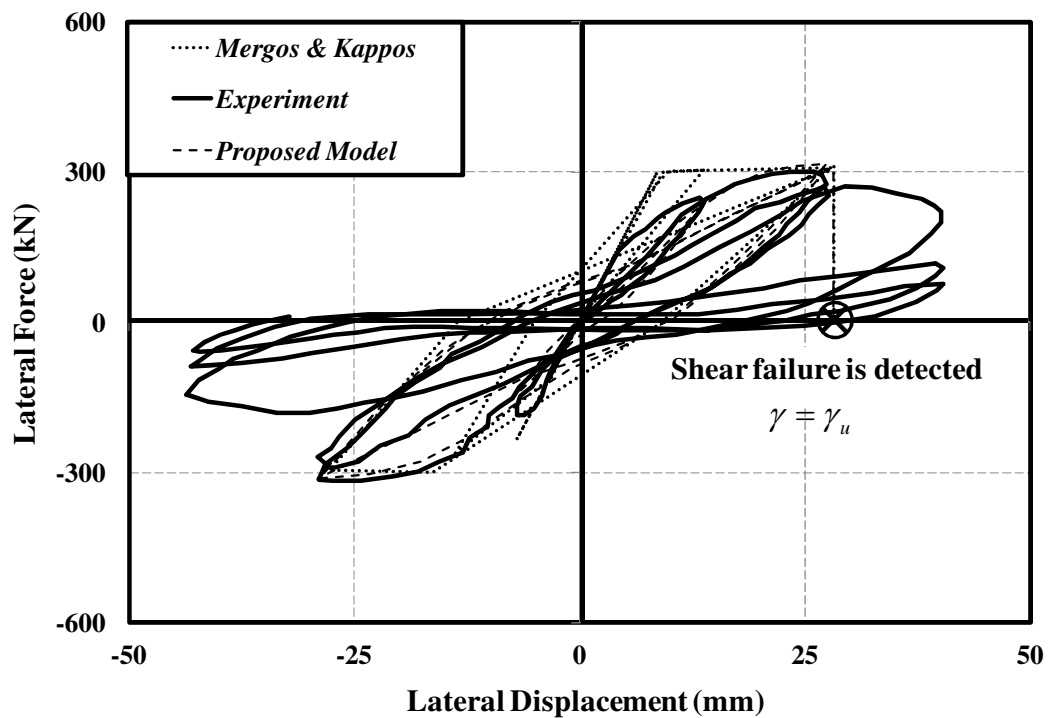


Figure 6-1 The specimen geometry of column 2CLD12 [Sezen, 2002]

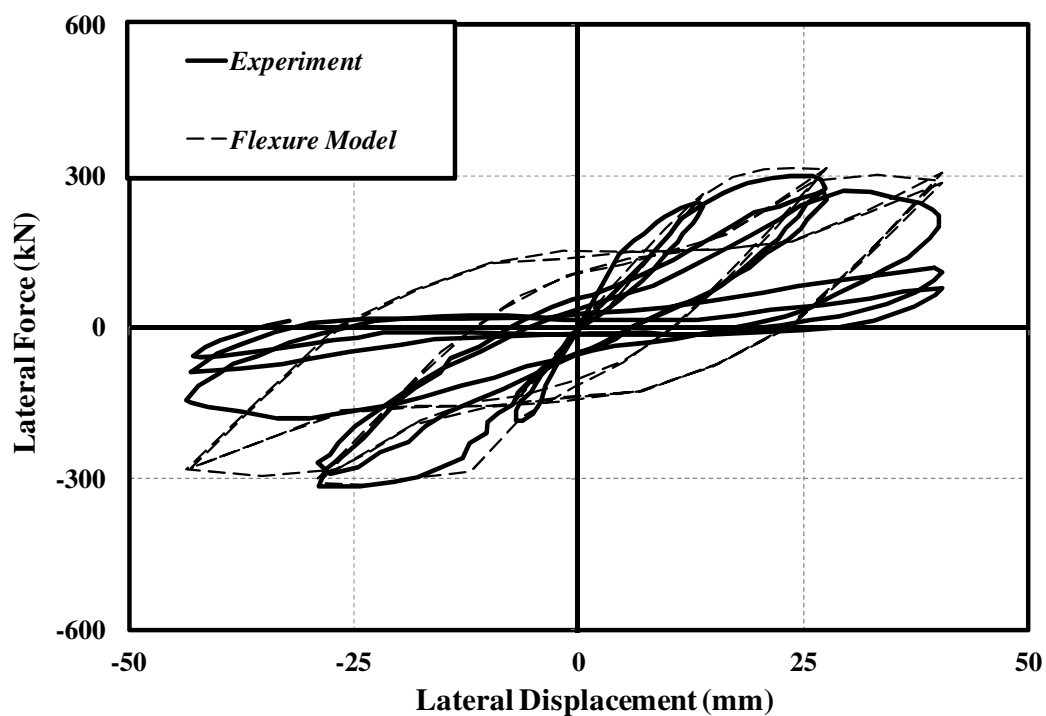
Figure 6-2 (a) shows the tip load-displacement response as derived by Mergos and Kappos model (2008) and proposed model while Figure 6-2 (b) demonstrates the tip load-displacement response obtained from the flexural model proposed by Spacone et al. (1996). The benchmark response is obtained from the experimental data tested by Sezen (2002). To compare with the experimental result as shown in Figure 6-2 (a), it can be seen that the proposed model is able to represent the complex behavior of the experimental result very well, though the initial stiffness is lower estimation because the tensile strength of concrete is not included in the numerical model as discussed in Chapter 5. According to the results, the proposed model can capture the member capacity, stiffness degradation with increasing displacement amplitude, amount of dissipated hysteretic energy, and general shape of hysteretic response. Moreover, the proposed model can represent a smoother load-displacement response when compared to the Mergos and Kappos model (2008). This benefit is because of the fiber-section model used to represent the characteristic of the column cross-section responses while the Mergos and Kappos model used the bilinear yield-oriented moment-curvature curve to represent the characteristic of the column responses. As the result, the Mergos and Kappos

model (2008 and 2012) failed to represent the smooth yielding process of column cross-section in flexure. From the numerical analysis result, the proposed model can predict the first plastic-hinge formation at the lateral displacement Δ_y about 13.80 mm and shear strain γ_y about 1.58×10^{-3} . Based on the experimental observation [Sezen, 2002], the lateral displacement Δ_u associated with the onset of rapid shear strength degradation is equal to 28.00 mm while the proposed model can predict the column failure in shear at the lateral displacement Δ_u about 28.21 mm. This value is in good agreement for the numerical prediction.

Figure 6-2 (b) presents the importance of considering the shear-flexure interaction effects from the numerical responses obtained with the flexural model [Spacone et al., 1996] when compared to the experimental result. It can observe that the flexural model can predict well the column strength but the shear failure due to the shear-flexure interaction at the plastic-hinge formation cannot be predicted by the flexural model. Therefore, the frame element with inclusion of the shear-flexure interaction effects is necessary and essential in the simulating the response of RC columns that fails in shear following the flexure yielding (Ductile shear failure).



(a)

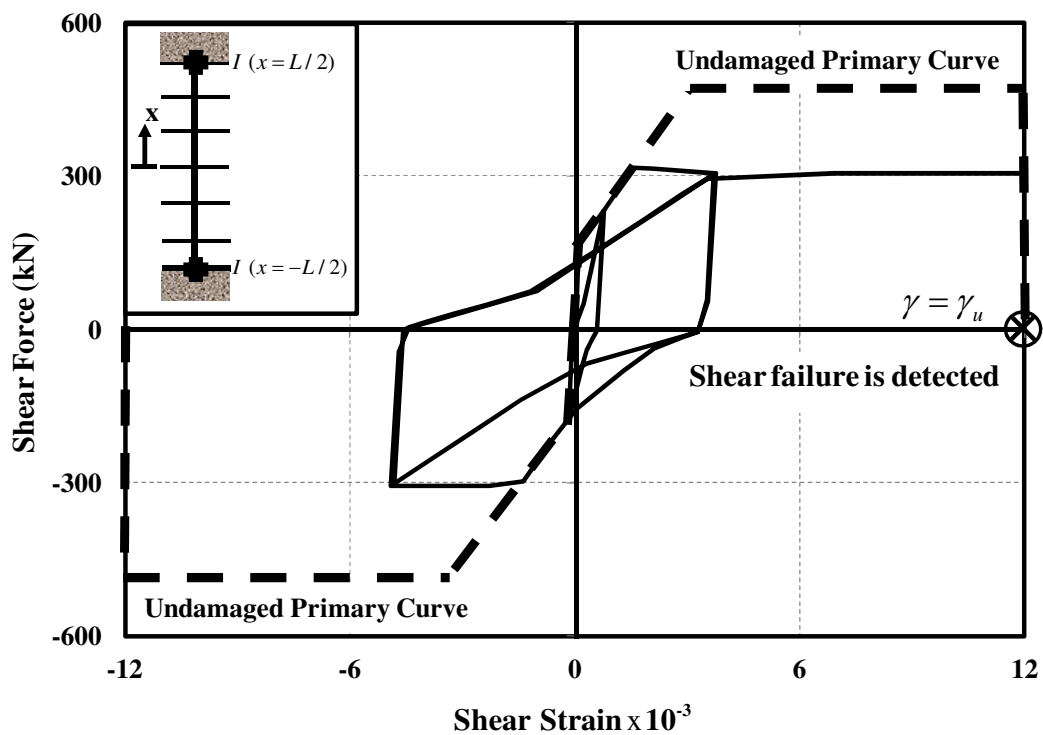


(b)

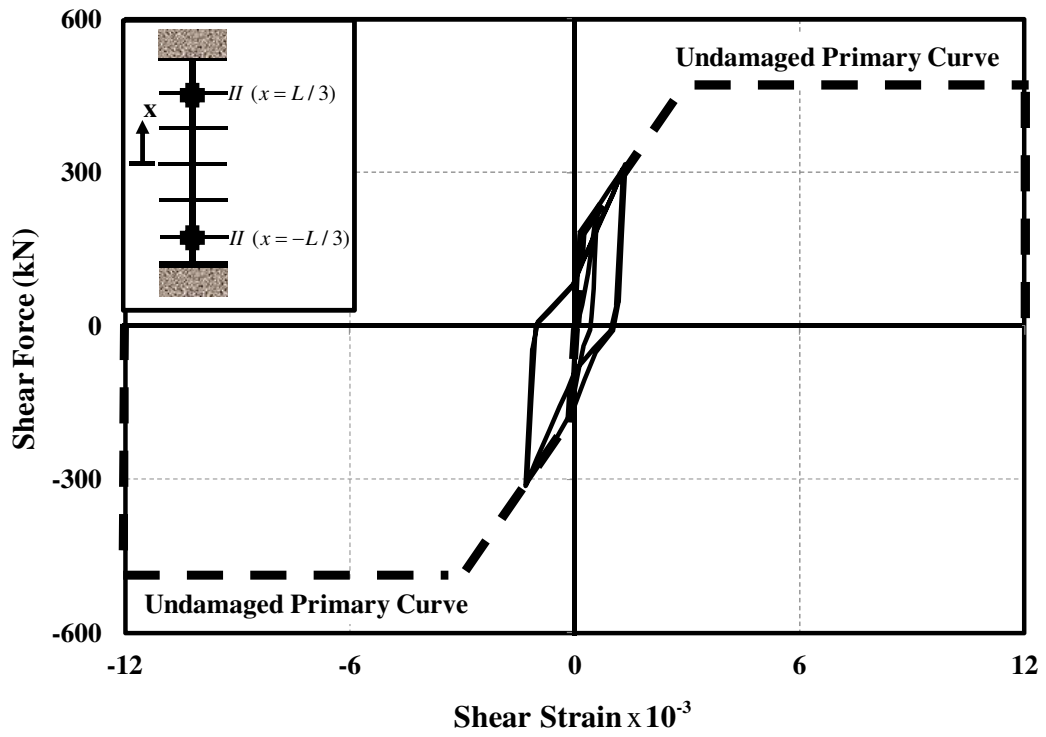
Figure 6-2 The lateral load-displacement response of the end column 2CLD12 obtained from: (a) the Mergos and Kappos model and the proposed model and (b) the flexure model

Figure 6-3 presents the hysteretic shear responses at various monitoring sections (Section I, II, III, and IV) along the column length. Based on the restrained conditions at column ends, the plastic hinges only form at the end of the columns (Section I). Therefore, the hysteretic shear response within the plastic-hinge regions (Section I) as shown in Figure 6-3 (a) is different from the hysteretic shear responses outside the plastic-hinge regions (Section II, III, and IV) due to the shear-flexure interaction effects as shown in Figure 6-3 (b) to (d). From the numerical result in Figure 6-3 (a), the sectional shear response starts to deviate from the undamaged envelope curve to the damaged envelope curve due to the shear-flexural interaction as predicted by the UCSD shear-strength model [Priestley et al., 1993] when the sectional curvature ductility reaches its threshold value of 3. On the other hand, the numerical results in Figure 6-3 (b) to (d) are almost identical. This relies on the fact

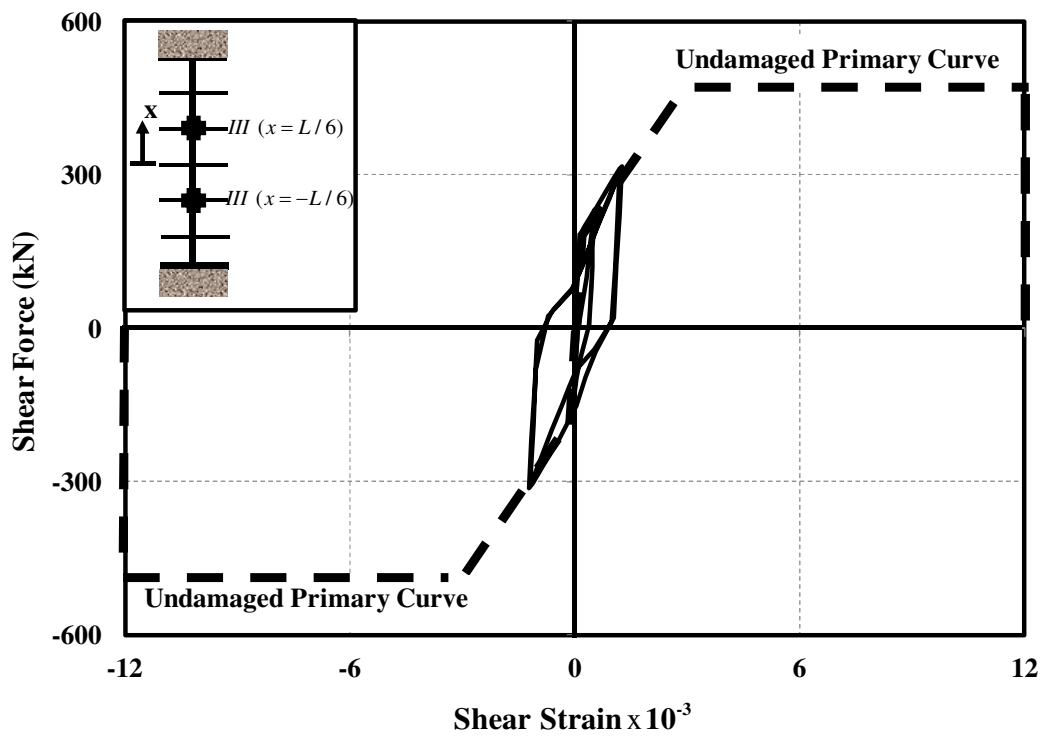
that the sectional shear responses outside the plastic-hinge regions (Section II, III, and IV) are not experienced with the shear-flexure interaction. As the result, it is observed from the hysteretic shear responses at all sections (Figure 6-3 (a) to (d)) that while the magnitude of shear force is the same value along the column length as governed by the equilibrium, the sectional shear strain at section I is much larger than the sectional shear strain at section II, III, and IV. Finally, the shear failure is detected at the hysteretic shear response within the plastic-hinge regions (Section I) when the sectional shear strain reaches its ultimate value of $\gamma_u = 1.2 \times 10^{-3}$. This value is obtained from Eq. (5-25) as suggested by Mergos and Kappos (2012). It is worth noting that this value is in good agreement with the experimental result of 1.00×10^{-3} as proposed in the research work of Mergos and Kappos (2012).



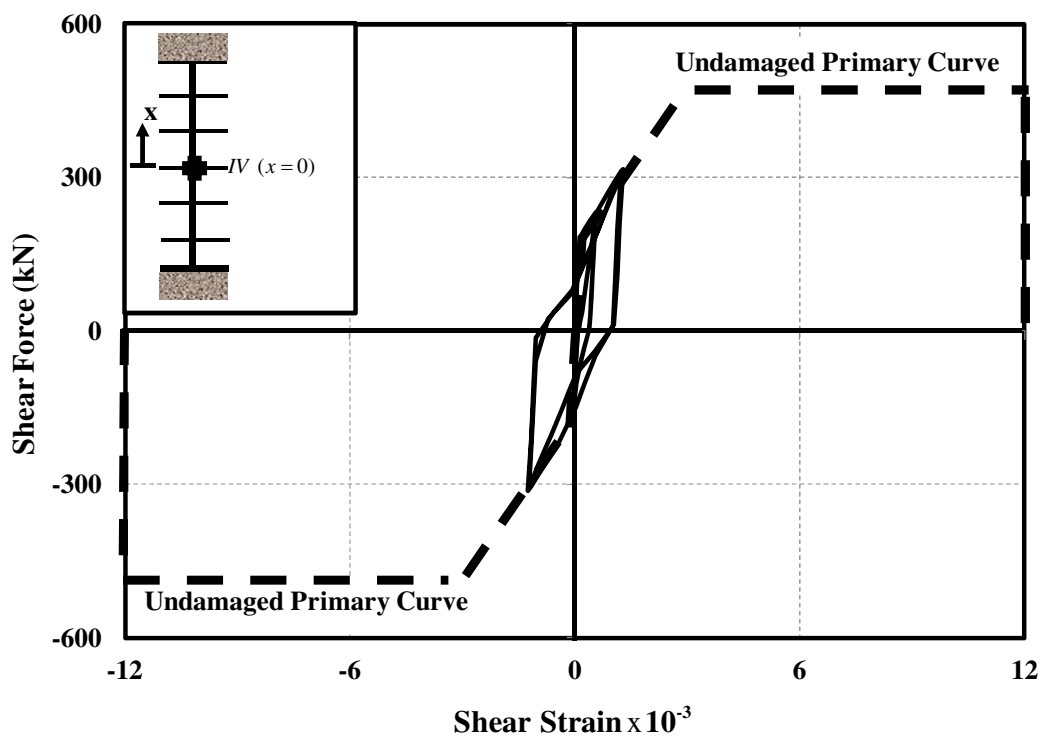
(a)



(b)



(c)



(d)

Figure 6-3 The hysteretic shear responses of column 2CLD12 at various monitoring sections: (a) section I ($x = L / 2$); (b) section II ($x = L / 3$); (c) section III ($x = L / 6$) and (d) section IV ($x = 0$)

Figure 6-4 illustrates the variations of shear force (Demand) and shear strength (Capacity) with the curvature ductility at the end of a column (Section I). From Figure 6-4, the shear failure envelope is constructed based on the UCSD shear-strength model [Priestly et al., 1993]. It is observed that the shear-flexure interaction results in the degradation of shear strength with increasing curvature ductility ($\mu_\phi \geq 3$). As the result, the initial shear strength $V_{u0} = 515.6$ kN calculated from Eq. (2-24) is higher than the peak shear force $V_{\max} = 316.1$ kN. Finally, the shear failure in this column occurs when the shear demand meets the shear failure envelope with associated value of the curvature ductility $\mu_\phi = 14.83$. However, it is crucial to point out that the shear failure would not have occurred in the column 2CLD12 if the flexural and shear actions had been independent.

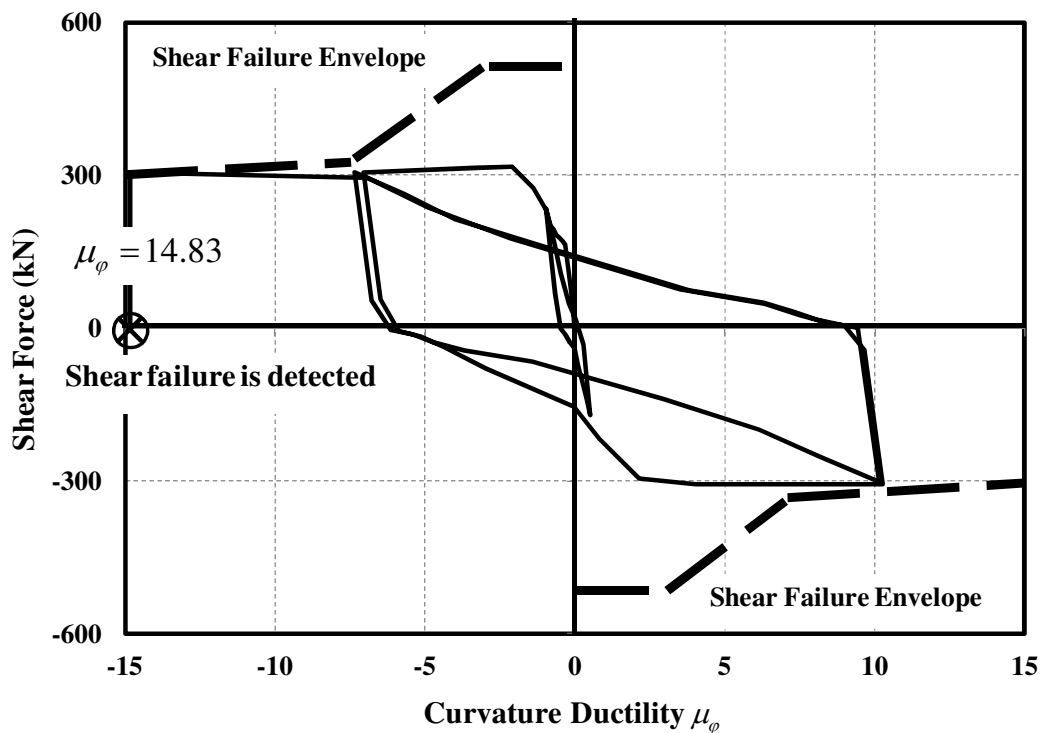


Figure 6-4 Shear force vs curvature ductility at the end of column 2CLD12 (Section I)

6.2.2 Example II: Column 2CMH18 [Lynn, 2001]

The second numerical example is selected from a series of eight RC square columns contained a variety of reinforcement details and subjected to two different levels of axial loading conducted by Lynn (2001). The column, labeled column 2CMH18, is one of those columns which are constructed to represent the existing RC columns built before the 1970's and is used to verify the accuracy and efficiency of the proposed RC frame element and to show the importance of including for the shear-flexure interaction effects in this study.

Figure 6-5 illustrates the column 2CMH18 geometry. The column is the square cross-section with dimension of $457.2 \times 457.2 \text{ mm}^2$. Eight #8 deformed longitudinal bars (25.4 mm diameter) are placed uniformly along the column perimeter. The transverse reinforcement of this column represents by the square hoops of #3 deformed bars (9.5 mm diameter) with 90° hooks and has a spacing of 457.2 mm. The volumetric ratio of transverse reinforcement is 0.0007 based on the transverse reinforcement details. It is worth mentioning that the transverse

reinforcement details and amount as above are indicated for the characteristic of the substandard seismic reinforcement details used before the 1970's. The column was design the concrete ultimate compressive strength of 25.5 MPa and the yield strengths of longitudinal and transverse reinforcing bars of 331 and 400 MPa, respectively. The column clear height was 2,946 mm. Moreover, the column was subject to a constant axial compressive load of 1,512 kN (Corresponding to approximately $0.28\% f'_c A_g$) and cyclic lateral displacement inducing flexure about the y axis. The above data of the column 2CMH18 is based on the information available in the research work of Lynn (2001). From numerical model, the column is discretized into 16 elements with 7 Gauss-Lobatto integration points and the frame cross-section is discretized into 40 fibers to represent the nonlinear responses of this numerical example. The initial shear strength V_{u0} can predict based on the UCSD shear-strength model [Priestley et al., 1993] in Eq. (2-24) about 477.2 kN.

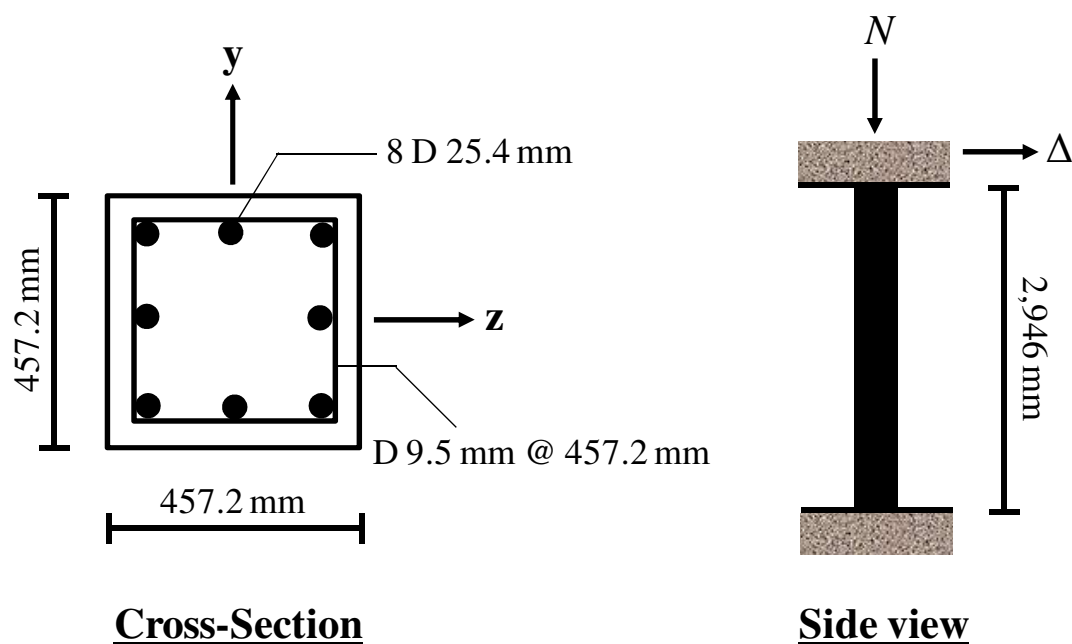
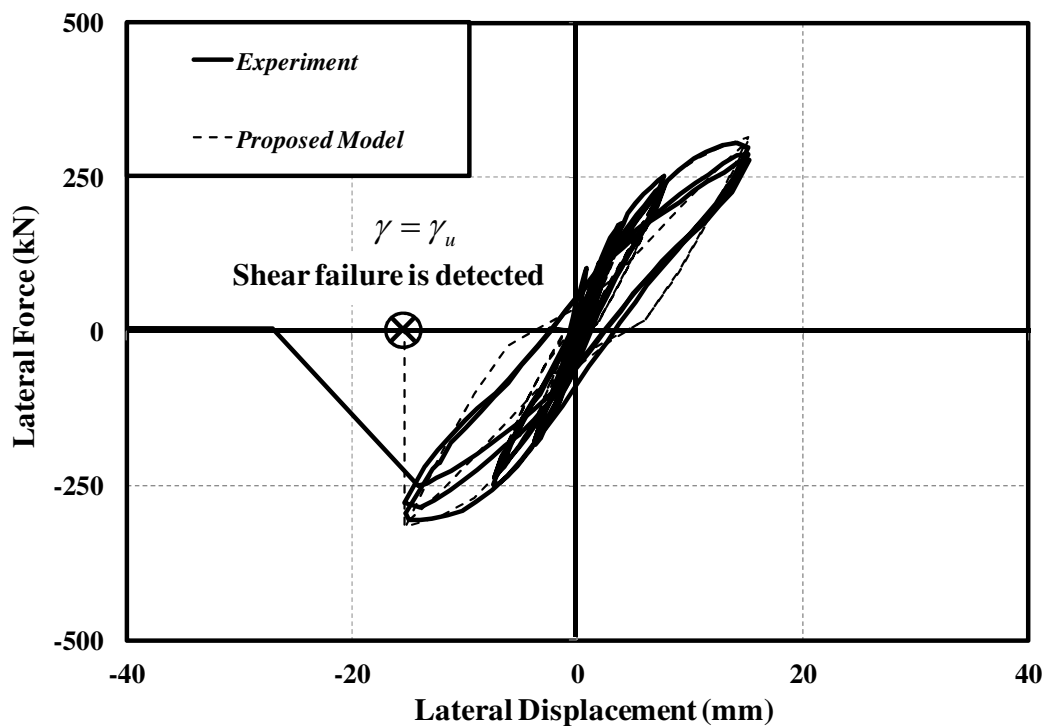


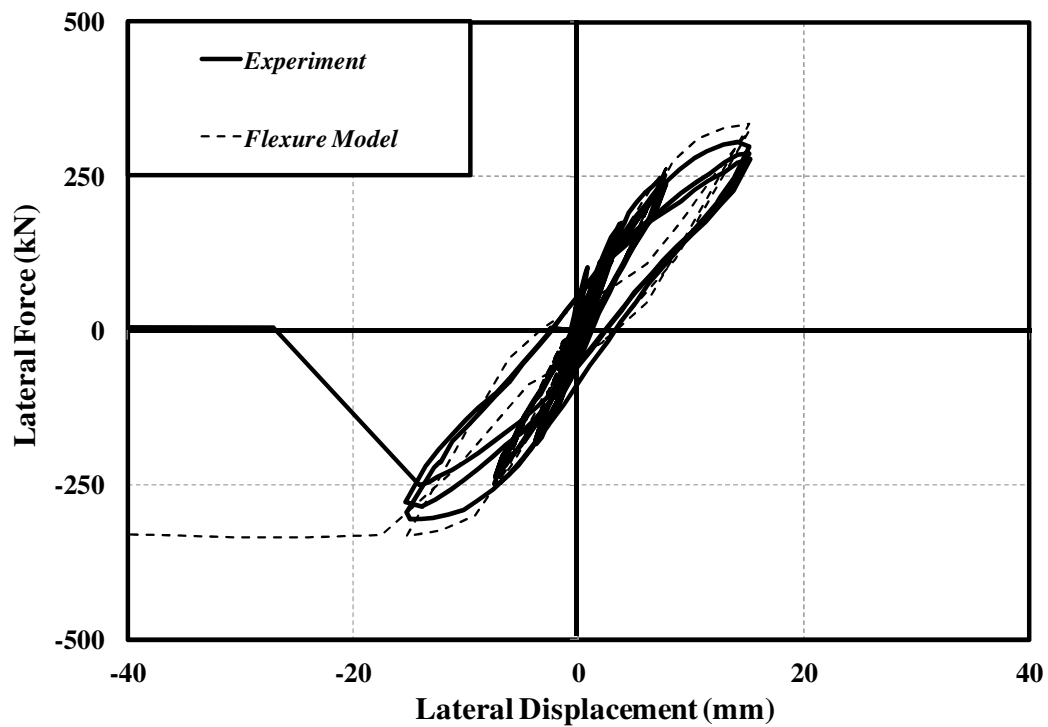
Figure 6-5 The specimen geometry of column 2CMH18 [Lynn, 2001]

Figure 6-6 (a) presents the relationship between the tip lateral load and total displacement obtained from the analysis result of the proposed model while Figure 6-6 (a) shows the tip load-displacement response obtained from the flexural model proposed by Spacone et al. (1996). The experimental data tested by

Lynn (2001) is defined as the benchmark response and used to compare with the numerical results. From the responses as shown in Figure 6-6 (a) and (b), both models succeed in the behavior capture of the characterizing experimental load-displacement response, such as the member capacity, amount of dissipated hysteretic energy, and general shape of hysteretic response. From the numerical result in Figure 6-6 (a), the proposed model can predict the first plastic-hinge formation at the lateral displacement Δ_y , about 8.30 mm and shear strain γ_y , about 1.21×10^{-3} . Finally, the proposed model can predict the lateral displacement Δ_u associated with the ultimate shear strain γ_u is equal to 15.30 mm. This value corresponds well with the experimental observation [Lynn, 2001] that the lateral displacement associated with the onset of rapid shear strength degradation occurs at about 15.30 mm. Furthermore, the experimental keynote of Lynn (2001) indicated that the column 2CMH18 collapse because the axial load loss it's carry capacity.



(a)



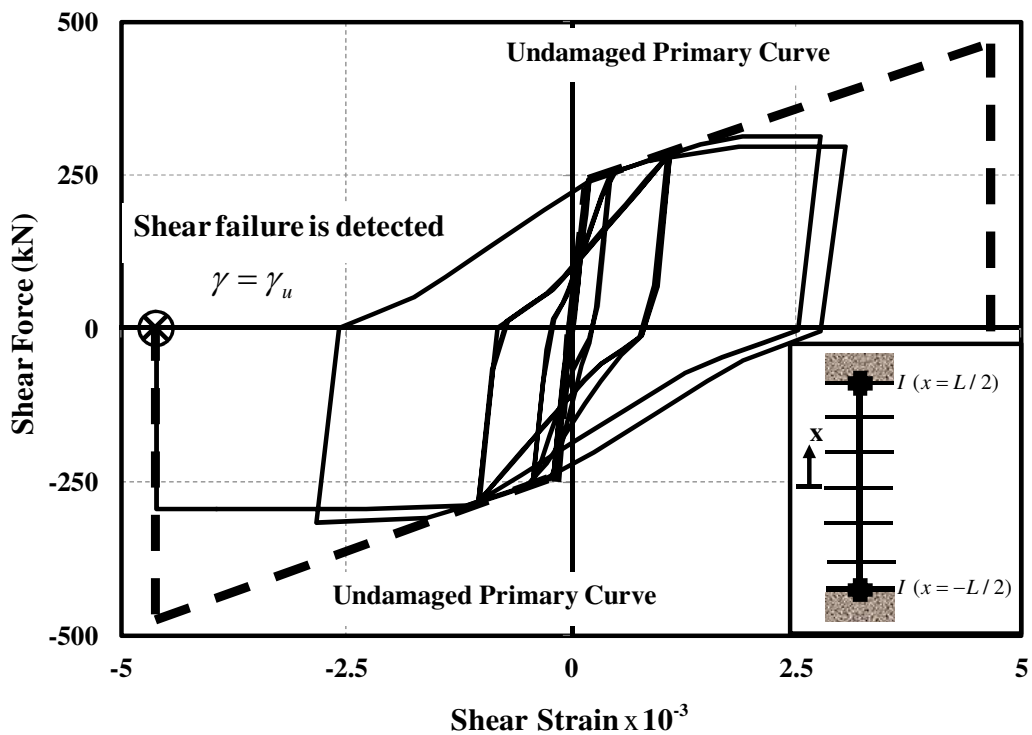
(b)

Figure 6-6 The lateral load-displacement response of the end column 2CLD12M obtained from: (a) the proposed model and (b) the flexure model

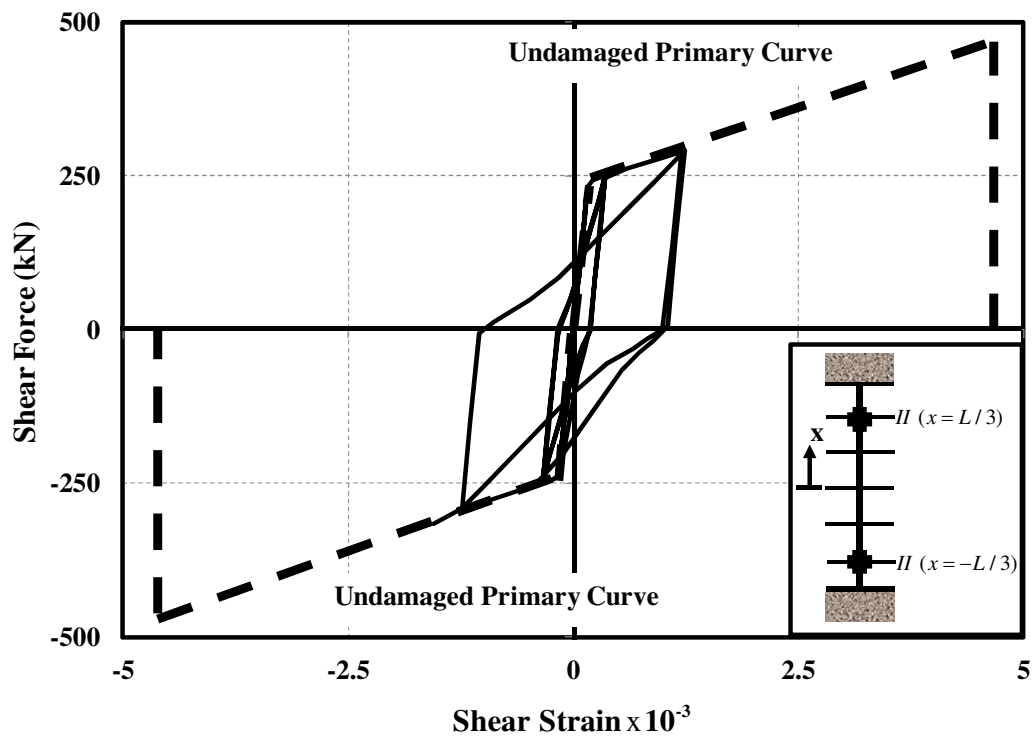
Figure 6-6 (b) illustrates the essence of including the shear-flexure interaction effect from the numerical responses obtained with the flexural model [Spacone et al., 1996] when compared to the experimental result. Although the flexural model can predict reasonably well the experimental result, the flexural model cannot predict the shear failure following the plastic-hinge formation. Therefore, the frame element with inclusion of the shear-flexure interaction effects is necessary and essential in the simulating the response of RC columns that fail in shear due to the shear-flexural interaction (Ductile shear failure).

Figure 6-7 represents the hysteretic shear responses at various monitoring sections (Section I, II, III, and IV) along the column length. The hysteretic shear response at section I locates on the plastic-hinge region due to their restrained conditions while The hysteretic shear response at section II, III, and IV rest outside the plastic-hinge region. Therefore, the hysteretic shear response at section I is different

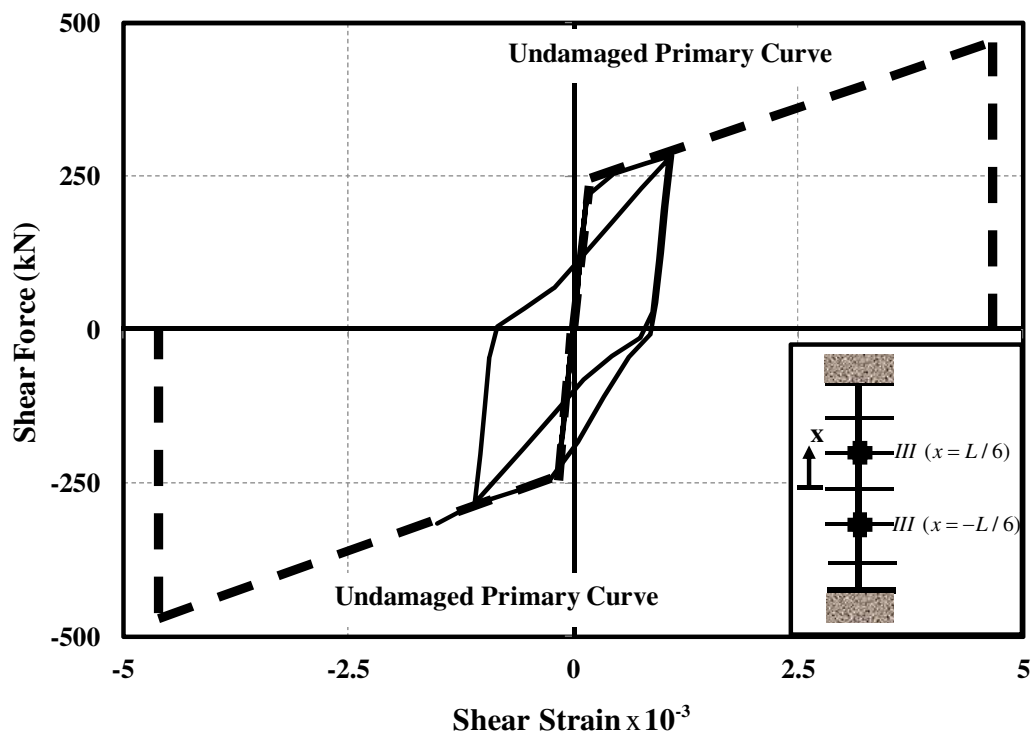
from the hysteretic shear responses outside the plastic-hinge regions (Section II, III, and IV). Based on the UCSD shear-strength model [Priestley et al., 1993], the sectional shear response begins to deviate from the undamaged envelope curve to the damaged envelope curve due to the shear-flexural interaction when the sectional curvature ductility reaches its threshold value of 3 as shown in Figure 6-3 (a). On the other hand, it is observed that the hysteretic shear responses at section II, III, and IV are almost identical. This relies on the fact that the sectional shear responses outside the plastic-hinge regions (Section II, III, and IV) are not experienced with the shear-flexure interaction. To compare the sectional shear response in Figure 6-3 (a) and 6-3 (b)-(d), it is observed that although all sections experience with the same magnitude of shear force as governed by the equilibrium, the sectional shear strain at section I is much higher than the sectional shear strain at section II, III, and IV. Finally, the column failure in shear can be detected by the proposed model when the sectional shear strain reaches its ultimate value of $\gamma_u = 4.6 \times 10^{-3}$ at section I. It is worth noting that the shear strain at onset of stirrup yielding γ_{st} is equal to shear strain at onset of shear failure γ_u based on the undamaged primary curve proposed by Mergos and Kappos (2012).



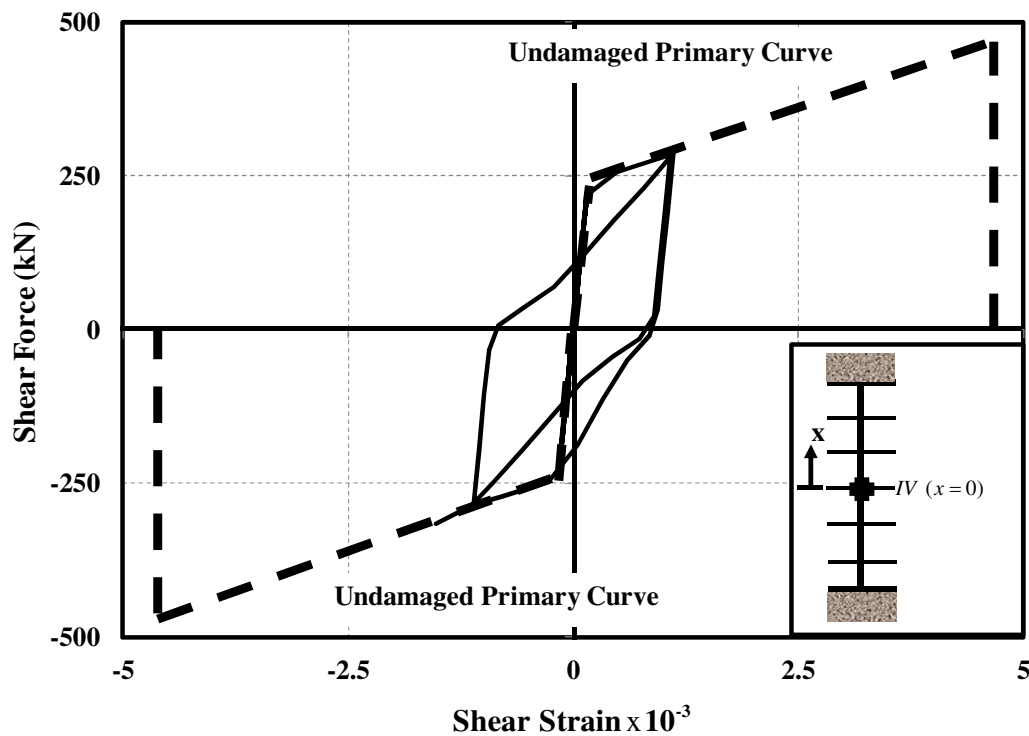
(a)



(b)



(c)



(d)

Figure 6-7 The hysteretic shear responses of column 2CMH18 at various monitoring sections: (a) section I ($x = L / 2$); (b) section II ($x = L / 3$); (c) section III ($x = L / 6$) and (d) section IV ($x = 0$)

Figure 6-8 presents the variations of shear force (Demand) and shear strength (Capacity) with the curvature ductility at the end of a column (Section I). The shear-strength capacity envelope in Figure 6-8 based on the UCSD shear-strength model [Priestly et al., 1993] is used to consider as the failure envelope. From the analytical response, the initial shear strength V_{u0} calculated from Eq. (2-24) is 477.2 kN while the peak shear force V_{max} can predict approximately 316.0 kN. It is observed that the column 2CMH18 would not have failed in shear if the shear-flexure relation had not interacted. The shear failure in this column occurs when the shear demand meets the shear failure envelope with associated value of the curvature ductility $\mu_{\phi} = 5.86$. Compare to the previous numerical example I (Column 2CLD12), the curvature ductility of column 2CLD12 at the shear failure ($\mu_{\phi} = 14.83$) is much larger

than the curvature ductility of column 2CMH18 ($\mu_\phi = 5.86$). It relies on the fact that the column 2CMH18 experiences the higher axial loading while the column 2CLD12 is the more ductile sectional shear envelope.

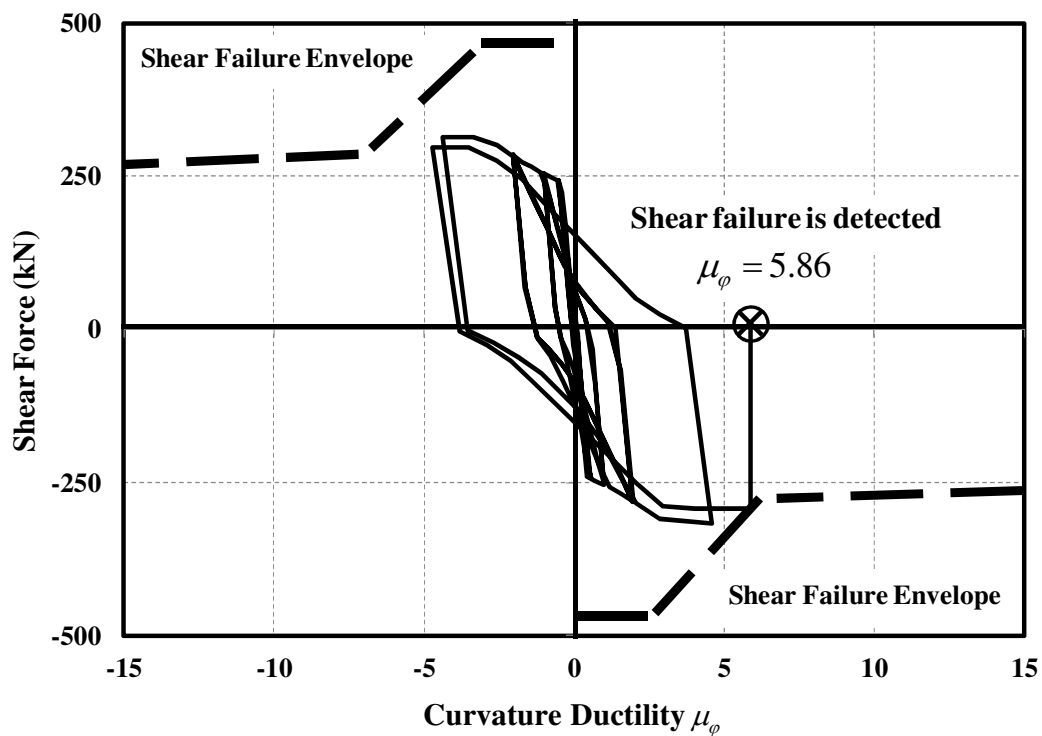


Figure 6-8 Shear force vs curvature ductility at the end of column 2CMH18 (Section I)

6.3 Shear critical RC member

A shear critical RC member refers to the RC column that fails in shear before the flexural yielding. The hysteretic shear response follows the undamaged primary curve as shown in Figure 5-4.

6.3.1 Example III: Column Specimen No. 1-1 [Batt et al., 1985]

The specimen No. 1-1 was one of the RC columns with a square cross-section under a constant axial load and cyclic lateral displacement tested by Bett et al. (1985). This specimen was approximated by 2/3 scale test in double bending and designed to fail in shear. The main objective of this experimental test was to

evaluate the efficiency of the strengthening and repairing techniques for short column designed in seismic regions of the U.S. in the 1950's and 1960's. The specimen geometry is given by Batt et al. (1985). The dimension of cross section specimen was $304.8 \times 304.8 \text{ mm}^2$ with eight #6 deformed longitudinal reinforcement bars (19 mm diameter). Square hoops of 6-mm deformed bars and spacing of 203 mm were used for the transverse reinforcement. The specimen was designed with the concrete strength of 29.9 MPa, longitudinal reinforcement yielding strength of 462 MPa and transverse reinforcement yielding strength of 414 MPa. The clear height of the specimen was 920 mm and was subjected to lateral load cycles under a constant axial load of 288 kN (Corresponding to approximately $0.10\% f'_c A_g$) as shown in Figure 6-9. In this numerical example, the column is discretized into 16 elements with seven Gauss-Lobatto integration points. Forty fibers (Layers) are used to discretize the column cross section.

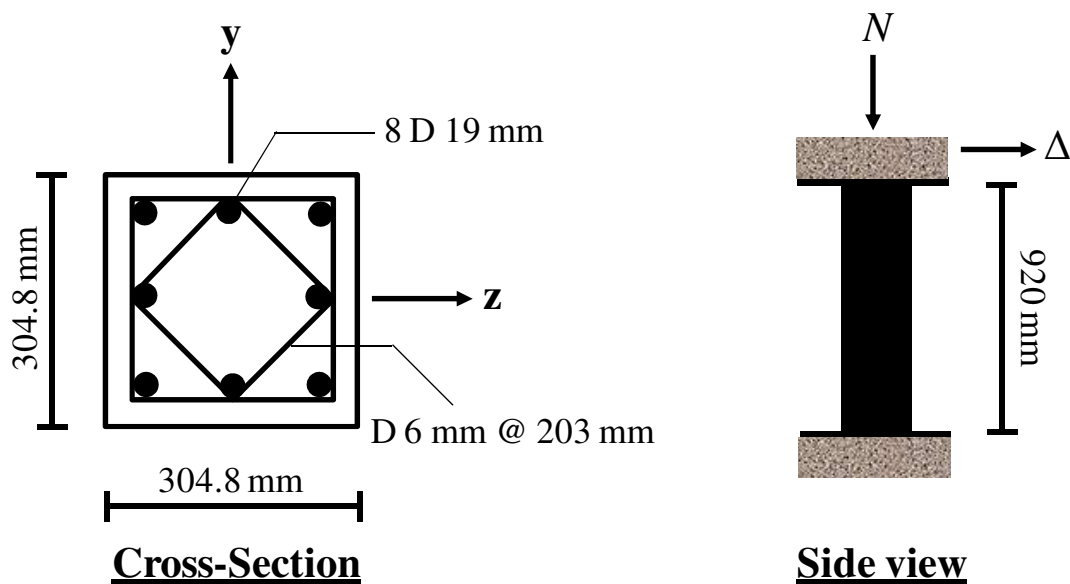
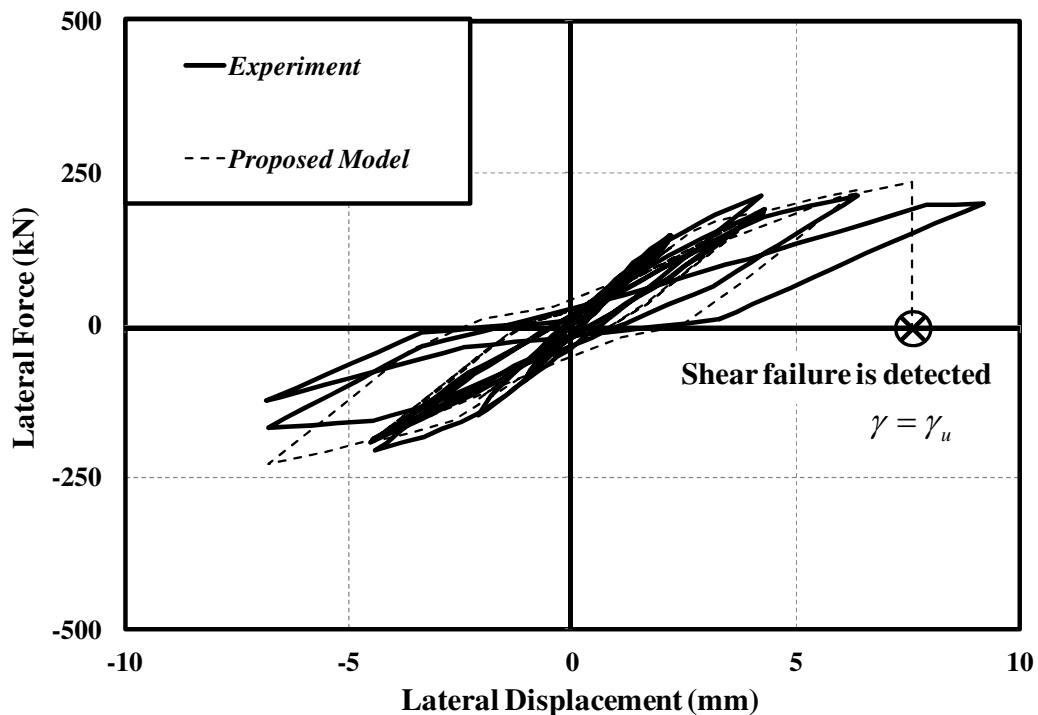


Figure 6-9 The specimen geometry of column No. 1-1 [Bett et al., 1985]

Figure 6-10 (a) present the lateral load-displacement response obtained from the experimental test and the numerical result analyzed with the proposed model while Figure 6-10 (b) shows the result comparison between the experimental result and the numerical result obtained with the flexural model proposed by Spacone et al. (1996). The analytical result in Figure 6-10 (a) proves the

performance of the proposed element that the proposed element can capture reasonably well the salient features of the experimental load-displacement result, such as the member capacity, the stiffness degradation with increasing displacement amplitude, amount of dissipated hysteretic energy, and general shape of hysteretic response. As expected, the pinching of hysteretic loop can be clearly noticed in the load-displacement response of this example. Thus, the column No. 1-1 is considered as a shear-dominated member. Furthermore, the proposed model predicts that the shear failure occur when the shear strain reaches its ultimate value of $\gamma_u = 7.10 \times 10^{-3}$ and the lateral displacement value of $\Delta_u = 7.6$ mm. It can observe that there is no plastic hinge formation in the column No. 1-1. On the other hand, the load-displacement response obtained with the flexure model in Figure 6-10 (b) shows that the flexure model fails to simulate the load-displacement response of the shear-dominated member like the column No. 1-1. From Figure 6-10 (b), the member strength and amount of dissipated hysteretic energy are drastically overestimated. As the result, it can be discussed that the frame element with inclusion of section shear response is necessary and essential in assessing the seismic performance of shear-dominated RC member.



(a)

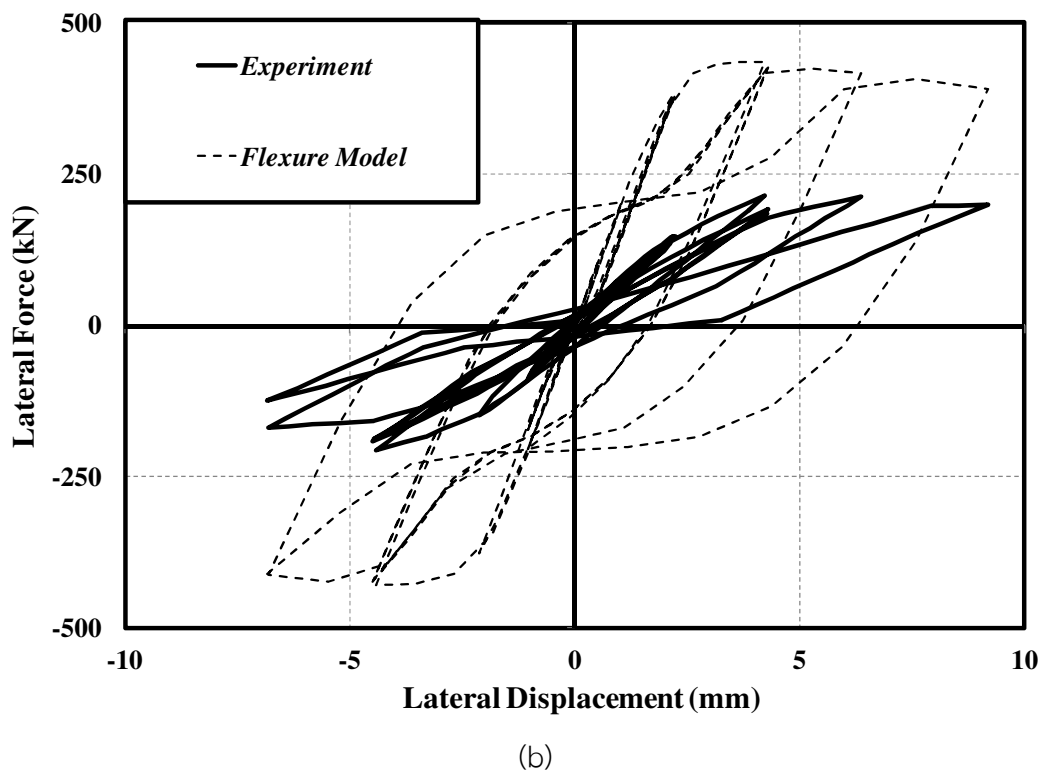


Figure 6-10 The lateral load-displacement response of the end column No. 1-1 obtained from: (a) the proposed model and (b) the flexure model

Figure 6-11 demonstrates the hysteretic shear responses at various monitoring sections (Section I, II, III, and IV) along the column length. The analytical results of this example show that the hysteretic shear responses at all monitoring sections along the column length are similar. It is different from the sectional shear responses of the previous examples (Column 2CLD12 and 2CMH18). This relies on the fact that all column sections of specimen No. 1-1 have not experienced yielding in flexure. Therefore, the hysteretic shear responses follow the undamaged primary curve and the sectional shear-flexure interaction does not occur in the column No. 1-1. Furthermore, the pinching characteristic is noticeable in the sectional shear responses. Finally, the column shear failure occurs when the sectional shear strain reaches its ultimate value of $\gamma_u = 7.10 \times 10^{-3}$.

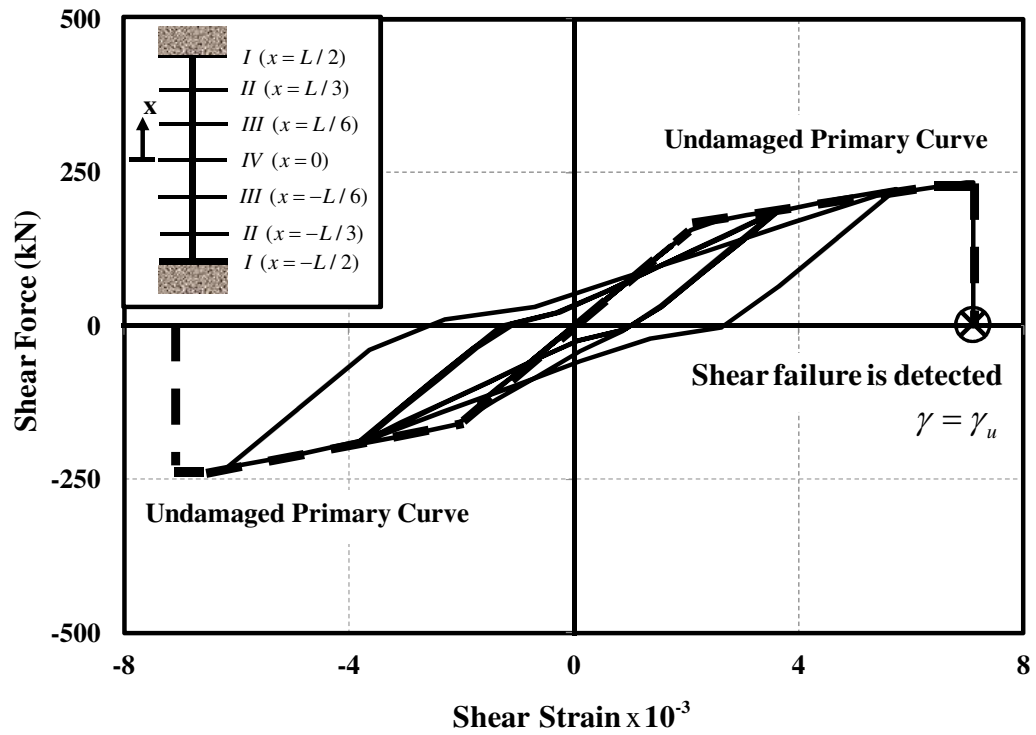


Figure 6-11 The hysteretic shear responses of column No. 1-1 at various monitoring sections

CHAPTER 7

Conclusions

7.1 Summary

This study presents a fiber frame element for cyclic analysis of reinforced concrete (RC) members prone to the flexure-shear failure as well as shear failure. The proposed frame element formulates from the displacement-based method and is based on the classical Timoshenko beam theory. Under Timoshenko beam kinematics assumption, the choice of displacement interpolation functions is selected with care to obtain the locking-free Timoshenko frame element. To overcome the shear-locking problem, the consistent interpolation approach is used to derive the displacement interpolation functions of two nodes Timoshenko frame element, thus resulting in the so-called “*linked*” displacement interpolation functions. Moreover, the nonlinear behaviors of material models are considered in the uniaxial hysteretic laws for concrete, reinforcing steel and sectional shear.

According to the influences of shear-flexure interaction on the shear responses, these effects lead to the degradation of shear capacity and sectional shear stiffness due to the increase of inelastic flexural deformation (Plastic-hinge formation). To include these effects into the shear hysteretic law, the presented framework of the shear-flexure interaction procedure within the implement displacement-based formulation is adapted and modified from the Mergos and Koppas procedure combined with the UCSD shear-strength model. This procedure is based on the general input properties of RC member. Therefore, the proposed model is simple but accuracy and computationally efficient which are confirmed by the numerical simulations.

From the numerical simulation analysis, the results of the flexure-shear critical columns confirm that the proposed model can reasonably well predict the salient features of the experimental data, such as the member capacity, stiffness

degradation with increasing displacement amplitude, amount of dissipated hysteretic energy, the general shape of hysteretic response, and failure mode. Moreover, the proposed model can accurately represent the degradation of shear strength and the drastic increase of shear deformations following the increase of inelastic flexural deformation (Plastic-hinge formation). The importance of accounting the shear-flexure interaction is proved when compared with the flexural model that the flexural model cannot predict the shear failure due to the shear-flexure interaction effects.

In case of the shear critical column, the proposed model can represent reasonably well the characteristic of the experimental data, such as the member capacity, stiffness degradation with increasing displacement amplitude, amount of dissipated hysteretic energy, the general pinched shape of hysteretic response, and failure mode. The importance of accounting the shear response is clearly discussed when compared to the flexural model that the model without considering the shear response (e.g. the flexural model) fails to simulate the responses of the shear critical column.

7.2 The Development and Future Work

The development and future work of the proposed frame element including the shear-flexure interaction effects for analysis of non-ductile reinforced concrete column is a step forward in establishing a computational framework that includes the anchorage bond-slip effect. From the previous research works (e.g. Sezen, 2002; Moehle and Sezen, 2006; Mergos and Kappos, 2008 and 2012; Schoettler et al., 2012; Terzic et al., 2015; and Feng and Xu, 2018a), the bond slip is found to play an important role in the responses. Therefore, it should be carefully considered in the next steps. Furthermore, the future studies will concentrate on the accurate formulas for the prediction of the response after plastic hinge rotation forming and extend for using in the force-based and two fields mixed formulations.

References

- Aboutaha, R. S., Engelhardt, M. D., Jirsa, J. O., and Kreger, M. E. (1999). "Rehabilitation of shear critical concrete columns by use of rectangular steel jackets." *ACI Structural Journal*, **96**(1), 68-78.
- Alim, R. (2014). "Reliability based seismic performance analysis of retrofitted concrete bridge bent." M. Engineering Thesis, Department of Civil Engineering, Chittagong University of Engineering and Technology (CUET), Chittagong, Bangladesh.
- American Concrete Institute (ACI). (2014). "Building code requirements for structural concrete." *ACI Committee 318*, Farmington Hills, Mich.
- Amitsu, S., Shirai, N., Adachi, H., and Ono, A. (1991) " Deformation of reinforced concrete column with high or fluctuating axial force." *Transactions of the Japan Concrete Institute*, **13**, 355-362.
- Ang, B. G., Priestley, M.J. N., and Paulay, T. (1989). "Seismic shear strength of circular reinforced concrete columns." *ACI Structure Journal*, **86**(1), 45-59.
- Arakawa, T., Arai, Y., Mizoguchi, M., and Yoshida, M. (1989). "Shear resisting behavior of short reinforced concrete columns under biaxial bending-shear." *Transactions of the Japan Concrete Institute*, **11**, 317-324.
- Armstrong, P. J. and Frederick, C. O. (1966). "A mathematical representation of the multiaxial bauschinger effect" *G.E.G.B. Report*, RD/B/N 731.
- ASCE-ACI Task Committee 426 (1973). "The shear strength of reinforced concrete members." *ASCE Journal of the Structural Division*, **99**(6), 1091-1187.
- Bairan, J. M. (2005). "A nonlinear coupled model for the analysis of reinforced concrete sections under bending, shear and torsion and axial forces." Ph.D. thesis, Technical University of Catalonia, Barcelona, Spain.

- Bairan, J. M. and Mari, A. R. (2006a). "Coupled model for the nonlinear analysis of anisotropic sections subjected to general 3D loading. Part 1: Theoretical formulation." *Computers and Structures*, **84**(31-32), 2254-2263.
- Bairan, J. M. and Mari, A. R. (2006b). "Coupled model for the nonlinear analysis of anisotropic sections subjected to general 3D loading. Part 2: Implementation and validation." *Computers and Structures*, **84**(31-32), 2264-2276.
- Barbato, M. (2009). "Efficient finite element modelling of reinforced concrete beams retrofitted with fibre reinforced polymers." *Computers and Structures*, **87**(3-4), 167-176.
- Bazant, Z. P. and Prat, P. C. (1988). "Microplane model for brittle-plastic material: Part I and II." *ASCE Journal of Engineering Mechanics*, **114**(10), 1672-1702.
- Bentz, E. C. (2000). "Sectional analysis of reinforced concrete members." Ph. D. Thesis, University of Toronto, Toronto, Canada.
- Bett, B., Klingner, R. E., and Jirsa, J. O. (1985). "Behavior of strengthened and repaired reinforced concrete columns under cyclic deformations." *PMFSEL Report No. 85-3*, The University of Texas, Austin, USA.
- Biscaia, H. C., Chastre, C., and Silva, M. A.G. (2013). "A smeared crack analysis of reinforced concrete T-beams strengthened with GFRP composites." *Engineering Structures*, **56**(11), 1346-1361.
- Biskinis, D., Roupakias, G. and Fardis, M. N. (2004). "Degradation of shear strength of R/C members with inelastic cyclic displacement." *ACI Structure Journal*, **101**(6), 773-783.
- Brocca, M. and Bazent, Z. P. (2001). "Size effect in concrete columns: finite-element analysis with microplane model." *Journal of Structural Engineering*, **127**(12), 1382-1390.

- Cai, G. and Degee, H. (2017). "Ultimate strengths of FRC rectangular columns subjected to simulated seismic loading: Experimental database and new models." *Archives of Civil and Mechanical Engineering*, **17**(1), 96-120.
- Ceresa, P., Petrini, L., and Pinho, R. (2007). "Flexure-shear fiber beam-column elements for modeling frame structures under seismic loading: State of the art." *Journal of Earthquake Engineering*, **11**(supplement 1), 46-88.
- Ceresa, P., Prtrini, L., and Pinho, R. (2008). "A fibre flexure-shear model for cyclic nonlinear behaviour of RC structural elements." *Research Report ROSE-2008/07*. IUSS Press: Pavia, Italy.
- Ceresa, P., Petrini, L., Pinho, R., and Sousa, R. (2009). "A fibre flexure-shear model for seismic analysis of RC-framed structures." *Earthquake Engineering and Structural Dynamics*, **38**(5), 565-586.
- Cervenka, V. (1985). "Constitutive model for cracked reinforced concrete." *ACI Structural Journal*, **82**(6), 877-882.
- Chan, E. C. (1982). "Nonlinear geometric, material and time-dependent analysis of reinforced concrete shells with edge beams." Ph.D. Thesis, University of California, Berkeley.
- Chapra, S. C. and Canale, R. P. (2002). *Numerical methods for engineers*, McGraw-Hill, New York.
- De Veubeke, B. F. (1965). *Displacement and equilibrium models*, Chapter 9 in Stress Analysis, Wiley, London, 145-197.
- Dogangun, A. (2004). "Performance of reinforced concrete buildings during the May 1, 2003 Bingol Earthquake in Turkey." *Engineering Structures*, **26**(6), 841-856.
- Erguven, M. E. and Gedikli, A. (2003). "A mixed finite element formulation for Timoshenko beam on Winkler foundation." *Computational Mechanics*, **31**(3-4), 229-237.

Faria, R., Oliver, J., and Cervera, M. (1998). "A strain-based plastic viscous-damage model for massive concrete structures." *International Journal of Solids and Structures*, **35**(14), 1533-1558.

Federal Emergency Management Agency (FEMA). (1997). "NEHRP guidelines for the seismic rehabilitation of buildings." *FEMA 273*, Washington, D.C.

Feng, D. C., Koley, C., Ricels, J. M., and Li, J. (2016). "Collapse simulation of reinforced concrete frame structures." *The Structural Design of Tall and Special Buildings*, **25**(12), 578-601.

Feng, D. C. and Xu, J. (2018a). "An efficient fiber beam-column element considering flexure-shear interaction and anchorage bond-slip effect for cyclic analysis of RC structures." *Bulletin of Earthquake Engineering*, 1-28.

Feng, D. C., Ren, X. D., and Li, J. (2018b). "Softened damage-plasticity model for analysis of cracked reinforced concrete structures." *Journal of Structural Engineering*, **144**(6), 04018044.

Filippou, F. C., Popov, E. P., and Bertero, V. V. (1983a). "Modelling of R/C joints under cyclic excitations." *Journal of Structural Engineering*, **109**(11), 2666-2684.

Filippou, F. C., Popov, E. P., and Bertero, V. V. (1983b). "Effects of bond deterioration on hysteretic behavior of reinforced concrete joints." *EERC Report 83-19*, Earthquake Engineering Research Center, University of California, Berkeley.

Filippou, F. C., D'Ambrisi, A., and Issa, A. (1992). "Nonlinear static and dynamic analysis of reinforced concrete subassemblages." *Earthquake Engineering Research Center Report No. UCB/EERC-92/08*, University of California, Berkeley, USA.

Grastka, B., Kratzig, W. B., and Stangenberg, F. (1993). "Damage assessment in cyclically loaded reinforced concrete members." *Structural Dynamics, EURO-DYN'93*, Moan, Ed. Balkema, Rotterdam 1, 121-128.

Gerin, M. and Adebar, P. (2004). "Accounting for shear in seismic analysis of concrete structures." *Proceeding of 13th world conference on earthquake engineering*, Vancouver, Paper No. 1747.

Ghasemi, H., Otsuke, H., Cooper, J. D., and Nakajima, H. (1996). "Aftermath of the Kobe earthquake." *Public Road*, Fall 1996, 60(2).

Ghee, A., Priestley, M.J. N., and Paulay, T. (1989). "Seismic shear strength of circular reinforced concrete columns." *ACI Structural Journal*, **86**(1), 45-59.

Giberson, M. F. (1967). "The response of nonlinear multi-story structures subjected to earthquake excitation." *Earthquake Engineering Research Laboratory*, California Institute of Technology, Pasadena, USA.

Guedes, J., Pegon, P., and Pinto, A. V. (1994). "A fibre/Timoshenko beam element in CASTEM 2000." *Special Publication Nr. I.94.31*, Applied Mechanics Unit, Safety Technology Institute, Commission of the European Communities, Joint Research Centre, Ispra Establishment, Italy.

Guedas, J. and Pinto, A. V. (1997). "A numerical model for shear dominated bridge piers." *Proceedings of the Second Italy-Japan Workshop on Seismic Design and Retrofit of Bridges*, Rome, Italy.

Hafezolghorani, M., Hejazi, F., Vaghei, R., Jaafar, M. S. B., and Karimzade, K. (2017). "Simplified damage plasticity model for concrete." *Structural Engineering International*, **27**(1), 68-78.

Hamilton, C. H., Pardoen, G. C., and Kazanjy, R. P. (2002). "Experimental testing of bridge columns subjected to reversed-cyclic and pulse-type loading histories." *Report 2001-03*, Civil Engineering Technical Report Series, University of California, Irvine.

Hsu, T. T.C. (1988). "Softened truss model theory for shear and torsion." *ACI Structure Journal*, **85**(6), 624-635.

Imai, H. and Yamamoto, Y. (1986). "A study on causes of earthquake damage of Izumi high school due to Miyagi-Ken-Oki earthquake in 1978." *Transactions of the Japan Concrete Institute*, **8**, 405-418.

Ismail, K. S., Guadagnini, M., and Pilakoutas, K. (2016). "Numerical investigation of the shear strength of RC deep beams using the microplane model." *Journal of Structural Engineering*, **142**(10), 04016077.

Issa, A. (1989). "Nonlinear static and dynamic analysis of reinforced concrete frames." Ph.D. thesis, Department of Civil and Environmental Engineering, University of California, Berkeley, USA.

Ju, J. (1989). "On energy-based coupled elastoplastic damage theories: constitutive modeling and computational aspects." *International Journal of Solids and Structures*, **25**(7), 803-833.

Kagermanov, A. and Ceresa, P. (2016). "Physically based cyclic tensile model for RC membrane elements." *Journal of Structural Engineering*, **142**(12), 04016118.

Kagermanov, A. and Ceresa, P. (2017). "Fiber-section model with an exact shear strain profile for two-dimensional RC frame structures." *Journal of the structural Engineering*, **143**(10), 04017132.

Karsan, I.D. and Jirsa, J.O. (1969). "Behavior of concrete under compressive loadings." *ASCE Journal of the Structural Division*, **95**(12), 2543-2563.

Kent, D.C. and Park, R. (1971). "Flexural members with confined concrete." *ASCE Journal of the structural Division*, **97**(7), 1964-1990.

Kim, J., Kwon, M., Jung, W., and Limkatanyu, S. (2013). "Seismic performance evaluation of RC columns reinforced by GFRP composite sheets with clip connectors." *Construction and Building Material*, **43**, 563-574.

Kotronis, P. (2000). "Cisaillement dynamique de murs en beton arme. Modeles simplifies 2D et 3D." Ph.D. Thesis, Ecole Normale Superieure de Cachan.

- Kotronis, P., Chambon, R., Mazars, J., and Collin, F. (2005). "Local second gradient models and damage mechanics: application to concrete." *ICFXI-Proceeding of the 11th International Conference on Fracture*, Turin (Italy), March 20-25, (in print).
- Lee, J. and Fenves, G. L. (1998). "Plastic-damage model for cyclic loading of concrete structures." *Journal of Engineering Mechanics*, **124**(8), 892-900.
- Li, X., Park, R., and Tanaka, H. (1995). "Reinforced concrete columns under seismic lateral force and varying axial load." *Research Report 95-5*, Department of Civil Engineering, University of Canterbury, Christchurch, New Zealand.
- Li, Z. X., Gao, Y., and Zhao, Q. (2016). "A 3D flexure-shear fiber element for modeling the seismic behavior of reinforced concrete columns." *Engineering Structures*, **117**, 372-383.
- Limkatanyu, S. (2002). "Reinforced concrete models with bond-interfaces for the nonlinear static and dynamic analysis of reinforced concrete frame structures." Ph.D. Engineering Thesis, Department of Civil, Environmental and Architectural Engineering, University of Colorado, Boulder.
- Limkatanyu, S. and Spacone, E. (2002). "Reinforced concrete frame element with bond interfaces. I: Displacement-based, force-based, and mixed formulations." *Journal of Structural Engineering*, **128**(3), 346-355.
- Limkatanyu, S. (2008). *Matrix structural analysis*. (1st ed.). Hadyai, Songkla, Thailand, 90110 : Faculty of Engineering.
- Limkatanyu, S., Sae-Long, W., Prachasaree, W., and Kwon, M. (2014). "Improved nonlinear displacement-based beam element on a two-parameter foundation." *European Journal of Environmental and Civil Engineering*, **19**(6), 1-23.
- Long, X., Bao, J. Q., Tan, K. H., and Lee, C. K. (2014). "Numerical simulation of reinforced concrete beam/ column failure considering normal-shear stress interaction." *Engineering Structures*, **74**, 32-43.

Lynn, A. C., Moehle, J. P., Mahin, S. A., and Holmes, W. T. (1996). "Seismic evaluation of existing reinforced concrete building columns." *Earthquake Spectra*, **12**(4), 715-739.

Lynn, A. C. (2001). "Seismic evaluation of existing reinforced concrete building column." Ph.D. Engineering Thesis, Department of civil engineering, Engineering, University of California, Berkeley.

Ma, S. M., Bertero, V. V., and Popov, E. P. (1976). "Experimental and analytical studies on hysteretic behavior of RC rectangular and T-beam." *Earthquake Engineering Research Center Report No. UCB/EERC-76/02*, University of California, Berkeley, USA.

Mander, J. B., Priestley, M.J. N., and Park, R. (1988). "Theoretical stress-strain model for confined concrete." *ASCE Journal of Structural Engineering*, **114**(8), 1804-1826.

Marini, A. and Spacone, E. (2006). "Analysis of reinforced concrete elements including shear effect." *ACI Structure Journal*, **103**(5), 645-655.

Martinelli, L. (1998). "Modellazione di pile di ponti in C. A. a travata soggetti ad eccitazione sismica." Ph. D. Thesis, Dipartimento di Ingegneria Strutturale, Politecnico di Milano, Milano, Italy. (in Italian)

Martino, R. (1999). "Nonlinear Pushover Analysis of Reinforced Concrete Structures." Master thesis, Department of Civil, Environmental, Architectural Engineering, University of Colorado, Boulder, USA.

Menegotto, M. and Pinto, P. E. (1973). "Method of analysis for cyclically loaded reinforced concrete plane frames including changes in geometry and inelastic behavior of elements under combined normal force and bending." *Proceeding of IABSE symposium on resistance and ultimate deformability of structures acted on by well-defined repeated loads*, Lisbon, 17-22.

Menegotto, M. and Pinto, P. E. (1977). "Slender RC compressed members in biaxial bending." *ASCE Journal of Structural Division*, **103**(3), 587-605.

Mergos, P. E. and Kappos, A. J. (2008). "A distributed shear and flexural flexibility model with shear-flexure interaction for R/C members subjected to seismic loading." *Earthquake Engineering and Structural Dynamics*, **37**(1), 1349-1370.

Mergos, P. E. and Kappos, A. J. (2012). "A gradual spread inelasticity model for R/C beam-columns, accounting for flexure, shear and anchorage slip." *Engineering Structure*, **44**(1), 94-106.

Minelli, F. (2005). "Plain and fiber reinforced concrete beams under shear loading: structural behavior and design aspects." Ph.D. thesis, Università degli Studi di Trento, Italy.

Moehle, J. P. and Mahin, S. A. (1991). "Observations on the behavior of reinforced concrete buildings during earthquakes." *ACI SP-127: Earthquake-Resistant Concrete Structures Inelastic Response and Design*, American Concrete Institute, Detroit.

Moehle, J. P., Sezen, H., and Elwood, K. J. (2001). "Response of reinforced concrete building lacking details for ductile response." *Proceeding of 4th International symposium on earthquake engineering for the moderate seismicity regions*, 117-131.

Moehle, J. P. and Sezen, H. (2006). "Seismic tests of concrete columns with light transverse reinforcement." *ACI Structural Journal*, **103**(6), 842-849.

Monegato, G. (1994). "Numerical evaluation of hypersingular integrals." *Journal of Computational and Applied Mathematics*, **50**(1-3), 9-31.

Mullapudi, T.R. S. and Ayoub, A. S. (2013). "Analysis of reinforced concrete columns subjected to combined axial, flexure, shear and torsional load." *Journal of Structural Engineering*, **139**(4), 561-573.

Nagasaka, T. (1982). "Effectiveness of steel fiber as web reinforcement in reinforced concrete columns." *Transactions of the Japan Concrete Institute*, **4**, 493-500.

Ning, L., Zhongxian, L., and Lili, X. (2013). "A fiber-section model based Timoshenko beam element using shear-bending interdependent shape function." *Earthquake Engineering and Engineering Vibration*, **12**(3), 421-432.

Ohue, M., Morimoto, H., Fujii, S., and Morita, S. (1985). "The behavior of R.C. short columns failing in splitting bond-shear under dynamic lateral loading." *Transactions of the Japan Concrete Institute*, **7**, 293-300.

Onate, E. (2013). *Structural analysis with the finite element method volume 2: beam, plates and shells*. Springer, Netherlands.

Ozcebe, G. and Saatcioglu, M. (1989). "Hysteretic shear model for reinforced concrete members." *Journal of Structural Engineering*, **115**(1), 132-148.

Ozbolt, J. and Bazant, Z. P. (1992). "Microplane model for cyclic triaxial behavior of concrete." *Journal of Engineering Mechanics*, **118**(7), 1365-1386.

Palermo, D. and Vecchio, F. J. (2002). "Behavior and analysis of reinforced concrete walls subjected to reversed cyclic loading." *Publication No. 2002-01*, Department of Civil Engineering, University of Toronto, Canada.

Palermo, D. and Vecchio, F. J. (2003). "Compression field modeling of reinforced concrete subjected to reversed loading: Formulation." *ACI Structural Journal*, **100**(5), 616-625.

Panto, B., Rapicavoli, D., Caddemi, S., and Calio, I. (2017). "A smart displacement based (SDB) beam element with distributed plasticity." *Applied Mathematical Modeling*, **44**, 1339-1351.

Park, H. and Kim, H. (2003). "Microplane model for reinforced-concrete planar members in tension-compression." *Journal of Structural Engineering*, **129**(3), 337-345.

Park, R. and Paulay, T. (1975). *Reinforced concrete structures*. New York: Wiley.

- Pelekasis, N. A. and Tsamopoulos, J. A. (1995). "Dynamics of charged and conducting drops via the hybrid finite-boundary element method." *Engineering Analysis with Boundary Elements*, **15**(4), 339-348.
- Petrangeli, M. (1996). "Modelli numerici per strutture monodimensionali in cemento armato." Ph.D. thesis, Universita di Roma "La Sapienza", Roma, Italy (in Italian).
- Petrangeli, M. Pinto, P. E., and Ciampi, V. (1999). "Fiber element for cyclic bending and shear of RC structure I: theory." *ASCE Journal of Engineering Mechanics*, **125**(9), 994-1009.
- Pincheira, J., Dotiwala, F. and Souza, J. (1999). "Seismic analysis of older reinforced concrete columns." *Earthquake Spectra*, **15**(2), 245-272.
- Prathap, G. and Bhashyam, G. (1982). "Reduced integration and the shear-flexible beam element." *International Journal for Numerical Methods in Engineering*, **18**(2), 195-210.
- Priestley, M.J. N., Seible, F., Verma, R., and Xiao, Y. (1993). "Seismic shear strength reinforced concrete columns." *Structural Systems Research Project Report No. SSRP-93/06*, University of California, San Diego, USA.
- Priestley, M.J. N., Verma, R., and Xiao, Y. (1994). "Seismic shear strength of reinforced concrete columns." *ASCE Journal of Structure Engineering*, **120**(8), 2310-2329.
- Priestley, M.J. N. and Benzoni, G. (1996). "Seismic performance of circular columns with low longitudinal reinforcement ratios." *ACI Structural Journal*, **93**(4), 474-485.
- Ranzo, G. and Petrangeli, M. (1998). "A fibre finite beam element with section shear modelling for seismic analysis of RC structures." *Journal of Earthquake Engineering*, **2**(3), 443-473.
- Recupero, A. D' Aveni, A. and Ghersi, A. (2005). "Bending moment-shear force interaction domains for prestressed concrete beams." *ASCE Journal of Engineering Mechanics*, **131**(9), 1413-1421.

- Reddy, J. N. (1997). "On locking-free shear deformable beam finite elements." *Computer Method in Applied Mechanics and Engineering*, **149**(1-4), 113-132.
- Remino, M. (2004). "Shear modelling of reinforced concrete structures." Ph.D. Thesis, Dipartimento di Ingegneria Civile, Universita degli Studi di Brescia, Brescia, Italy.
- Ricles, J. M., Yang, Y. S. and Priestley, M.J. N. (1998). "Modelling nonductile R/C columns for seismic analysis of bridges." *Journal of Structure Engineering*, **124**(4), 415-425.
- Rose, B. W. (2001). "A constitutive model for the analysis of reinforced concrete beam-columns subjected to lateral loads." Ph.D. Thesis, CEAE Dept., University of Colorado, Boulder, Colorado.
- Saatcioglu, M. and Ozcebe, G. (1989). "Response of reinforced concrete columns to simulated seismic loading." *ACI Structural Journal*, **81**(1), 3-12.
- Saritas, A. (2006). "Mixed formulation frame element for shear critical steel and reinforced concrete members." Ph.D. Thesis, University of California, Berkeley.
- Schoettler, M. J., Restrepo, J. I., Guerrini, G., Duck, D., and Carrea, F. (2012). "A full-scale, single-column bridge bent tested by shake-table excitation." *Center for Civil Engineering Earthquake Research*, Department of Civil Engineering, University of Nevada, Reno.
- Scordelis, A. C. (1984). "Computer models for nonlinear analysis of reinforced and prestressed concrete structures." *PCI Journal*, **29**(6), 116-135.
- Scott, B. D., Park, R., and Priestley, M.J. N. (1982). "Stress-Strain behavior of concrete confined by overlapping hoops at low and high strain rates." *ACI Structural Journal*, **79**(1), 13-27.
- Sezen, H. (2002). "Seismic behavior and modeling of reinforced concrete building columns." Ph.D. thesis, Department of Civil and Environmental Engineering, University of California, Berkeley, USA.

Sezen, H., Whittaker, A. S., Elwood, K. J., and Mosalam, K. M. (2003). "Performance of reinforced concrete buildings during the August 17, 1999 Kocaeli, Turkey earthquake, and seismic design and construction practice in Turkey." *Engineering Structures*, **25**(1), 103-114.

Sezen, H. and Moehle, J. P. (2004). "Shear strength model for lightly reinforced concrete column." *Journal of Structure Engineering*, **130**(11), 1692-1703.

Sezen, H. (2008). "Shear deformation model for reinforced concrete columns." *Structural Engineering and Mechanics*, **28**(1), 39-52.

Sinha, B. P., Gerstle, K. H., and Tulin, L. G. (1964). "Stress-strain relations for concrete under cyclic loading." *ACI Structural Journal*, **61**(2), 195-211.

Soleimani, D. (1978). "Reinforced concrete ductile frames under earthquake loadings with stiffness degradation." Ph.D. thesis, University of California, Berkeley, USA.

Spacone, E., Filippou, F. C., and Taucer, F. F. (1996). "Fiber beam-column model for nonlinear analysis of R/C frames. part I: formulation." *Earthquake Engineering and Structural Dynamics*, **25**(7), 711-725.

Spacone, E. and Limkatanyu, S. (2000). "Responses of reinforced concrete members including bond-slip effects." *ACI Structural Journal*, **97**(6), 831-839.

Stramandinoli, R. and Rovere, H. L.L. (2012). "FE model for nonlinear analysis of reinforced concrete beams considering shear deformation." *Engineering Structures*, **35**, 244-253.

Stroud, A. H. and Secrest, D. (1966). *Gauss quadrature formulas*. Prentice Hall, New Jersey.

Taylor, R. L. (2000). *FEAP: A Finite Element Analysis Program*, User manual: version 7.3, Department of Civil and Environmental Engineering, University of California, Berkeley.

Terzic, V., Schoettler, M. J., Restrepo, J. I., and Mahin, S. A. (2015). "Concrete column blind prediction contest 2010: out-comes and observations." *PEER Report1*.

Tessler, A. and Dong, S. B. (1981). "On a hierarchy of conforming Timoshenko beam elements." *Computers and Structures*, **14**(3-4), 335-344.

Tonti, E. (1977). "The reason for analogies between physical theories." *Applied Mathematical Modeling*, **1**(1), 37-50.

Umehara, H. and Jirsa, J. O. (1982). "Shear strength and deterioration of short reinforced concrete columns under cyclic deformations." *PMFSEL Report No. 82-3*, Department of Civil Engineering, University of Texas at Austin, Austin Texas.

Vecchio, F. J. and Collins, M. P. (1986). "The modified compression field theory for reinforced concrete elements subjected to shear." *ACI Structural Journal*, **83**(2), 219-231.

Vecchio, F. J. and Collins, M. P. (1988). "Predicting the response of reinforced concrete beams subjected to shear using modified compression field theory." *ACI Structural Journal*, **85**(3), 258-268.

Vecchio, F. J. and Selby, R. G. (1991). "Towards compression-field analysis of reinforced concrete solids." *ASCE Journal of Structural Engineering*, **117**(6), 1740-1758.

Vecchio, F. J. (1999). "Towards cyclic load modelling of reinforced concrete." *ACI Structural Journal*, **96**(2), 193-202.

Watanabe, F. and Ichinose, T. (1991). "Strength and ductility design of RC members subjected to combined bending and shear." *Proceeding of workshop on concrete shear in earthquake*, University of Houston, Texas, 429-438.

Wight, J. K. and Sozen, M. A. (1973). "Shear strength decay in reinforced concrete columns subjected to large deflection reversals." *Structural Research Series No. 403*, Civil Engineering Studies, University of Illinois, Urbana-Champaign.

Wight, J. K. and Sozen, M. A. (1975). "Strength decay of RC columns under shear reversals." *ASCE Journal of Structural Division*, **101**(5), 1053-1065.

Wolfram, S. (1992). *Mathematica Reference Guide*, Addison-Wesley Publishing Company, Redwood City.

Wong, Y. L., Paulay, T., and Priestley, M.J. N. (1993). "Response of circular reinforced concrete columns to multi-directional seismic attack." *ACI Structural Journal*, **90**(2), 180-191.

Wu, J. Y., Li, J., and Faria R. (2006). "An energy release rate-based plastic-damage model for concrete." *International Journal of Solids and Structures*, **43**(3-4), 583-612.

Wu, J. Y. (2017). "A unified phase-field theory for the mechanics of damage and quasi-brittle failure." *Journal of the Mechanics and Physics of Solids*, **103**, 72-99.

Wu, J. Y. (2018). "A geometrically regularized gradient-damage model with energetic equivalence." *Computer Methods in Applied Mechanics and Engineering*, **328**, 612-637.

Xiao, Y. and Martirosyan, A. (1998). "Seismic performance of high-strength concrete columns." *Journal of Structural Engineering*, **124**(3), 241-251.

Xucheng, W. and Xiaoning, W. (1995). "Simplified method for elasto-plastic finite element analysis of hardening materials." *Computers and Structures*, **55**(4), 703-708.

Yalcin, C. (1997). "Seismic evaluation and retrofit of existing reinforced concrete bridge columns." Ph.D. thesis, Department of Civil Engineering, University of Ottawa, Canada.

Yassin, Mohd H.M. (1994). "Nonlinear analysis of prestressed concrete structures under monotonic and cyclic loads." Ph.D. dissertation, Department of Civil and Environmental Engineering, University of California, Berkeley.

Zeris, C. A. and Mahin, S. A. (1991). "Behavior of reinforced concrete structures subjected to biaxial excitation." *Journal of Structural Engineering*, **117**(9), 2657-2673.

Zhou, X., Satoh, T., Jiang, W., Ono, A., and Shimizu, Y. (1987). "Behavior of reinforced concrete short column under high axial load." *Transactions of the Japan Concrete Institute*, **9**, 541-548.

Zienkiewicz, O. C. and Taylor, R. L. (1991). "The finite element method volume 2 solid and fluid mechanics dynamics and non-Linearity." Fourth Edition, McGraw Hill, London.

APPENDIX A

APPENDIX A: Euler-Bernoulli beam theory

Euler-Bernoulli beam theory has the fundamental hypothesis that “Plane sections remain plan and normal to the longitudinal beam axis” [Limkatanyu, 2008]. Thus, the kinematics and deformation of cross sections points a and b for Euler- Bernoulli beam can present in Figure a-1. It can be observed that the point a’ and b’ in deformed configuration remain plane and is normal to the longitudinal axis of beam.

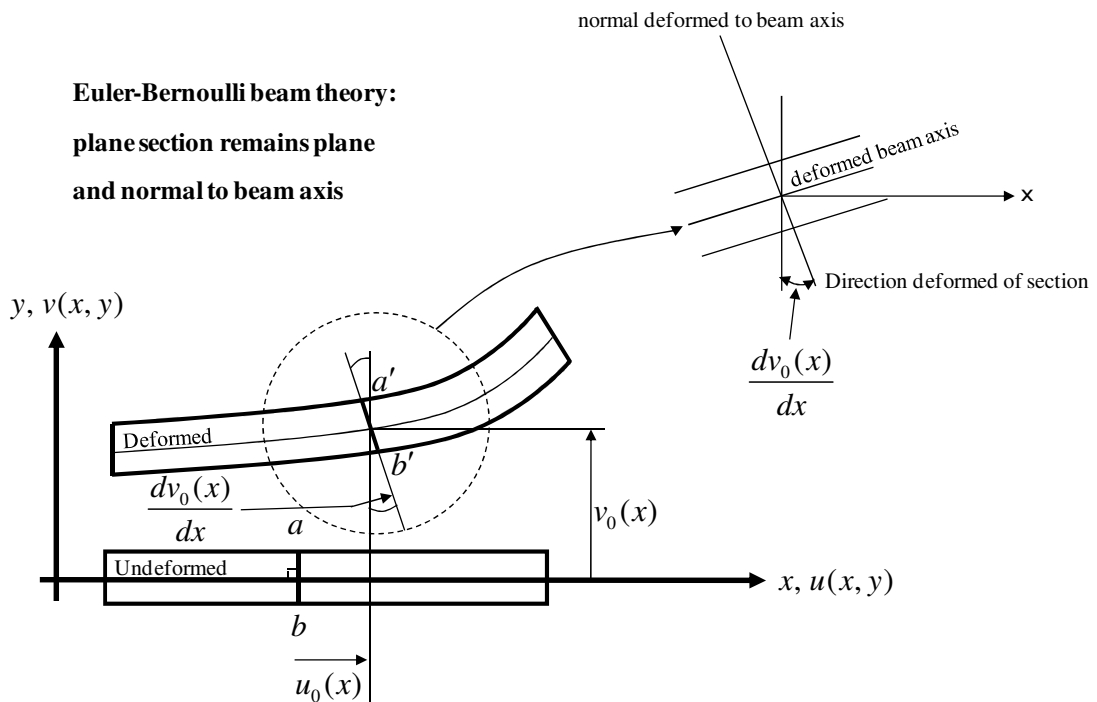


Figure A-1 Kinematics description of the Euler-Bernoulli beam element before deformation and after deformation [Limkatanyu, 2008]

From the kinematics assumption of Euler-Bernoulli beam, the axial strain $\varepsilon_{xx}(x)$ and shear strain $\gamma_{xy}(x)$ can be written as:

$$\varepsilon_{xx}(x) = \frac{du(x)}{dx} = \frac{du_0(x)}{dx} - y \frac{d\theta(x)}{dx} = \varepsilon_0(x) - y\varphi(x) \quad (\text{A-1})$$

APPENDIX B

APPENDIX B: List of Proceeding

1. Sae-Long, W. and Limkatanyu, S. (2018). "Shear model with shear-flexure interaction for non-linear analysis of reinforced concrete frame element." MATEC Web of Conferences 192, 02003, <https://doi.org/10.1051/matecconf/201819202003>.

Shear model with shear-flexure interaction for non-linear analysis of reinforced concrete frame element

Worathep Sac-Long^{1*}, and Suchart Limkatanyu¹

¹Department of Civil Engineering, Faculty of Engineering, Prince of Songkla University, Hat Yai, Songkhla, Thailand

Abstract. This paper presents the shear constitutive model for the reinforced concrete (R/C) frame structures analysis under monotonic and cyclic loading. The proposed model is adopted and modified from Mergos and Koppas model [1] that accounts the shear stiffness degradation effect by the shear-flexure interaction in the plastic hinge region. Firstly, the proposed shear model starts from the primary curve without the damages due to the shear-flexure interaction effect. Then, the shear-flexure interaction effect is taken into consideration at the locations of plastic hinges and this effect leads to the degradation of the shear strength and shear stiffness on the undamaged primary curve that is replaced with the damaged primary curve. To determine the sectional shear stiffness with the shear-flexure interaction, an alternative way of the iterative procedure is proposed here. Finally, a numerical example is used to verify the characteristics and behavior of the R/C frame system and confirm accuracy and computational efficiency of the proposed model among the experimental data.

1 Introduction

The reinforced concrete structures (R/C-Structure) have been used extensively in engineering works, for example, the building and bridge structures etc. From the past earthquakes, the R/C members before the proposed seismic codes were often collapsed and heavily damaged due to the member without ductile design requirement. The most dangerous damage mechanism was related to shear that occurred suddenly because of the insufficient shear strength. However, the characteristics of R/C member failure didn't account only the shear failure but also included the flexural failure and the flexure-shear failure [2].

The flexure-shear failure might be significant in some cases such as the lightly R/C columns. To represent the accurate responses of those members, there were several researchers [2-3] who developed the analytical procedures to include the shear-flexure interaction into the assessment of element by using the different strategies. Although these procedures were attractive, these methods were not successful with the degradation of shear strength in the plastic hinge region. Later, Mergos and Kappos [1, 4] presented the shear model and the shear-flexure interaction procedure that was able to capture the degradation of the shear strength in the plastic hinges region. However, although these methods were attractive, it didn't seem reasonable in the real analysis because their method approximated the shear stiffness with the shear-flexure interaction which based on a constant stiffness in every step.

In the light of this reason, this paper proposes an alternative of a shear model with the modified technique

for the degraded shear stiffness estimation due to the shear-flexure interaction effect. Moreover, a numerical example is used to confirm the accuracy and efficiency of the proposed model. The example presents the member with failing in shear after the flexural yielding that is defined to the shear-flexure critical member. All the responses of the model in this paper are implemented in the general-purpose finite element platform FEAP [5].

2 Shear model

The shear model represents the shear force-shear strain relation of the R/C member. The original shear model was proposed by Mergos and Kappos [1] and their model covered all the behaviors of R/C member prior and after concrete cracking, the flexural yielding and the transverse reinforcement yielding or failure as indicated in the primary curve for this paper.

2.1 Primary curve of shear model

The primary curve presents the initial shear force-shear strain relation that is first derived without considering the damage due to the shear-flexure interaction effect. As shown in Fig. 1, it comprises four branches with three different slopes. The first branch oa with uncracked slope (GA_0) shows the elastic behavior of uncracked section in shear. The origin point o connects to the cracking point a (V_{cr}, γ_{cr}) at which the nominal principal tensile stress becomes larger than the nominal tensile strength of concrete. The cracking shear force (V_{cr}) [4],

*Corresponding author: s.worathep@yahoo.com

the uncracked slope (GA_0) and the cracking shear strain (γ_{cr}) can be written as:

$$V_{cr} = \frac{f'_t}{L_u/h} \sqrt{1 + \frac{N}{f'_t A_g}} 0.80 A_g \quad (1)$$

$$GA_0 = 0.80 GA_g \quad (2)$$

$$\gamma_{cr} = V_{cr} / GA_0 \quad (3)$$

Where f'_t is the mean concrete tensile strength, A_g is the gross area of the concrete section, L_u is the shear span, h is the section height, N is the compressive axial load and G is the shear modulus respectively.

The second branch ab and third branch bc have the same slope of GA_1 . The second branch ab links the cracking point a (V_{cr}, γ_{cr}) to the flexural-yielding point b (V_y, γ_y) at which the longitudinal reinforcement yields for the first time. The third branch bc joins the flexural-yielding point b (V_y, γ_y) to the shear-yielding point c (V_{s0}, γ_{st}) at which shear strain corresponds to the onset of the transverse reinforcement yielding (γ_{st}) while shear force reaches its ultimate value (V_{u0}).

To estimate the shear strength (V_u) on the primary curve, the shear strength model, proposed by Priestly et al. [6], is used in this study. The model is able to account for the shear strength degradation with increasing curvature ductility demand that can be defined as:

$$V_u = k_p \sqrt{f'_c} (0.80 A_g) + \frac{A_s f_{yv} D' \cot 30^\circ}{s} + \frac{d-c}{2L_u} N \quad (4)$$

Where k_p is a parameter associated the curvature ductility demand μ_p [1], f'_c is concrete strength, A_s is the area of the transverse reinforcement, f_{yv} is the yield strength of transverse reinforcement, D' is the distance measured parallel to the applied shear between the centres of transverse reinforcement, s is the spacing of transverse reinforcement, d is the section depth and c is the neutral axis depth respectively.

The slope of the second and third branch (GA_1) can be expressed as:

$$GA_1 = \frac{V_{u0} - V_{cr}}{\gamma_{st} - \gamma_{cr}} \quad (5)$$

Where V_{u0} is the non-degraded shear strength that can determine from Eq. (4) by setting the curvature ductility demand which becomes lesser than 3.

The shear strain at the onset of transverse reinforcement yielding (γ_{st}) can simply be determined by using the truss analogy. However, it is not corresponding well with experimental results due to the axial load and aspect ratio effects. Mergos and Kappos [1] suggested two modification factors (κ and λ) to improve the accuracy of these equations. The value of γ_{st} was given by

$$\gamma_{st} = \frac{V_{cr}}{GA_0} + \frac{A_s f_{yv} \left(\sin^4 45^\circ + \frac{E_s}{E_c} P_v \right)}{s E_s b p \sin^4 45^\circ \cot 45^\circ} \quad (6)$$

$$\kappa = 1 - 1.07\nu \quad \text{and} \quad \lambda = 5.37 - 1.59 \min(2.5, L_u/h) \quad (7)$$

$$\gamma_{st} = \kappa \lambda \gamma_{st0} \quad (8)$$

Where γ_{st0} is the shear associated with the yielding of transverse reinforcement based on truss analogy, E_s is the elastic modulus of steel, E_c is the elastic modulus of concrete, ν is the volumetric ratio of transverse reinforcement, b is the section width and $\nu = N / (f'_c A_g)$ is the normalized compressive axial load.

Finally, the last branch cd represents the plastic behavior of shear and connects the shear-yielding point c (V_{s0}, γ_{st}) to the ultimate point d (V_{u0}, γ_u) which associates with the onset of shear failure. The value of γ_u is based on regression analysis of experimental results and suggested by Mergos and Kappos [1]:

$$\lambda_1 = 1.0 - 2.5 \min(0.40, \nu) \quad \text{and} \quad \lambda_2 = \min(2.5, L_u/h)^{2.0} \quad (9)$$

$$\lambda_3 = 0.31 + 17.8 \min\left(\frac{A_s f_{yv}}{(b s f'_c)}, 0.08\right)$$

$$\gamma_u = \lambda_1 \lambda_2 \lambda_3 \gamma_{st} \geq \gamma_{st} \quad (10)$$

Where λ_1 , λ_2 and λ_3 are the parameter accounting for axial load, aspect ratio and amount of transverse reinforcement respectively. It is important to note that the Mergos and Kappos formula for γ_{st} and γ_u estimation suggested the criteria: $1.11 \leq L_u/h \leq 3.91$, $0 \leq \nu \leq 0.61$ and $0.47\% \leq (A_s f_{yv}) / (b s f'_c) \leq 8.13\%$ [1].

2.2 The modified Mergos-Kappos shear-flexure interaction procedure (MMKSFIP)

According to the primary curve, there are two phenomena results due to the shear-flexure interaction effect on the undamaged primary curve. The first one is the degradation of the shear strength because of the increasing curvature ductility demand as defined by the shear strength model in Eq. (4). From this result, the last branch cd is degraded from the undamaged primary curve to the new portion that associates with the shear strength at the start of load increment step. Moreover, the reduction of the shear strength also leads to the degradation of the shear stiffness as defined in the second phenomena result. The authors refer to the degraded shear stiffness as "the effective shear stiffness (GA_{eff})". As shown in Fig. 1, there are three cases to be confronted when the shear-flexure interaction appears after the flexural reinforcement yielding.

The first case refers to the case of the non-degradation of the shear strength, the sectional curvature ductility is lesser than 3 that based on the shear strength model in Eq. (4). In this case (Fig.1), the sectional shear force at the start and end of load increment step are located on the undamaged primary curve with the cracked sectional shear stiffness (GA_1).

The second case presents the case of the degradation of the shear strength for the first time, the sectional curvature ductility is larger than 3 for the first time. From this case, the sectional shear force at the start of

load increment step lies on the undamaged primary curve but the sectional shear force at the end of load increment step is situated on the damage primary curve due to the shear-flexure interaction effect with the effective shear stiffness $((GA)_{eff})^k$ as shown in Fig.1.

The last case shows the case after the degradation of the shear strength for the first time. The sectional shear force at the start and end of load increment step are located on the damaged primary curve with the effective shear stiffness $((GA)_{eff})^k$.

According to the effective shear stiffness estimation, the original procedure proposed by Mergos and Kappos [1] is adopted and modified herein. The authors refer to this procedure as “modified Mergos-Kappos shear-flexure interaction procedure (MMKSFIP)”. From all three possible cases, The incremental sectional shear force (ΔV) and the effective shear stiffness $((GA)_{eff})^k$ can determine form a given incremental sectional shear strain $(\Delta\gamma)$ by using the MMKSFIP through the proposed reference slope that links the sectional shear force at the start of load increment step to the sectional shear force at the end of load increment step on the undamaged primary curve as shown in Fig. 1. In this procedure, the so-called reference sectional shear stiffness $((GA_{ref})_i)^k$ can define as:

$$(GA_{ref})_i^k = \frac{V_{0,j}^{k+1} - V^k}{\Delta\gamma_i^k} \quad (11)$$

Where $V_{0,j}^{k+1}$ is the non-degradation sectional shear force that corresponds to the sectional shear strain $\gamma_i^{k+1} = \gamma_i^k + \Delta\gamma_i^k$ and can be written as:

$$V_{0,j}^{k+1} = V_{cr} + GA_i(\gamma_i^{k+1} - \gamma_{cr}) \quad (12)$$

It is worth noting that, the reference sectional shear stiffness $((GA_{ref})_i)^k$ in the first and second cases is simply equal to the cracked sectional shear stiffness (GA_i) as shown in the Fig. 1. Considering the relation between incremental sectional shear force (ΔV) and shear strain $(\Delta\gamma)$ in Fig. 1 leads to the following expression:

$$\Delta\gamma_i^k = \frac{\Delta V_i^k}{(GA_{eff})_i^k} = \frac{\Delta V_i^k + (\Delta V_c^{deg})_i^k}{(GA_{ref})_i^k} \quad (13)$$

Where $(\Delta V_c^{deg})_i^k$ is the degradation of the concrete shear resisting mechanism can calculate by:

$$(\Delta V_c^{deg})_i^k = (GA_{ref})_i^k \Delta\gamma_i^k - \frac{(V_{0,j}^k - V_i^k)}{(V_{0,j}^k - \gamma_i^k)} \Delta\gamma_i^k \quad (14)$$

The effective shear stiffness $((GA_{eff})_i)^k$ can calculate by solving Eq. (13). The following equation is obtained.

$$(GA_{eff})_i^k = \frac{\Delta V_i^k}{\Delta V_i^k + (\Delta V_c^{deg})_i^k} (GA_{ref})_i^k \quad (15)$$

It is observed from Eq. (15) that the effective shear stiffness $((GA_{eff})_i)^k$ is a function of the incremental sectional shear force (ΔV_i^k) but both quantities are unknown. To overcome this problem, an iterative

analytical scheme is applied within the iterative step i of the load increment k . It needs to note that the following parameters $\Delta\gamma_i^k$, $(GA_{ref})_i^k$ and $(\Delta V_c^{deg})_i^k$ aren't changed during an iterative scheme except $(GA_{eff})_i^k$ and ΔV_i^k . For this reason, the additional subscript “ j ” is added into $(GA_{eff})_i^k$ and ΔV_i^k to define the iterative step of the shear-flexural interaction process. The iterative process within the shear-flexural interaction procedure in this study is adopted from Newton-Raphson iterative technique. Firstly, an initial effective shear stiffness $((GA_{eff})_{i,j-1})^k$ is assumed. Shear force increment $(\Delta V_{i,j}^k)$ is calculated from $\Delta V_{i,j}^k = (GA_{eff})_{i,j}^k \Delta\gamma_i^k$ in the second step and Eq.(15) is enforced to a residual function by moving $(GA_{eff})_{i,j}^k$ into the opposite side in the third step. The fourth step is the derivative of residual function determination. Next, the new value of $(GA_{eff})_{i,j+1}^k$ is updated from the residual function and its derivative. Finally, the iterative procedure terminates, when the value of residual function converges with the specified tolerance.

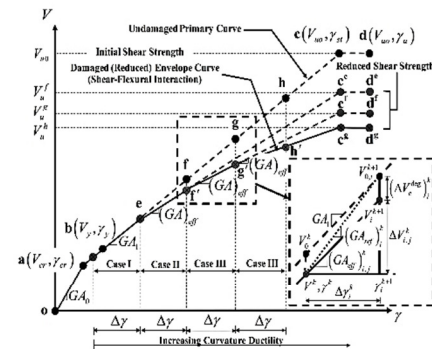


Fig. 1. Primary curve of the shear model

2.3 The hysteretic shear behavior

In this study, the hysteretic relation between the shear force and shear strain is based on the uniaxial behaviors and expressed in term of shear strain. Moreover, the hysteretic law is adapted from the hysteretic moment-rotation relation with pinching and damage, proposed by Filippou et. al. [7]. It comprises of three parts. The first one is the monotonic envelop curve (Primary curve). The second and third parts are unloading and reloading curves respectively.

3 Numerical example

To verify the accuracy and efficiency of the proposed model, a numerical example is presented herein. The example is presented by using 16 elements with 7 Gauss-Lobatto integration points under the displacement-based

method that are enough for the convergent responses. Moreover, the frame section is discretized into 40 fibers (Layers) to represent the nonlinear responses under the fiber-section model.

The specimen 3SMD12 was one of the full-scale R/C column tests by Lynn [8]. The column was a double curvature specimen under a constant axial load and cyclic lateral displacements at the end of the column and collapsed in shear after the longitudinal reinforcement bars yielding. It's so-called "Flexure-shear failure". The initial shear strength can predict from Eq. (4) about 597.93 kN by using the properties in Table 1.

Table 1. Properties of specimen 3SMD12

Properties	Value	Properties	Value
f'_c	25.5 (MPa)	s	305 (mm)
b and h	457.2 (mm)	p_s	0.0017
f_{st}	331 (MPa)	L	2,946 (mm)
f_{yv}	400 (MPa)	N	1,512 (kN)

Fig. 2 shows the lateral load vs. lateral displacement response as derived by the proposed model and the experimental data. It can be seen that the proposed model is able to represent the complex behavior of the experimental results very well. These include the member capacity, stiffness degradation with increasing displacement amplitude, amount of dissipated hysteretic energy and general shape of hysteretic response. Moreover, the proposed model can capture the degradation of the shear strength and shear stiffness due to the increasing curvature ductility demand before the shear failure occurs at the displacement about 17.12 mm.

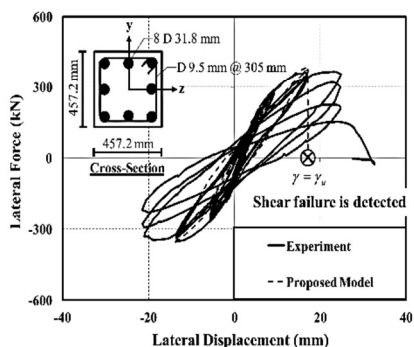


Fig. 2. The lateral load and total displacement relationship between the proposed model and experimental data

Fig. 3. presents the shear force vs. shear strain hysteretic relationship of a specimen 3SMD12 at the end of a column (Inside plastic hinge regions). It can be observed that after the curvature ductility demand value exceeds 3, the shear strain increases immediately and shear stiffness is degraded from the undamaged primary curve into the damaged primary curve. Finally, the

models can predict shear failure when the shear strain reaches γ_u , that is found to be 3.33×10^{-3} .

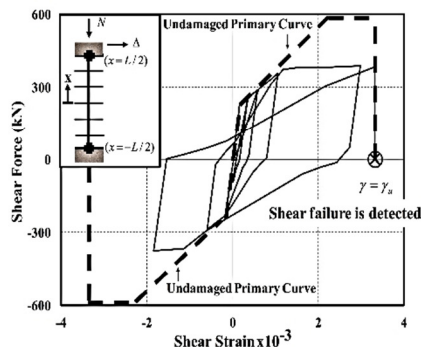


Fig. 3. Shear force vs. shear strain hysteretic loops at the end of a column (inside plastic hinges)

4 Conclusions

This paper presents an alternative of the shear model for the R/C frame structures analysis under monotonic and cyclic loading. The degradation of the shear strength and shear stiffness due to the shear-flexure interaction effect is included in this model. Moreover, the modified Mergos-Kappos shear-flexure interaction procedure (MMKSFIP) is proposed here and used to estimate the effective shear stiffness. Finally, the response analysis of a numerical example confirms the accuracy and computational efficiency of the proposed model.

Funding

This study was partially supported by Faculty of engineering, Prince of Sonkla University.

References

1. P.E. Mergos, A.J. Kappos, Eng. Struct., **44**, 94-106 (2012)
2. P. Ceresa, L. Petrini, R. Pinho, IUSS, Pavia, Italy (2008)
3. F.J. Vecchio, M.P. Collins, ACI Struct. J., **83**, 219-231 (1986)
4. P.E. Mergos, A.J. Kappos, Earthquake Eng. Struct. Dyn., **37**, 1349-1370 (2008)
5. R.L. Taylor, User manual: version 7.3 (Department of Civil and Environmental Engineering, UC, Berkeley, 2000)
6. M.J.N. Priestley, F. Seible, R. Verma, Y. Xiao, Report no SSRP-93/06 (USD, Calif., 1993)
7. F.C. Filippou, E.P. Popov, V.V. Bertero, EERC Report 83-19 (EERC, UC, Berkeley, 1983)
8. A. Lynn, Ph.D. thesis (UCB, Berkeley, Calif., 2001)

VITAE

Name Mr.Worathep Sae-Long

Student ID 5810130013

Educational Attainment

Degree	Name of Institution	Year of Graduation
Bachelor of Engineering (Civil Engineering)	Prince of Songkla University	2012
Master of Engineering (Civil Engineering)	Prince of Songkla University	2014

Scholarship Awards during Enrolment

- Scholarship Awards for Thai Ph.D. Students under Thailand's Education Hub for Southern Region of ASEAN Countries
- Scholarship from Faculty of Engineering, Prince of Songkla University

List of Publication and Proceedings

- Sae-Long, W. and Limkatanyu, S. (2018). "Shear model with shear-flexure interaction for non-linear analysis of reinforced concrete frame element." MATEC Web of Conferences 192, 02003, <https://doi.org/10.1051/matecconf/201819202003>.